



Journal of Madenat Alelem University College

www.jmauc.edu.iq

E-mail: jmauc@mauc.edu.iq

TEL: 7801099835

Publisher:

Madenat Alelem University College

كلية مدينة العلم الجامعة

www.mauc.edu.iq

رقم الايداع في دار الكتب والوثائق 1333 لسنة 2009

Editor in chief

Dr. Shaker M. Al-Jobori

Deputy editor in Chief

Dr. Jabbar F. Al-Maadhidi

Editorial board

Lect. Isam Atta Ajaj

Editor

Dr. Saeed Selman Kamoon

Dr. Mousa M. Al-jobori

Dr. Sabah Abdul Latif Nassif

Dr. Usama Aladdin Ibrahim

Dr. Saad Abdolridha Makki

Dr. Abd Almonem K. Hammadi

Dr. Ali Mahdi

Dr. Hussain H. Ahmed

Dr. Farooq Abdul Azeez Mohammed

Dr. Ayaid K. Zgair

Advisori Board

Prof. Dr. AbdolHazim Al-Rawi, Alrashed University

Prof. Dr. TawficNajim, Al-mammon University College

Prof. Dr. Ghazi Faisal, Al-Nahrin University

Prof. Dr. Nabil Hashim, Babel University

Dr. Ayad A. Al-Taweel, Ministry of Science and Technology

Assis. Prof. Ahmed Mossa, Technical University

Dr. Ammer M. Ali, MadentAlelem College

Dr. IbrahimKhammas, MadentAlelem College



INSTRUCTIONS to AUTHERS

Submitted articles to the Journal of Madinat Al-Elem University College can be published in all fields related to the Academic Departments of the College (Biology, Law, programming Engineering Sciences, Computer Techniques Engineering Law, Medical Physics, Civil Engineering, and Accounting).

Written request for publication and signing a consent form to publish must be for articles which have not been published or submitted for publication to other journals. Three copies with CD are needed. Manuscripts should be typed on: A4 white paper, double spaced, written in Times New Roman font size 14. Margins should be 3cm from top, bottom, left and right. The main title should be in: bold Times New Roman font size 14. Author names should be written in the following sequence: first name, middle name, the family name, followed by the names of departments and institutions of work. A footnote accompanies the first page stating the full address of correspondence author.

Articles need to contain the following items:

- Abstract in English and Arabic not more than 300 words.
- Article includes the following items: Introduction, Materials and Methods, Results and Discussion, Conclusion and References.
- References should be numbered in the text according to the sequence appeared in the text and listed in order.
- Tables and figures should be appropriately titled with size not exceed an A4 page.

The editor reserves the right to reject or accept any article submitted.

Publication charges: Each accepted paper is required to pay the publication charge (100,000 Iraqi dinars). Five thousands Iraqi dinar are requested for each extra page extra printed page.

Contents

	Page
<p>1-Function of thyroid gland of normal healthy pregnant women during the second trimester of pregnancy.</p> <p>Noor Salman Dalis, Sami Z. Akrim, Alaa Saber Shihab, Mossa M. Marbut.</p>	1
<p>2-The use of Interleukin -10 as a biomarker for diagnosis of viral hepatitis type C Infections and related liver function in beta-thalassemic major patients.</p> <p>Sarah M. Mahmoud, Zainb ER. Abass , Assis. Prof. Dr. Nihad Abdulhussain Jafar.</p>	10
<p>3- A Photoelastic Study of stresses in the femure</p> <p>Dr. Jamal A. Hassan , College ofEngineering, Al-Nahrain University</p> <p>Dr. Sadiq J. Abass, College of Engineering, Al-Nahrain University</p> <p>Eng. Zainabmajid, Electrical Engineering Technical College , Middle Technical University</p>	26
<p>4- Sensors Data Encryption Using TSFS Algorithm</p> <p>Shatha Habeeb Dr. Rehab F. Hassan</p>	32
<p>5-Evanescent Field Mach-Zehnder Interferometer Sensor for Concentration Measurement</p> <p>Ruaa Khalil Musa¹, Salah Al deen Adnan², Ali Mahdi Hammadi³</p>	44
<p>6-Single phase Cascaded H-Bridge Multilevel Inverter study and comparison of different levels</p>	56

Asst.prof.Jameel Kadhum Abed , Muhannad Jabbar Munati , Bassam Mohammed Yaseen

7-Design of Maximum power Tracking System by Automatic Control of Solar Cell Panel to the Sun Direction

Kader H.A. Al-Shara

71

8-Creating continuous model review for material cement in Kirkuk plant when fuzzy and randomly demand with acceleration (speed up) waiting period by application

Abdul muneem K. Hamadi Alshokri

84

Function of thyroid gland of normal healthy pregnant women during the second trimester of pregnancy.

Noor Salman Dalis, Ass. prof. Dr. Sami Z. Akrim, Alaa Saber Shihab, Prof. Dr. Mossa M. Marbut

Dept of Physiology, College of Medicine, Tikrit University.

Mossa 1955p@yahoo.com

Abstract :

Background : During pregnancy, the mother's thyroid gland undergoes many physiological changes, leading to an increase in thyroid volume which is often associated with higher urinary iodine excretion. **Aim of study:** To study the levels of thyroid function in second trimester of pregnancy. **Subjects and methods:** A longitudinal study was conducted in Gynecological clinics at Alalm city Salah din Government from the 1st of August 2016 to the end of march 2017. Ninety pregnant women were participated in the study. About 10 ml of venous blood was drawn from pregnant woman. Samples were collected between (9-11) A.M., after overnight fasting, the blood was drawn from the capital vein using disposable needles and syringes with using tourniquet in all cases. The blood was allowed to clot in plain tubes at room temperature. The serum was aspirated after centrifugation (at 3000 rpm) for 30 minutes, divided into liquates in plastic tubes and stored at deep freeze (-18_20C⁰) until the time of estimation. **Result:** The result show that, there is a high significant in T3 and T4 there are no significant difference between three month in TSH concentration as compare to its trimester. In other hand, there is no significant difference ($p \leq 0.001$) among pregnant of cholesterol , LDL and VLDL concentration. but there is there is significant difference ($p \leq 0.001$) among pregnant of triglyceride and HDL value when compare to different month. **Conclusion:** We calculated clinically relevant second trimester values for thyroid function tests through pregnancy to facilitate improved management of thyroid disease in pregnancy in our local population.

Key Words: Second trimester, Pregnancy, thyroid hormones, Lipid profile.

وظيفة الغدة الدرقية في النساء الحوامل السليمات طبيعية خلال الثلث الثاني من الحمل

نور سلمان دلس ، ا.م.د سامي زبار أكريم ، م.م علاء صابر شهاب, أ.د موسى محمود مربوط

فرع الفلسفة، كلية الطب ، جامعة تكريت

الخلاصة

المقدمة: خلال فترة الحمل ، تخضع الغدة الدرقية للكثير من التغيرات الفسيولوجية ، مما يؤدي إلى زيادة في حجم الغدة الدرقية والتي غالبا ما ترتبط بزيادة إفراز اليود في البول. **الهدف من الدراسة:** دراسة مستويات وظائف الغدة الدرقية في الثلث الثاني من الحمل. **طرق البحث:** تم إجراء دراسة طولية في عيادات أمراض النساء في مدينة علم بمدينة صلاح الدين من 1 أغسطس 2016 حتى نهاية مارس 2017. شاركت 90 سيدة في هذه الدراسة. تم سحب حوالي 10 مل من الدم الوريدي من امرأة حامل. تم جمع العينات بين (9-11) صباحا ، بعد صيام بين عشية وضحاها ، تم سحب الدم من الوريد باستخدام الحقن الطبية . كان يُسمح للدم بالتجلط في أنابيب عادية عند درجة حرارة الغرفة. تم رش المصل بعد الطرد المركزي (عند 3000 دورة في الدقيقة) لمدة 30 دقيقة ، مقسمة إلى سوائل في أنابيب بلاستيكية وتخزينها في تجميد عميق حتى وقت التقدير. **النتائج:** تظهر النتيجة TSH لا يوجد فرق كبير بين ثلاثة أشهر في تركيز T4 و T3 أن هناك درجة عالية من الأهمية في بين العوامل من تركيز ($p \leq 0.001$) بالمقارنة مع الثلث الاول. من ناحية أخرى ، لا يوجد فرق كبير بين العوامل من قيمة الدهون ($p \leq 0.001$) ولكن هناك فرق كبير. VLDL و LDL الكوليسترول ، عند المقارنة بشهر مختلف. **الخلاصة:** حسبنا قيم الفصل الثاني ذات الصلة سريريا HDL الثلاثية و لاختبارات وظيفة الغدة الدرقية خلال الحمل لتسهيل إدارة محسنة لمرض الغدة الدرقية في الحمل في السكان المحليين.

الكلمات المفتاحية: الثلث الثاني- الحمل, مرئسم الدهون و وظيفة الغدة الدرقية

Introduction:

Pregnancy trimester were define according to the American College of Obstetricians and Gynecologist' definition: Frist trimester (1-3)weeks, second trimester (14_26) weeks, and third trimester (27) weeks .^[1] During pregnancy, the extrathyroid T4 pool is increase in order to maintain hemostasis of the free hormone concentration, so that at the beginning of pregnancy the thyroid adjustment is continuous and T4 and TBG levels are constantly change.^[2,3] During pregnancy, the mother's thyroid gland undergoes many physiological changes, leading to an increase in thyroid volume which is often associated with higher urinary iodine excretion. It is also associated with the formation of new thyroid nodules with the histological features of nodular hyperplasia,^[4] Very early in pregnancy, the increase in

estrogen levels causes an approximate doubling in thyroxine binding globulin (TBG) that can lead to an increases in total T4 concentration and a reduced free fraction In healthy women, the final effect consists of a significant increase in the total thyroxine pool, mainly in the first trimester^[4,5].

Evident maternal thyroid failure during the first half of pregnancy has been associated with several pregnancy complications including preeclampsia, premature labor, fetal death and low birth weight and intellectual impairment in the offspring,^[6]Most of the changes in maternal metabolism and inflammatory status are considered to be normal physiological responses to support fetal growth and development. These changes typically return to pre-pregnancy states soon after delivery. These adverse pregnancy outcomes are associated with increased future

risk of diabetes and cardiovascular disease both in mothers and offspring, though the extent to which these are causal or reflect pre-existing maternal risk is unclear^[7].

The **Aim** of study is to study the levels of thyroid function in second trimester of pregnancy.

Subjects & methods:

A longitudinal study was conducted on Gynecological clinics at Alalm city Salahdin Government from the 1st of August 2016 to the end of march 2017. Ninety pregnant women were participated in the study. healthy pregnant women, aged between 18 - 41 years. About 10 ml of venous blood was drawn from pregnant woman. Samples were collected between (9-11) A.M., after overnight fasting, the blood was drawn from the capital vein using disposable needles and

syringes with using tourniquet in all cases. Two ml blood was mixed with anticoagulant EDTA for analyzing hematological parameters. Four ml of clotted sample was used to determine the levels of thyroid hormone and four ml for determine lipid profile. The blood was allowed to clot in plain tubes at room temperature. The serum was aspirated after centrifugation (at 3000 rpm) for 30 minutes, divided into liquates in plastic tubes and stored at (-20C⁰) until the time of estimation. VIDAS Techniques used for estimated thyroid hormones and Cobas c 111 analyzer used for estimated lipid profile.

Results

The age range was (18 to 41) years. Regarding T3: there is a high significant differences ($p \leq 0.007$) in mean and stander deviation of T3 value of pregnant in month one (1.626 ± 0.325),

month two (2.187 ± 0.572) and month three (2.581 ± 0.618), as show in table (1).

There is 37.23% increase in concentration of T3 compare to normal range. Regarding T4: there is a high significant reduction ($p \leq 0.005$) in mean T4 value of pregnant in month one (140.00 ± 34.81), month two (121.43 ± 32.54) month three (97.77 ± 18.58), As show in table (1).

There is 30.2% reduction in concentration of T4 compare to normal range. Regarding TSH: there are no stander differences among three month ($P > 0.652$) in TSH value month one (1.127 ± 0.734), month two (1.265 ± 0.542) and month three (1.266 ± 0.624).), As show in table (1).

There is 10.98% change in concentration of TSH compare to normal range. Regarding

cholesterol : there is no significant difference ($p \leq 0.001$) among pregnant of cholesterol value in month one (198.67 ± 36.47 mg/dl), month two (209 ± 29.04 mg/dl) and month three (193.73 ± 26.55), As show in table (2).

Regarding triglyceride: there is significant difference ($p \leq 0.052$) among pregnant of triglyceride value in month one (152.40 ± 40.45 mg/dl), month two (170.63 ± 35.12 mg/dl) and month three (168.93 ± 32.75 mg/dl), As show in table (2).

Regarding HDL : there is significant difference ($p \leq 0.001$) among pregnant of HDL value in month one (59.65 ± 11.78 mg/dl), month two (64.16 ± 14.11 mg/dl) and month three (54.26 ± 13.34 mg/dl), As show in table (2).

Regarding LDL: there is no significant difference ($p \leq 0.866$) among pregnant of cholesterol

value in month one (107.66 ± 25.59 mg/dl), month two (108.37 ± 25.32 mg/dl) and month three (104.97 ± 26.85 mg/dl), As show in table (2).

Regarding VLDL: there is no significant difference ($p \leq 0.117$)

Regarding HB: there is highly significant difference ($P \leq 0.001$) in HB among three months month one (10.123 ± 1.040 gm/dl), month two (9.403 ± 1.144 mg/dl) and month three (10.727 ± 1.562 mg/dl), as show in table (4.3) & figure (1).

In present study we found elevated T3, which was significant and decrease in T4 value and TSH is stay stable in second trimester as compared to other trimester.

Kumar et al¹⁶ measured serum levels of T3, T4, and TSH in 124 pregnant women that were apparently normal, healthy young primigravidas with no known

among pregnant of cholesterol value in month one (30.77 ± 7.91 mg/dl) , month two (34.12 ± 7.02) and month three (34.68 ± 8.48 mg/dl), As show in table (2).

Regarding PCV: there is a significant reduction ($P \leq 0.004$) in mean PCV value in month one ($33.553 \pm 3.431\%$), month two ($31.230 \pm 3.761\%$) and month three (28.060 ± 4.645) , as show in table (3).

Discussion

metabolic disorders and normal carbohydrate gestational intolerance test. They found that mean TT3 increased during the second trimester and then declined in the third trimester compared to the first trimester. This is in agreement to our study where TT3 level increased the Kumar *et al.* also showed mean TT4 level rose

in the second trimester and then decreased during the third trimester . Kumar et al. also found

that the mean of TSH levels rising progressively through the trimesters of pregnancy.^[8]

Reference:

1. Bourjeily, G., Chalhoub, M., phornphutkul, C., *et al.* Neonatal thyroid function: effect of a single exposure to iodinated contrast medium in utero. Radiology . rsna.org ; 2010. 256(3), 744_750.
2. Mansourian, A. R. Thyroid function tests during first-trimester of pregnancy: A review of literature. Pakistan journal of biological sciences; 2010. 13(14), 664_673.
3. Pe'rez_Lo'pez F. R. (2007). Iodine and thyroid hormone during pregnancy and postpartum. Gynecological endocrinology, 22 (5), 1_15.
4. Shah MS, Davies TF, Stagnaro-Green A. The thyroid during pregnancy: a physiological and pathological stress test. Minerva Endocrinol. 2003; 28: 233-45.
5. Alexander EK, Marqusee E, Lawrence J, *et al.* Timing and magnitude of increases in levothyroxine requirements during pregnancy in women with hypothyroidism. N Engl J Med. 2004; 351: 241-9
6. Brent GA. The debate over thyroid-function screening in pregnancy. New Eng J Med. 2012; 366: 562–563.
7. Rich-Edwards JW, Fraser A, Lawlor DA, Catov JM. Pregnancy characteristics

and women's future cardiovascular health: an underused opportunity to improve women's health? *Epidemiol Rev.* 2014; 36: 57–70.

8. Kumar A, Gupta N, Nath T, Sharma JB, Sharma S. Thyroid function tests in pregnancy. *Indian J MedSci* 2003; 57: 252-8.

Table (1) the mean and standard deviation of thyroid hormone

Parameters	Month 1	Month 2	Month 3	P-value
T3	1.626 ± 0.325	2.187 ± 0.572	2.581 ± 0.618	0.001
T4	140 ± 34.81	121 ± 32.54	97.77 ± 18.58	0.001
TSH	1.127 ± 0.734	1.265 ± 0.542	1.266 ± 0.624	NS

Table (2) The mean & SD of lipid profile

Parameters	Month 1	Month 2	Month 3	P-value
Cholesterol (mg/dl)	198.67 ± 36.47	209 ± 29.04	193.73 ± 26.55	NS
Triglyceride (mg/dl)	152.40 ± 40.45	170.63 ± 35.12	168.93 ± 32.75	0.052
HDL mg/dl	59.65 ± 11.78	64.16 ± 14.11	54.26 ± 13.34	0.017
LDL mg/dl	107.66 ± 25.59	108.37 ± 25.32	104.97 ± 26.85	NS
VLDL mg/dl	30.77 ± 7.91	34.12 ± 7.02	34.68 ± 8.48	NS

Table (3) the mean and standard deviation of Hemoglobin and pack cell volume (PCV) in the 1st, 2nd and 3rd month of pregnancy.

Parameters	Month 1	Month 2	Month 3	P- value
HB g/dl	10.123 ± 1.040	9.403 ± 1.144	10.727 ± 1.562	0.001
PCV %	33.553 ± 3.431	31.230 ± 3.761	28.060 ± 4.645	0.001

The use of Interleukin -10 as a biomarker for diagnosis of viral hepatitis type C Infections and related liver function in beta-thalassemic major patients.

Sarah M. Mahmoud, Assis prof. Dr. Zainb ER. Abass , Assis. Prof. Dr. Nihad Abdulhussain Jafar.

Dept. of medical microbiology, College of Medicine, Tikrit University.

E-mail Sarah1992@yahoo.com

Abstract

Introduction; IL-10 is an important cytokine in the pathogenesis of both infectious and inflammatory processes. The central and necessary role of IL- 10 in protecting against severe or inflammatory pathology has been clearly shown in models of experimental infection with intracellular pathogens using IL-10 genetically deficient mice. IL-10 is a multifunctional cytokine with potent immunoregulatory and anti-inflammatory properties. It prevents the release and function of a number of proinflammatory cytokines. It has been postulated that inadequate levels of IL-10 can determine long-term escape of pathogens from immune control and give rise to persistent infections. The **aim** of the study is to use of Interleukin -10 as a biomarker for diagnosis of viral hepatitis type C Infections and its relation to liver enzymes in thalassemia patients with viral hepatitis. **Patients and methods:** A cross sectional study was done on thalassemia patients in gastrointestinal center – Medical city directory in Baghdad from the beginning of March to the end of August 2017. A total of 80 subjects were participated in the present study, (45 thalassemia patients without hepatitis and 35 patients with Thalassemia who receive regular blood transfusion and diagnosed having viral hepatitis type C and were participated in the study. liver enzymes, and IL-10. Alanine transaminase (ALT), and aspartate transaminase (AST) were measured according to standard procedures. **Result;** there is significant increase in the concentration of IL-10 in the serum of HCV positive patients as compare with control patients. Also, there were significant increase in serum liver enzymes (ALT and AST and ALP), in patients with positive HCV, as compare to control with those with non-viral thalassemia hepatitis.

Key words; HCV, Liver enzymes, IL-10, thalassemia patients.

استعمال الإنترلوكين -10 كعلامة بايولوجية لتشخيص التهاب الكبد الفيروسي و ما يتعلق بها من نشاط انزيمات الكبد لدى مرضى الثلاثيميا نوع بيتا الكبرى المصابين بالتهاب الكبد الفيروسي.

سارة موسى محمود، ا.م.د. زينب ارزيج عباس أ.م.د. نهاد عبد الحسين جعفر.
قسم الأحياء المجهرية الطبية، كلية الطب، جامعة تكريت.

الخلاصة:

الانترلوكين -10 هو سيتوكين متعدد الوظائف منضم للمناعة قوي وله خصائص مضادة للالتهابات. ويمنع تحرر و الإفراج عن وظيفة عدد من السيتوكينات المضادة للالتهابات. وقد افترض أن مستويات غير كافية من إيل-10 يمكن أن تحدد الهروب على المدى الطويل من مسببات الأمراض من السيطرة المناعية وتؤدي إلى الإصابات المستمرة. **الهدف** من الدراسة هو تحديد تركيز الانترلوكين -10 وعلاقته بإنزيمات الكبد في مرضى الثلاثيميا المصابين بالتهاب الكبد الفيروسي الوبائي. **المرضى وطرق العمل** : دراسة مقطعية اجريت لمرضى الثلاثيميا المحالين الى مركز الجهاز الهضمي و امراض الكبد- دائرة مدينة الطب في بغداد. بدأت الدراسة من بداية مارس وحتى نهاية أغسطس 2017. و شارك في الدراسة 80 شخصا، (45 مريضا بالثلاثيميا بدون التهاب الكبد و 35 مريضا مصابا بالثلاثيميا مع التهاب الكبد الفيوسي نوع سي. وقد تم قياس انزيمات الكبد و الانترلوكين -10. **النتائج**: هناك زيادة كبيرة في تركيز الانترلوكين -10 في مصل مرضى التهاب الكبد الفيروسي نوع سي مقارنة مع مرضى السيطرة. كذلك هنالك زيادة معنوية لمستوى انزيمات الكبد في المرضى الذين يعانون مرضى التهاب الكبد الفيروسي نوع سي مقارنة مع السيطرة الذين لا يعانون من التهاب الكبد الفيروسي.

الكلمات المفتاحية: الانترلوكين -10، إنزيمات الكبد، مرضى الثلاثيميا

Introduction

In the United States, viral hepatitis is most commonly caused by hepatitis A virus (HAV), hepatitis B virus (HBV), and hepatitis C virus (HCV). These three viruses can all result in acute disease with symptoms of nausea, abdominal pain, fatigue, malaise, and jaundice. Furthermore, chronic hepatitis carriers remain infectious and may transmit the disease for many years.^(1,2)

HCV can be transmitted parenterally, perinatally, and sexually. Transmission occurs by percutaneous exposure to infected blood and plasma. The virus is transmitted most reliably through transfusion of infected blood or blood products, transplantation of organs from infected donors, and sharing of contaminated needles among IV drug users,⁽³⁾

Hepatitis is an infection of the liver caused by several viruses,

the most common of which are Hepatitis A, B and C. Both Hepatitis B Virus (HBV) and Hepatitis C Virus (HCV) spread mainly through contaminated blood, blood products, sexual contact and contaminated needles,^(1,4)

Interleukin (IL)-10 is a member of the IL-10 cytokine family and one of the most crucial suppressors and regulators of the immune system.

IL-10 and other members of the IL-10-like family have been shown to confer hepatoprotection^(2,3). IL-10 family cytokines are categorized into three subgroups based primarily on their biological functions. The first group contains only IL-10 itself which mainly represses excessive inflammatory responses. The second group, namely IL-20 subfamily cytokines, is composed of IL-19, IL-20, IL-22, IL-24, and IL-26^(4,5). IL-10, protects epithelial cells from invasion by extracellular pathogens such as

bacteria and yeast. Also, they enhance tissue remodeling and wound-healing activities, which help to maintain tissue integrity and restore homeostasis of epithelial layers during infection and inflammatory responses, ⁽⁶⁾.

Finally, the last group is the type III IFN group (or IFN λ s), which contains cytokines IL-28A, IL-28B, and IL-29 (7). IL-10 is a multifunctional cytokine with potent immunoregulatory and anti-inflammatory properties. It prevents the release and function of a number of proinflammatory cytokines ⁽⁸⁾.

It has been postulated that inadequate levels of IL-10 can determine long-term escape of pathogens from immune control and give rise to persistent infections ⁽⁹⁾. Therefore, the physiological role of IL-10 during infectious diseases is likely to reduce tissue damage resulting from the unfavorable and excessive effects of inflammation. However, an

inappropriate production of IL-10 during a virulent infection may compromise the effectiveness of the immune system, allowing fulminant or persistent infection ^(3,4).

Hepatitis is an infection of the liver caused by several viruses. The most common were Hepatitis A, B and C. Both HBV and Hepatitis C Virus (HCV) spread mainly by contaminated blood, blood products, sexual contact and contaminated needles, ⁽¹⁰⁾.

Hepatitis C virus (HCV) is one of the most important etiologic agents of posttransfusional hepatitis and a common cause of chronic hepatitis, cirrhosis and hepatocarcinoma, ^(10, 11).

Approximately, two billion people in the world have been infected by Hepatitis B virus (HBV), 350 million of whom are chronic carriers of the virus [1,2]. Worldwide HBV isolates have been classified into eight genotypes: A, B, C, D, E, F, G and H. The eight genotypes have

a characteristic geographical distribution, ⁽¹²⁾. Several studies have revealed the association of HBV genotypes with the severity of chronic liver disease, but the results are not consistent, ⁽¹²⁻¹³⁾.

The **aim** of the study is to evaluate the relation between of some biochemical markers in viral hepatitis C patients namely AST, ALT, alkaline phosphatase.

Subjects and methods

A cross sectional study was done in gastrointestinal center – Medical city directory on Thalassemia patients in Baghdad from the beginning of March to the end of August 2017. One hundred and forty patients referred to gastroenterology center (GIT) in medical city in Baghdad for further investigation for detection of viral hepatitis and other liver diseases.

Only eighty patients with Beta Thalassemia patients were

completed the whole investigation and participated in the study. 45 neo diagnosed and untreated thalassemia patients affected by HCV-related chronic hepatitis.

A total of 80 subjects were participated in the present study, (35 thalassemia patients without viral hepatitis and 45 thalassemia patients who receive regular blood transfusion and diagnosed having viral hepatitis were participated in the study.

An informed written consent was obtained from every subject before taking blood sample.

Excluded Criteria;

Patients with liver diseases other than HCV, or other medical diseases such as; hypertension, diabetes mellitus, endocrinal disorders or neurological diseases, autoimmune diseases, alcohol abuse, and drug induced

liver injury were excluded. In addition, patients with evidence of other chronic or acute infective processes (altered white blood cells count, temperature, urinary tract infection, airway infections) were excluded. Or patients receiving antiviral drugs were also, excluded from this study.

Diagnosis of patients was based on clinical (medical history, physical examination), instrumental (ultrasonography), and laboratory investigations (serum HCV antibodies, HCV-RNA and liver function tests) data.

Age and body weight was recorded. Also, about 5 ml of venous blood was drawn from all subjects. The blood lifted to clotted then centrifuged to separate the serum. The separated serum kept in deep freezing, until collection of all

samples to be used in measurement of liver enzymes, and IL-10. Alanine transaminase (ALT= SGPT), and aspartate transaminase (AST= SGOT) were measured according to standard procedures,⁽¹⁴⁾.

The circulating IL-10 levels were determined using a quantitative sandwich ELISA according to the manufacturer's instructions (R &D systems, Germany). ELISA plate wells were coated with 100 µl/well of anti-human IL-10 capture antibody in coating buffer and incubated overnight at 4°C. After incubation, excess coating buffer was discarded and wells blocked with 100 µl/well of blocking buffer (1% BSA in PBS) followed by incubation at 37°C for 1 h. Plates were washed 3 times in washing buffer (0.05% tween-20 in PBS), 100 µl of plasma samples and IL-10 standards diluted in buffer were added to appropriate wells, and

incubation at 37°C for 2 h followed. Plates were washed as before and detector biotinylated antibody (100 µl) added to each well followed by incubation at 37°C for 1 h, then washed as before. Streptavidin-HRP (Horse-Radish Peroxidase) conjugate (100 µl) was added to each well followed by incubation of plates at 37°C for 1 h, and washing as before. Substrate solution, 100 µl was added to each well and plates incubated at room temperature for 15 minutes for color development. Stop solution (50 µl) was added to each well and plates were read at 450 nm, ⁽¹⁵⁾.

Detection of viral markers:-

1-ELISA for detection of hepatitis B surface antigen (HBsAg), also ELISA was used for detection of

antibodies for HCV (screening test, ^(16,17).

SPSS was used for **statistical** analysis was used. All data were presented as Mean and Slandered deviation (SD). Unpaired student T test was used to compare between means of variables. P value less than 0.05 or 0.01 was used as significant value.

Results

Thalassemia Patients distributed into two groups;

Group 1 consist of 45 thalassemia patients without liver hepatitis as control group, and 35 thalassemia patients diagnosed as having viral hepatitis type c (patients with positive HCV).

Table 1 The age and body weight of all patients'

Parameters	Control (45)	HCV patients (35 patients)
Age (years)	30.14 ± 9.2	22.3 ± 6.5
Body weight (KG)	7.8 ± 54.5	46.9 ± 6.6
IL-10 (pg./ml)	8.74 ± 2.5	33.62 ± 7.3

In **table 1** , there is significant increase in the concentration of IL-10 in HCV patients (33.62 ± 7.3) as compare with control patients (8.74 ± 2.5).

In addition, by comparing the mean level of liver enzymes (ALT and AST), ALP, in patients with +ve Anti-HCV as compare to control with those with non-viral hepatitis. (**Table 2**).

Table 2 showed a significant increase in AST enzyme activity (GOT) in the thalassemia patients suffering viral hepatitis (HCV=47.3 ± 6.54 UI/L) as compare with thalassemia

patients without viral hepatitis, (23.6 ± 3.4 UI/L).

Moreover, there is significant increase in ALT enzyme activity (GPT) in the thalassemia patients suffering viral hepatitis (HCV= 70.56 ± 8.2 UI/L) as compare with thalassemia patients without viral hepatitis, (24.6 ± 2.15 UI/L).

Also, there is significant increase in ALP activity in the thalassemia patients suffering viral hepatitis (HCV= 224.6 ± 61.1 UI/L) as compare with thalassemia patients without viral hepatitis, (54.43 ± 4.4 UI/L).

Furthermore, there is significant increase in total bilirubin concentration in the thalassemia patients suffering viral hepatitis (HCV=2.68 ± 0.31mg/dl) as compare with thalassemia patients without viral hepatitis, (0.51 ± 0.09 mg/dl).

Table 2 Show the concentration of GOT, GPT, ALP and total bilirubin in thalassemia patients

Parameters	Control (45)	HCV patients (35 patients)	P value
AST (SGOT) (UI/I)	23.6 ± 3.4	47.3 ± 6.54	0.05
ALT (SGPT) (UI/I)	24.6 ± 2.15	70.56 ± 8.2	0.01
ALP (UI/I)	54.43 ± 4.4	224.6 ± 61.1	0.01
Total bilirubin (mg/dl)	0.51 ± 0.09	2.68 ± 0.31	0.05

Forty percent (40% of thalassemia patients suffered from jaundice and 43 % had thalassemia features. All patients were on regular blood transfusion with a mean frequency of 12.94 ± 4.31 times per year.

There was a significant decrease in the frequency of blood transfusion per year in patients who underwent splenectomy, compared to the pre-splenectomy period (P ≤ 0.05).

Discussion

In the present study, there was a significant increase in the concentration of IL-10 in the serum of HCV patients as compare with control patients.

Previous human studies have investigated this balance using neutralizing antibodies against IL-10 in vitro. HCV-specific T cell responses in chronically infected patients were restored by blocking IL-10, resulting in increased IFN- γ production, ^(18, 19).

Previous study was found in chronically HCV infected patients significant increase in IL-10 and IL-4, and they suggested that Th2 response during chronic HCV infection and this finding is concordant with the present study, ^(19, 20).

The significant increase in the concentration of IL-10 in the

serum of viral hepatitis patients of the present study (HCV patients), may be these patients have a chronic state of liver damage by the virus. This result agree with previous study which done HCV patients who found there were significant increase I the concentration of IL-10 and IL-18 in the serum of chronic hepatitis C patients, ⁽²¹⁾.

In study done in Baghdad by Mahmood (2005), who found a significant increase in the mean of levels of serum IL-6, IL-10, IL-8, and TNF- α and in contrast, a significant reduction in the IFN- γ levels in hepatitis patients with maintenance haemodialysis therapy in comparison to healthy control group, ⁽²²⁾.

These results indicates the predominance of Th2 cytokine which promote the persistency of virus, also HCV core and NS3 induced production of the anti-

inflammatory cytokines, IL-10, ^(23, 24).

IL-10 by itself and through cooperation with Th1 cytokines (such as IL-12) also regulates Th2 responses to prevent the overproduction of IL-4, IL-5 and IL-13, cytokines that can lead to severe fibrosis in, for example hepatitis C virus, ^(25, 26).

In the present study, In Thalassemia patients, there were an increase in serum concentrations of Alanine transaminase (ALT) and Aspartate transaminase (AST), and ALP in HCV positive patients as compare with control patients.

Hepatitis virus C infection is the main risk factor for liver injury in transfusion-dependent thalasseemics, ⁽²⁷⁾.

Interrelationship between iron overload, HCV infection and liver injury is still controversial.

Multicenter cross-sectional studies have reported that the development and the severity of liver injury are strongly related to the extent of liver iron overload and to the presence of chronic HCV infection ⁽²⁸⁾.

Dimitrios *et al*, (2013), on the other hand suggested that in the late stages of liver disease in BTM patients, iron overload may be the critical determinant, since fibrosis is related to the minimal haemosiderosis, independently of HCV history, ⁽²⁹⁾.

In present study, anti-HCV positive patients had higher mean serum ALT, AST and ALP levels than the negative group, and the same finding was true for total bilirubin in HCV positive patients.

A study done by Ocak *et al.*, (2006), found that the HCV positive patients had a significantly higher increase in

the activity of serum ALT level than anti-HCV-negative patients, Ameli *et al.*, (2008), found that serum iron was significantly higher in anti-HCV positive patients compared to the negative group, ⁽³¹⁾.

A previous pilot studies had suggested that IL-10 was well tolerated, normalized serum alanine aminotransferase (ALT), decreased hepatic inflammation and reduced liver fibrosis in patients with chronic hepatitis C who had not responded to previous IFN-based therapy. These data suggested that IL- 10 has an important role in chronic inflammation and fibrogenesis in HCV and that IL-10 might be used in the treatment of chronic hepatitis C and other chronic liver diseases, ^(26, 32).

So in the present study, data suggest that IL-10 can be used as a non-invasive marker for

⁽³⁰⁾.

detection of the chronicity and severity of liver inflammation in chronic hepatitis C.

Conclusions

1-Threre is significant increase in the concentration of IL-10 in the serum of patients of HCV.

2- There is significant increase in liver enzymes activities in patients with viral hepatitis.

3- From the present result, it can be concluded that there is a relation between level of IL-10 and liver function tests and it could be used as a biomarker for the infectivity with HCV .

Recommendations.

1. Measurement of the concentrations of IL-6, IL-12 and TNF In the sera of the positive HBV and HCV patients.

2. Study the effect of splenectomy on outcome on the concentration of interleukin in viral hepatitis.

3. Extend the study on all types of viral hepatitis.

References.

1-Cosimo Marcello Bruno,^a Maria Valenti,^a Gaetano Bertino,^a Annalisa Ardiri, *et al.* Relationship between circulating interleukin-10 and histological features in patients with chronic C hepatitis. *Ann Saudi Med.* 2011 Jul-Aug; 31(4): 360–364.

2. Mizukoshi E, Eisenbach C, Edlin BR, Newton KP, Raghuraman S, Weiler-Normann C. *et al.* Hepatitis C virus (HCV)-specific immune responses of long-term injection drug users frequently exposed to HCV. *J. of Infectious Dis.* 2008; 198(2): 203–12.

3. Pellicano R, Mladenova I, Dimitrova M, Bruno CM, Sciacca C, Rizzetto M. The epidemiology of

hepatitis C virus infection. An update for clinicians. *Minerva Gastroenterol Dietol.* 2004; 50: 1–7.

4. Nelson PK, Mathers BM, Cowie B, *et al.* Global epidemiology of hepatitis B and hepatitis C in people who inject drugs: results of systematic reviews. *Lancet.* 2011 Aug 13. 378 (9791):571-83.

5- Brooks DG, Trifilo MJ, Edelmann KH, Teyton L, McGavern DB and Oldstone MB. Interleukin-10 determines viral clearance or persistence in vivo. *Nat. Med.* 2006; 12(11): 1301–1309.

6. Nelson DR, Tu Z, Soldevila-Pico C, Abdelmalek M, Zhu H, Xu YL, *et al.* Long-term interleukin 10 therapy in chronic hepatitis C patients has a proviral and anti-inflammatory effect. *Hepatology.* 2003;38:859–68.

7. Cooper S, Erickson AL, Adams EJ, Kansopon J, Weiner AJ, Chien DY, Houghton M, *et al.* Analysis of a successful immune response

- against hepatitis C. Immunity. 1999;10: 439-449.
8. Ejrnaes M, Filippi CM, Martinic MM, Ling EM, Togher LM, Crotty S, *et al.* Resolution of a chronic viral infection after interleukin-10 receptor blockade. *J Exp Med.* 2006;203:2461–72.
9. Lio D, Caruso C, Di Stefano R, Colonna Romano G, Ferraro D, Scola L, *et al.*, (2003): IL-10 and TNF-alpha polymorphisms and the recovery from HCV infection. *Hum Immunol*; 64(7):674–680.
10. Kuo, G., Choo, Q., Alter, H. *et al.*, An assay for circulating antibodies to a major etiologic virus of human non-A, non-B hepatitis. *Science* 1989, 244 (4902): 362–4.
11. Rowan, AG., Fletcher, J.M., Ryan E.J. *et al.* Hepatitis C virus-specific Th17 cells are suppressed by virus-induced TGFbeta. *J. Immunol.* 2008, 181: 4485–94.
- 12 - Schaefer S. Hepatitis B virus: significance of genotypes. *J Viral Hepat.* 2005; 12: 111-124.
13. Kao JH. Hepatitis B viral genotypes: clinical relevance and molecular characteristics. *J Gastroenterol Hepatol* 2002; 17: 643-650
14. Bergmeyer HJ. Principles of enzymatic analysis. Verlag. Chemi (Bergmeyer HU., Ed). 1978: 35-40.
15. San Diego: Academic Press. Deshpande SS (1996): Antigen-Antibody Reactions. In text, Enzyme Immunoassays From Concept to Product Development by Deshpande SS, Chapter (2), 1st edition, 52-71, International Thomson Publishing.
16. Giles, RE; Burgess, C.; Gimore, M., Perry., KR. An evaluation of the bioelisa HBsAG colour assay. Medical Device agency evaluation report. MDA. 1999; 99: 68-69.
17. Uyttendale, S., Claeys, H., Mertens, W. Evaluation of 3rd generation screening and confirmatory assays for HCV antibodies. *Vox Sang.* 1994; 66: 122- 129.

18. Ji J, Sahu GK, Braciale VL, Cloyd MW. HIV-1 induces IL-10 production in human monocytes via a CD4-independent pathway. *Int Immunol.* Jun 1; 2005 17(6):729–36.
19. Flynn, KJ, Gregory J Dore, Margaret Hellard, Barbara Yeung. Early IL-10 predominant responses are associated with progression to chronic hepatitis C virus infection in injecting drug users. *J Viral Hepat.* 2011 August ; 18(8): 549–561.
20. Jankovic D, Trinchieri G. IL-10 or not IL-10: that is the question. *Nature Immunology.* 2007; 8(12):1281–3.
21. Jia HY, DU, J., Zhu SH. The roles of serum IL-18, IL-10 and TNF- α in patients with chronic hepatitis C. *Hepatobil and Pancreat Dis Int. J.* 2002; 1(3): 378-82.
22. Mahmood, A.E. (2005). Study of some immunogenetic aspects of viral hepatitis C patients of haemodialysis units. Ph.D. Thesis, College of Sciences, Baghdad University.
23. Al-Khozai, Z. M. Study some epidemiological and immunological aspects on Hepatitis B and C in Al-Qadisiyia province. Ph.D. Thesis, College of science, Baghdad university. 2006.
24. Sabat R, Gruetz G, Warszawska K, Kirsch S, Witte E, Wolk K and Geginat J. Biology of interleukin-10. *Cytokine Growth Factor Rev.* 2010; 21(5): 331–44.
25. Suvas S, Azkur AK, Kim BS, Kumaraguru U and Rouse BT. CD4₊CD25₊ regulatory T cells control the severity of viral immune inflammatory lesions. *J. Immunol.* 2004; 172(7): 4123–4132.
26. Nelson DR, Lauwers GY, Lau JY and Davis GL. Interleukin 10 treatment reduces fibrosis in patients with chronic hepatitis C: a pilot trial of interferon non-responders. *Gastroenterology.* 2000; 118(4): 655–660.

27. Di Marco V, Capra M, Gagliardotto F, Borsellino Z, *et al.* Liver disease in chelated transfusion-dependent thalassemics: the role of iron overload and chronic hepatitis C. *Haematologica*. 2008; 93(8): 1243–1246.
28. Li CK, Chik K, Lam C, To K, *et al.* Liver disease in transfusion dependent thalassemia major. *Arch Dis Child*. 2002; 86: 344–7.
29. Dimitrios K, Nikolaos J Tsagarakis, Evangelia F, Efthimios D, *et al.* Liver disease in adult transfusion -dependent beta-thalassaemic patients: investigating the role of iron overload and chronic HCV infection. *Liver International*. 2013;33(3):420–427.
30. Ocak S, Kaya H, Cetin M, Gali E, *et al.* Seroprevalence of hepatitis B and hepatitis C in patients with thalassemia and sickle cell anemia in a long-term follow-up. *Arch Med Res*. 2006; 37(7):895–8.
31. Ameli M, Besharati S, Nemati K, Zamani F. Relationship between elevated liver enzyme with iron overload and viral hepatitis in thalassemia major patients in Northern Iran. *Saudi Med J*. 2008; 29(11): 1611–5.
32. Bruno CM, Valenti M, Bertino G, Ardiri A, Amoroso A, Consolo M. *et al.* Relationship between circulating interleukin-10 and histological features in patients with chronic C hepatitis. *Ann Saudi Med*. 2011; 31(4): 360-4.

A PHOTOELASTIC STUDY OF STRESSES IN THE FEMURE

Dr. Jamal A. Hassan,* Dr. Sadiq J. Abass,* Eng. Zainab majid,**

* College of Engineering, Al-Nahrain University

** Electrical Engineering Technical College , Middle Technical University

E-mail: engzainabmajid@gmail.com

Abstract

The femur bone is the longest bone in the human body. The proximal end of femur contacted at hip joint and in the distal end contacted at knee joint. Femur bone affected with muscles attached with it and with contacts at joints and weight bearing of body, all of these applied loads on femur and stresses effect result. In this study we will discuss stress analysis on the femur bone when a compressive load applied on the head of the bone at the contact region with acetabulum by using the photo elasticity transmission technique. The normal femur bone scaling to prototype according to material properties an polariscope load applied. The effect of load on the prototype with passage of polarized light through it give fringes pattern which Interpretation to show the stress at head of femur and at the shaft of femur. The study was done in Baghdad during 2016 from Al-Nahrain University.

Keyword: Photoelasticity, femur bone and stress analysis.

دراسة الاجهادات على عظم الفخذ

الخلاصة

عظم الفخذ هو أطول عظمة في جسم الإنسان. النهاية القريبه من عظم الفخذ تتصل بمفصل الورك و النهاية البعيدة تتصل بمفصل الركبة . عظم الفخذ تتأثر بالعضلات المتصلة به وتتأثر باتصالاته مع المفاصل و وزن الجسم الذي تحمله, كل هذه الأحمال المسلطه على عظم الفخذ والاجهادات تؤثر على النتائج . في هذه الدراسة سوف نناقش تحليل الاجهادات على عظم الفخذ عند تسليط قوة الضغط على رأس العظم في منطقة اتصال مع العظم الحقي باستخدام تقنية المستقطب الضوئي الناقل. عظم الفخذ الطبيعيه تدرج الى نموذج بقياسات معينه وفقا لخصائص المادة المستخدمه والاحمال التي تسلط من المستقطب الضوئي المستخدم. تأثير الاحمال على نموذج العظم مع مرور الضوء المستقطب من خلاله يعطي ترتيب هديبي يفسر لكي يظهر الاجهادات على رأس عظم الفخذ وعلى رمح العظم

الكلمات المفتاحية: المرونة الضوئية, عظم الفخذ , تحليل الشد

INTRODUCTION

Photoelastic stress analysis is a technique that provides us with full field stress distribution at any examined model. It is based on the property of some transparent double refraction materials (birefringence material) [1]. If these materials are subjected to an applied load the refractive index of material change and the magnitude of the change is different in two plane of principal stress. This result in light passing through stressed material at different speed according to applied load [2].

The hip is a ball-and-socket joint as shown in figure (1). The socket is formed by the acetabulum, which is part of the large pelvis bone. The ball is the femoral head, which is the upper end of the femur [3]. The femur head subjected to compressive load that applied from the pelvis at contact with acetabulum region. Qualitative analyses of the stress distribution of the trabecular femoral head of a human femur by photoelasticity are presented and find that the porous bone model makes the stresses. Reduced at the contact with surface of the femoral head joint. That because of maximum stress concentration is shifted from the surface to the interior of the bone, results from the damping of external forces and diffused them towards the interior of the bone tissue [4]. The state of stress of an intact femur was analyzed using a three-dimensional finite element model and strain gauges for experimental measurements .several modes of loading, the deflections and the principal and comparison stresses were determined and compared. The upper one third and the diaphysis of the femur are differently affected in their state of stress. [5]

Use of photoelastic models to interpret and demonstrate biomechanical principles. Isochromatic fringes show bone stresses distribution in the femur is explained with respect to iliotibial tract loading, and he uses two-dimensional models to illustrate bone remodeling theories. [6]

Model from catalin made to femur bone with compressive load applied on the bone .the arrangement

of stresses line markedly show the trabecular structure at longitudinal section of femur . The greater number of stresses line appears to be at medial side and shifted toward the line of mechanical axis of normal femur. [7]

In this work a qualitative analysis of the stress distribution of a cross section of the medial condyle of a human femur by photoelasticity is presented. A model of the cross section was obtained by plaster casting, carefully maintaining the internal architecture of the Porous bone. The fringe patterns observed in the porous bone model showed that the maximum stress concentration is shifted from the surface to the interior of the bone and diffused [8].

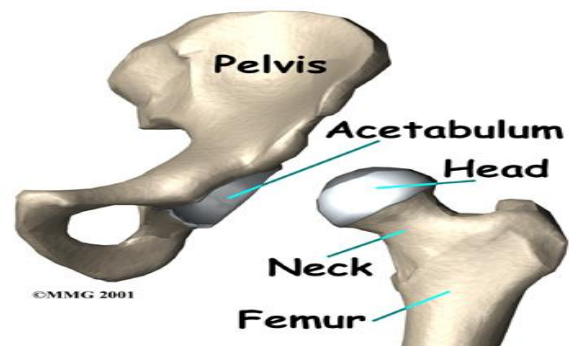


Fig.(1) Region of contact between femur head and acetabulum.

Aim of the study

In this study the photoelasticity used to find the stresses at femur bone of human body at hip joint. The stresses analyzed at different region in the femur bone and then compared with each other to find the higher stress which lead to fracture at some cases.

EXPERIMENTAL WORK

The first step on photoelasticity techniques calibration of material to find the material fringe values defined as number of fringes produced per unit load. Material fringe value used to accurately determine the stress distribution. The material fringe value depends on the type of birefringens material which used to make the

prototype. The calibration method used at this study by tensile specimen which have a specific dimensions depend on the thickness of material. The width of specimen w , the thickness h , and the load applied p , fringe order n , and the axial stress σ .

$$\text{So, } \sigma_1 = P/(wh) \text{ and } \sigma_2 = 0 \quad (1)$$

The birefringes material used at this study is the transparent polycarbonate. The load on tensile specimen increased gradually and order of fringes change with this increments as in figure(2). The material fringe value determined from equation (2).

$$P/(wh) = nf/h \quad \text{or} \quad f = P/(wn) \quad (2)$$

$$f = 25.523 / (3.8 * 1) = 6.7 \text{ N/mm fringes.}$$

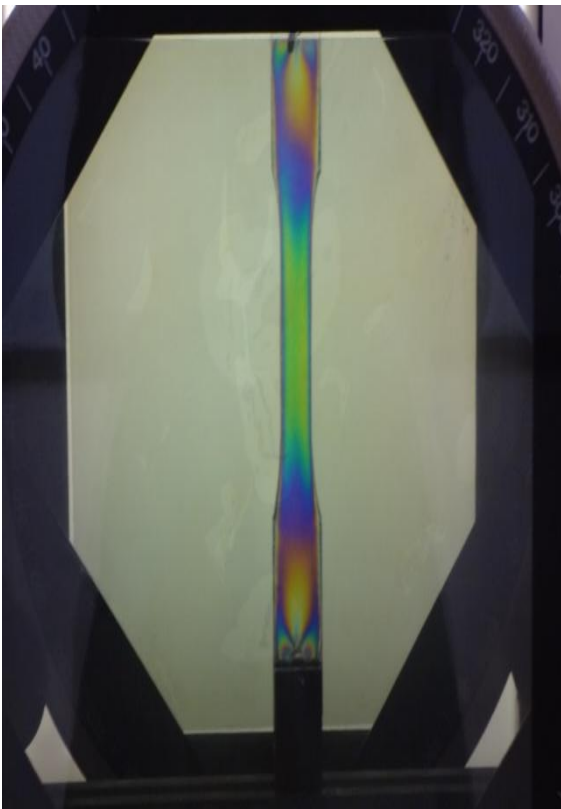


Fig.(2) Calibration of material by tensile specimen

After calibration the model of bone scaled to 2D prototype and the load applied on it founded as in figure(3). The prototype on polariscope with compressive load at 75degree on head of femur and

passage of polarized light give a fringe pattern to find the stress distribution at region of contact with acetabulum and stresses at the shaft of the bone as in figure(4).

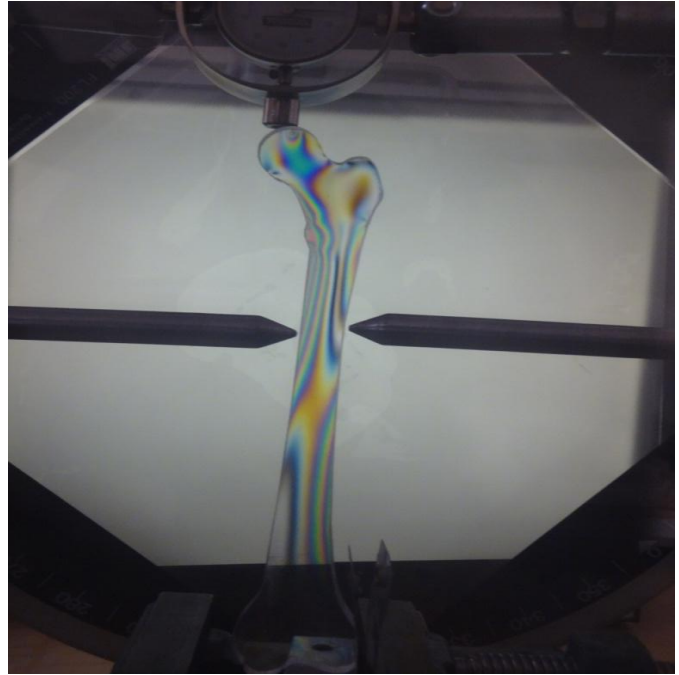


Fig.(3) Prototype of femur bone with applied load



Fig.(4) Fringes pattern on femur bone under load

The principal stress determined from fringe order appeared on the prototype with equation (3).

$$\sigma_1 - \sigma_2 = f \cdot n / h \quad (3)$$

h is the thickness of prototype.

Then find the stresses on the head of femur and shaft of femur with each load applied by mohrs circle as in figure(5).

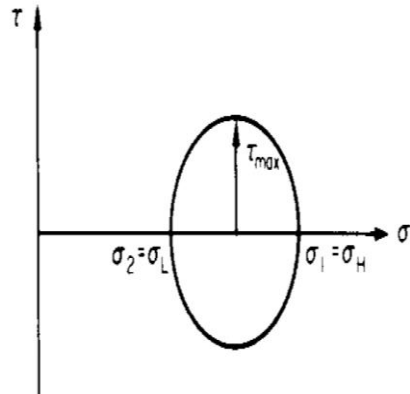


Fig. (5) Mohrs circle

Result:

The fringe order increase with the increasing of the load and find that the principal stresses and stresses in the femur head higher than the stress in the femur shaft as in table (1,2,3 and4).

Table 1: principal stresses on the femur head determined from fringe order

Load (N)	Fringe order(fringe)	Principal stresses on femur head(Mpa)
2.224	1	1.34
13.7322	2	2.68
17.9915	3	4.02
27.4646	4	5.36
31.7238	5	6.7
35.9830	6	8.04
40.24233	6	8.04
44.50159	7	9.32
48.76025	8	10.72
53.020111	9	12.06
57.2793	10	13.4
61.53862	10	13.4
70.5756	11	14.74

Table 2: principal stresses on the shaft of femur determined from fringe order.

Load (N)	Fringe order(fringe)	Principal stress on the shaft of bone(MPa)
2.224	0	0
13.7322	1	1.34
17.9915	1	1.34
27.4646	2	2.68
31.7238	2	2.68
35.9830	2	2.68
40.24233	3	4.02
44.50159	3	4.02
48.76025	3	4.02
53.020111	4	5.36
57.2793	4	5.36
61.53862	5	6.7
70.5756	6	8.04

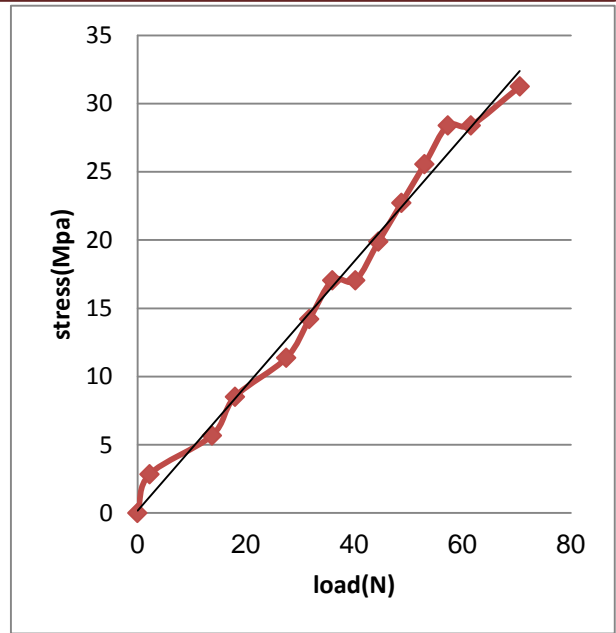


Fig. 6 Stress with load on head of femur

Table 4: stresses from Mohr circle on shaft of femur

Table3: stresses on the head of femur from Mohr circle.

Principal stresses on the head of femur bone (MPa)	Stress(MPa)
0	0
1.34	2.84
2.68	5.68
4.02	8.52
5.36	11.36
6.7	14.2
8.04	17.04
8.04	17.04
9.32	19.88
10.72	22.72
12.06	25.56
13.4	28.4
13.4	28.4
14.74	31.24

Principal stress on the shaft of bone(MPa)	Stresses(MPa)
0	0
1.34	2.84
1.34	2.84
2.68	5.68
2.68	5.68
2.68	5.68
4.02	8.52
4.02	8.52
4.02	8.52
5.36	11.36
5.36	11.36
6.7	14.2
8.04	17.04

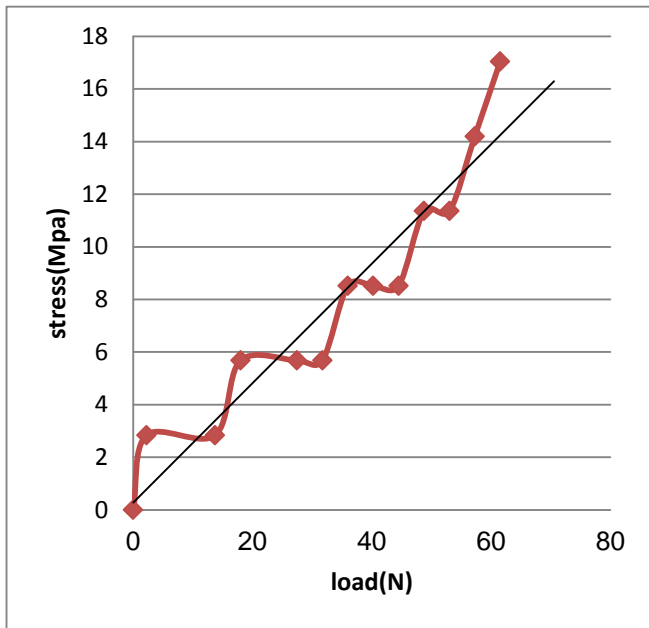


Fig. 7 Stresses with load on femur shaft

DISCUSSION

The fringe order on the head at contact more than the orders that reach at the shaft so , the stresses on the head of the bone higher than the stresses on the shaft of the bone .

Load applied directly from pelvis at contact region while the stresses on the shaft result from compression and decreased because of that the load not directly applied on it. So, with daily activity the hip joint may have arthritis or injury on the region of femur with hip contact or on the high stresses on the head of femur result from the load the femur neck that leads to hip replacement.

REFERENCES

[1] James F. Doyle and James W. Phillips, eds," **Manual on experimental stress analysis**"

[2] J. W. Dally and W. F. Riley, "**Experimental Stress Analysis**" (New York: McGraw-Hill, 1978)

[3] Gerard J. Tortoraand Mark T. Nielsen, "**principles of human anatomy**" , 12th Edition

[4] Rodríguez Lelis J.M., Marciano Vargas Treviño, Navarro Torres J., Arturo Abundez P, Sergio Reyes Galindo, and Dagoberto Vela Arvizo ,"**A qualitative stress analysis of a cross section of the trabecular bone tissue of the femoral head by photoelasticity**" Vol. XXVIII, Núm. 2 ,Diciembre 2007 ,pp 105 – 109

[5] A. Rohlmann, U. Mössner , G. Bergmann, R. Kölbl," **Finite-element-analysis and experimental investigation of stresses in a femur**".

[6] 8th Samuel Houghton Lecture," **Images from Waves – photoelasticmodellingofBones**" January 2002 .Page 209.

[7] HENRY MILCH." PHOTO-ELASTIC STUDIES OF BONE FORMS" J Bone Joint Surg Am. 1940;22:621-626.

[8] J.M. Rodríguez-Lelis , A. Abúndez-Pliego, Marciano Vargas-Treviño, J. Navarro-Torres, Dagoberto Vela-Arvizo, G. Piña-Piña," A Qualitative Stress Analysis of a Cross Section of the Trabecular Bone Tissue of a Distal Femur by Photoelasticity"

Sensors data encryption using TSFS Algorithm

Shatha Habeeb and Dr. Rehab F. Hassan

University of Technology, Computer Sciences Department

E-mail: shathahabeeb@yahoo.com

Abstract

Sensors data security has an increasing importance with the use of sensors in all kinds of real world applications, after being collected from sensors, huge amount of data will be stored in a database, with different types of analysis. It should be protected from all attack kinds considering sensor data as sensitive data. Several security algorithms are implemented to present database protection, and to have powerful protection, the sensitive data should be covered from the risk of being attacked and not stored as original text only, therefore, the key solution for protecting database is to encrypt it. This paper provides database encryption for data acquisition from sensor. TSFS (Transposition, Substitution, Folding, and Shifting) algorithm has been used with three strong and different keys matrices after two sub-steps for key generation using genetic algorithm and expansion by column shifting. By implementing the enhanced algorithm, an efficient and strong database security system has been achieved to data received from sensor.

Keywords: TSFS, Cryptographic, Key expansion, Database Security, Sensor Data Encryption.

تشفير بيانات اجهزة الاستشعار باستخدام خوارزمية TSFS

الجامعة التكنولوجية قسم علوم الحاسوب

الخلاصة: أمن بيانات أجهزة الاستشعار لها أهمية تتزايد مع استخدام أجهزة الاستشعار في جميع أنواع التطبيقات في العالم الحقيقي، بعد تجميعها من أجهزة الاستشعار، سيتم تخزين البيانات الضخمة في قاعدة بيانات. ينبغي حمايتها من جميع أنواع الهجمات و تعتبر بيانات الاستشعار بيانات حساسة. يتم تنفيذ العديد من خوارزميات الامنية لتوفير الحماية لقاعدة البيانات، ولها خصائص قوية في حماية البيانات، وينبغي حجب البيانات الحساسة من خطر التعرض للهجوم وليس تخزينها كنص أصلي فقط ، وبالتالي ، فإن الحل الرئيسي لقاعدة البيانات المحمية هو التشفير.

هذا البحث يقدم تشفير قاعدة البيانات المستلمة من أجهزة الاستشعار. وقد استخدمت خوارزمية TSFS مع ثلاثة مفاتيح قوية ومختلفة كما استخدمت المصفوفات لتسهيل التعامل مع هذه المفاتيح بعد ان تم الاستعانة الخوارزمية الجينية لتوليد المفاتيح الثلاثة ولاضافة قوة اكبر تم توسع عن طريق تحويل العمود. ومن خلال تنفيذ الخوارزمية المطورة، تم تحقيق نظام فعال وقوي لأمن قواعد البيانات للبيانات الواردة من أجهزة الاستشعار.

الكلمات المفتاحية: أمن بيانات, التشفير, خوارزمية TSFS, أجهزة الاستشعار

I. Introduction

The growing use of sensors in real world applications and linking these sensors to the Internet has its results obvious online on the Web, moreover, tens of devices can be communicating with each other in a real-time manner. Real world applications may connect and control several sensors and actuators with their data and services to be available at all times. [1]

The sensor can sense the physical world and convert it to electrical signals. There are many existing types of sensors that sense the environmental factors such as light power, temperature, audio waves, pictures, etc. [2] A number of sensor nodes (few tens to thousands) working simultaneously to observe a region to gain data about the environment.[3]

With data gained from sensors a database system can be build. The protection systems of database become critical, any damages or misusing will affect the sensitive data stored in that database and will also affect the entire system and the risk has been increased

with the increasing number of database developments.

For implementing database security systems, there are four techniques: DBMS, OS physical security systems and data encrypting. The security techniques are not completely acceptable solutions. A well-ordered light-weight encrypting techniques TSFS algorithm will be used for sensitive data only, an effective implementation of queries will afford and a fast response to the users. TSFS is the symmetric-key block algorithm, similar keys are used for data encrypting and decrypting and its power depends on the key length. [4]

II. Related work

Several schemes have more efficient and creative executions proposed for database security domain. An efficient light-weight database encryption techniques have been used, TSFS algorithm used with ordinary data and randomly generated key. [4] H. Al-Souly *et al*, used TSFS algorithm by spreading the data-set to separate characters, and by correcting shifting and substitution

operations, by supporting several modulo factors and four sixteen arrays correspondingly to avoid the inaccuracy that arises in the decryption steps [5].

Based on the Chinese Remainder theorem and using strong keys and sub-keys an implementation of encrypting the database structure in [3], a record encryption system for all the levels of columns and rows are implemented. Multilevel access control had been proposed in [6] to improve the security level.

A solution for confidentiality problem, a chip secured data access had been proposed in [7]. It is a quite effective and secure solution, however, still the cost is expensive and it is rather a complicated method.

III. TSFS Algorithm:

With 12 rounds, four types of conversions in TSFS algorithm: Substitution and transposition ciphers are considered the most significant essential techniques in building a new symmetric encryption algorithm. The advantage of this cipher is having the two aspects of security and cryptology, confusion and diffusion. TSFS uses the same sequence of these conversions for both encryption and decryption. Encryption algorithms are known as the ciphers and the opposite ciphers are the decryption algorithms. TSFS algorithms are a not Feistel ciphers, each conversion or set of conversions should be reversible. The keys have to be used in the reverse order also. Figure1 shows (illustrate) TSFS algorithm in general view. [4]

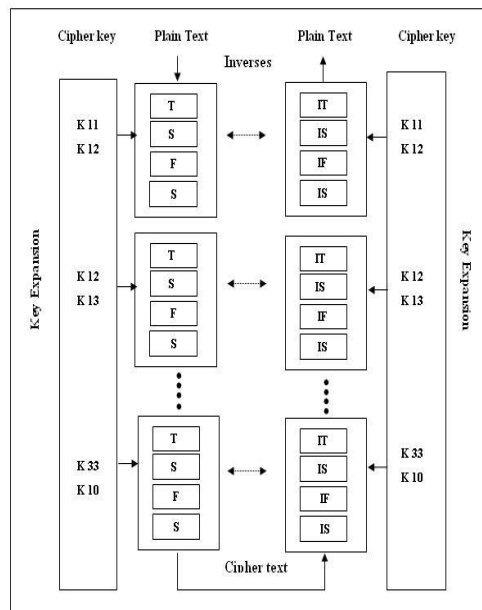


Figure 1: TSFS Algorithm

V. Proposed System

The proposed system collects data from the physical world by a set of sensors and stores it in a database. Then to secure the database by adapting the data in a form that cannot be stated by illegal people. The proposed system is an enhanced form of TSFS algorithms by using genetic algorithm to generate the key and extending it in a way to get strong key matrix. Besides adjusting its transposition and substitution steps, to avoid the error taking place through the decryption process. Experiment results demonstrate the power of the proposed system in the encryption of the sensitive data only.

To provide high security, the proposed system is a symmetric algorithm for database encryption with three keys after key expansion technique. For more security and effective system, these three keys had been expanded in twelve sub-keys by using the key expansion method.

1. Cryptographic Key:

Cryptography is often used in security environment to protect data that is sensitive, has a high value, or is susceptible to unauthorized disclosure or unnoticed modification through transmission or storage. It relies upon two basic components: a cryptographic algorithm (methodology) and a cryptographic key. [8]

1.1- Key Generation:

The proposed system generates three keys by using Genetic algorithm and with the help of random number generator to make the key complex. Key generation will go through a number of process and main criteria for key selection will be the fitness value of the population. [9]

Input: Threshold Number
Output: Key Matrix
<p>Process</p> <p>Generate population number random</p> <p>Do</p> <p>Step one</p> <p>Selection:</p> <ol style="list-style-type: none"> 1- To breed a new generation selected is a portion of the existing population. 2- Convert sample of the population into binary. <p>Step two</p> <p>Crossover: used to vary the programming of a chromosome or chromosomes from one generation to the next. It is analogous to reproduction and biological crossover, Crossover is a process of taking more than one parent solutions and producing a child solution from them.</p> <p>Step three </p> <p>Mutation: alters one or more gene values in a chromosome from its initial state</p> <p>Until Get all element of key matrix</p>

Algorithm 1: Key Generation

1.2- Key Expansion:

The proposed algorithm generates three keys to be used in 12 rounds. In each round, each key is expanded to several sub-keys. The extension operations for the keys are done by changing the column positions and by using add round key procedure. Here, to get these keys, an

arbitrary key generator have to be used only for getting the key values on the first step. Then the key is changed to numbers based on the sequence in the alphabets and stored in 4x4 matrix shape.

The following algorithm shows key extension:

Input Three keys of Array 4x4
Output 12 keys of Array
Process : Do Key I Expanded into key (i1,i2,i3,i4) For keyI1 - column 1 is not shifted, column 2 is shifted one position, column 3 is shifted two position column 4 is shifted three positions. For keyI2 - column 1 is shifted one position, column 2 is shifted 2 positions, column 3 is shifted three positions, column 4 not shifted. For keyI3 - column 1 is shifted two positions, column 2 is shifted three positions, column 3 is not shifted, column 4 is shifted one position. For keyI4 - column 1 is shifted three positions, column 2 is not shifted, column 3 is shifted one position, column 4 is shifted two positions. Until End keys

Algorithm 2: Key Expansion

Original Key Expansion to key I ,1	0	1	2	3
Original Key Expansion to key I ,2	1	2	3	0
Original Key Expansion to key I ,3	2	3	0	1
Original Key Expansion to key I ,4	3	0	1	2

Figure 1 Role of shift algorithm of three key

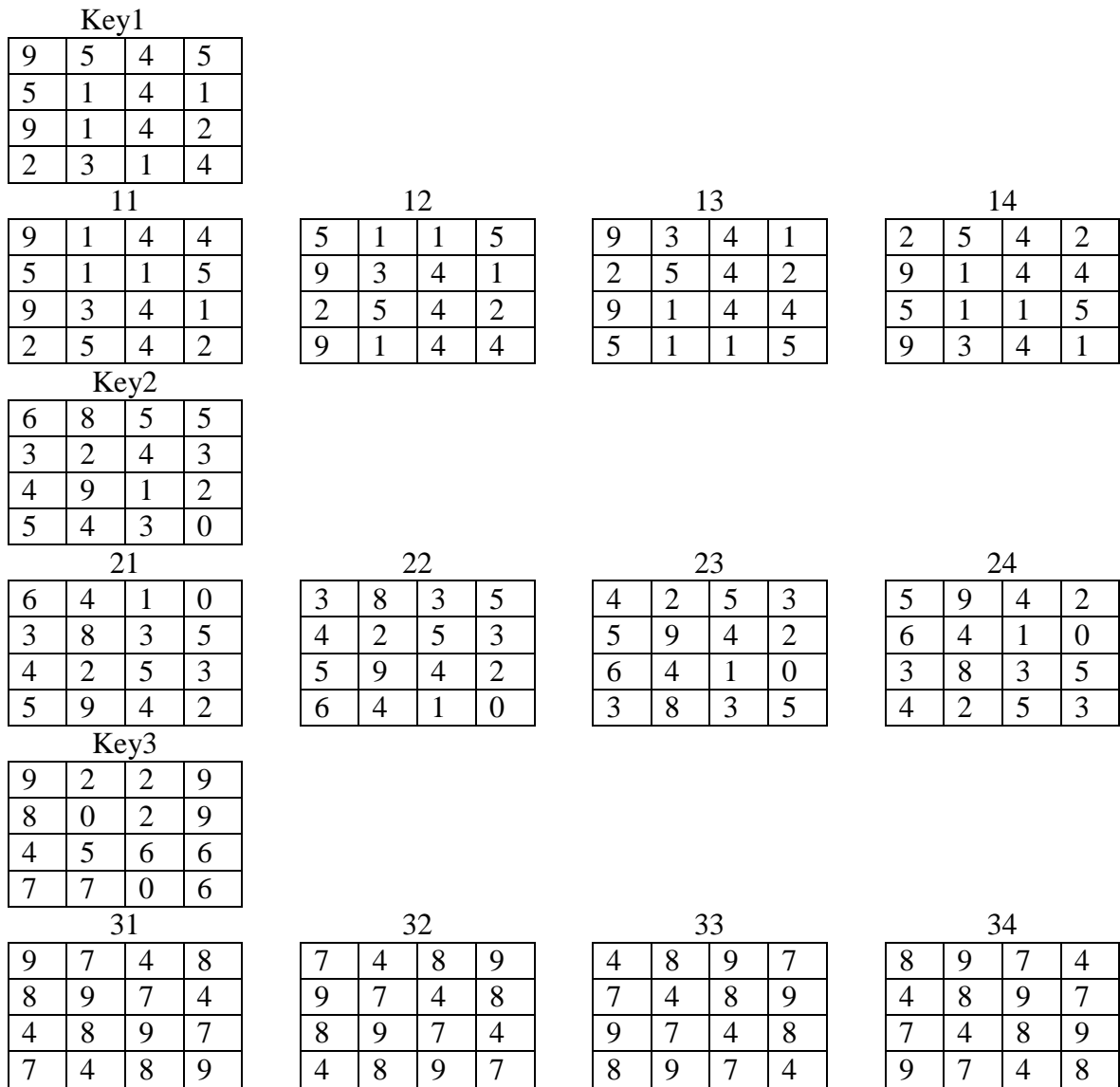


Figure.2 examples view key expansion process

2. Transposition

Transposition cipher is a significant type of traditional ciphers. It does not perform a replacement of one representation with another, alternatively modifies the position only. The symbol in the first position of the plain-text may

occur in different position of the cipher text. That means transposition ciphers rearranges symbols. TSFS algorithm uses *zigzag* diagonal transposition for storing data into 4 x 4 matrix forms. Figure 3 shows transposition procedure with example.

Where p is the plaintext, $key1$ and $key2$ represent the keys that should be in the same location as p , M is the size of modulo process. TSFS algorithm takes two values for M unlike the original TSFS algorithm which takes one value only. Substitution procedure illustrated in equation (1) has confusion if the data is collected of numeric digits and alphabetic

and M is equal to 26 for any digit, as exemplified in the next example. If plain data was 6, $key1=1$, $key2=7$, $M = 26$, then the result is 13. M in the proposed TSFS algorithm is equal to 26 if p represents alphabetic, and 10 if p equal to any numerical value. [5]

Decryption Equation (2) $D(E(x))$ can be written as follows:

$$D(E(x)) = (((E(x) - key2) \bmod M) / key1) \bmod M \quad (2)$$

Substitution procedure can be considered as poly-alphabetic or mono-alphabetic ciphers. [4]

3	7	9	0
4	F	0	0
S	D	0	8
A	8	4	2

→

17	9	14	9
18	J	5	6
C	k	8	11
L	14	12	8

Figure 4 Substitution

4. Folding

The next stage use folding procedure. Folding is considered as a transposition cipher, the matrix elements are folded vertically, horizontally, and diagonally.

The folding procedure mixes up the data from one location to other one. Figure 5 shows the result of folding procedure. [4,5]

17	9	14	9
18	J	5	6
C	k	8	11
L	14	12	8

→

8	14	12	L
6	11	K	18
8	5	J	C
9	9	14	17

Figure 5 Folding

Algorithm folding (Matrix data)**Input:** In_data is 4x4 matrix get from substitution technique.**Output:** data is data matrix after applying folding technique.

Matrix Out_data;

Out_data [0,0] = In_data [3,3];

Out_data [0,1] = In_data [3,1];

Out_data [0,2] = In_data [3,2];

Out_data [0,3] = In_data [3,0];

Out_data [1,0] = In_data [1,3];

Out_data [1,1] = In_data [2,2];

Out_data [1,2] = In_data [2,1];

Out_data [1,3] = In_data [1,0];

Out_data [2,0] = In_data [2,3];

Out_data [2,1] = In_data [1,2];

Out_data [2,2] = In_data [1,1];

Out_data [2,3] = In_data [2,0];

Out_data [3,0] = In_data [0,3];

Out_data [3,1] = In_data [0,1];

Out_data [3,2] = In_data [0,2];

Out_data [3,3] = In_data [0,0];

Return Out_data;

End folding**Algorithm 4 folding****5. Shifting**

The final stage of TSFS algorithms is shifting conversion, which offers an easy method for data encryption using a 16 element in array of numeric digits to replace the symbol with other one. Each array element contains a numeric representation of the data. Every digit must only appear once in each array element in any order. [4,11] In shifting procedure, within its array element, every element is

replaced in the data matrix by its location.[5]

Each array element contains 26 numeric digits from 0 to 25. For shifting decryption procedure, the location is given as an input considered on the position of the data, the data represents the plain text of the given cipher-text.

This process is illustrated in the following figure 6.

I/p	Array element	O/p
3	0 1 2 3 4 5 6 7 8 9 10.....22 23 24 25	3
17	1 2 3 4 5 6 7 8 9 10 11 23 24 25 0	16
7	2 3 4 5 6 7 8 9 10 11 12.....23 24 25 0 1	5
•	•	•
•	•	•
•	•	•
F	13 14 15 16 17 187 8 9 10 11 12	S
14	14 15 16 17 18 19 9 10 11 12 13	0
O	15 16 17 18 19 20 10 11 12 13 14	Z

Figure.6 Shifting

All above encryption procedures form the first round only from TSFS algorithm. And output of the first round is the input to the second round, output of the second round is the input to the third round, and so on. The round is repeated 12 times, the cipher-text of the given plain text is the last round output and that cipher-text is stored in the database. Decryption Algorithm is the opposite procedure of the Encryption. [4,10]

VI. Conclusion

The exchanging and storing of sensor data between networks is increasing rapidly around the world. Attacks at that data raise the danger of data discovery. Many organizations must deal with regulation and legislation on data confidentiality. In this environment, the proposed security development contains an

approach for protecting sensitive data against any attacker. The experimental result shows that TSFS algorithm with key generated by using genetic algorithm profitably important cipher, in addition to alphanumeric data. Improved performance approaches without compromising query processing time or database size.

Reference

1- **Sensor Similarity Search in the Web of Things.** Cuong Truong, Kay Römer, Kai Chen. Institute of Computer Engineering,2012.

- 2- **Application based Study on Wireless Sensor Network.** Kiran Maraiya, Kamal Kant, Nitin Gupta, International Journal of Computer Applications *Volume 21– No.8, May 2011.*
- 3- **Wireless sensor network survey.** Jennifer Yick, Biswanath Mukherjee, Dipak Ghosal *. Department of Computer Science, Computer Networks 52 (2008) 2292–2330.
- 4- **Light Weight and Secure Database Encryption.** Using TSFS Algorithm. D. Manivannan¹, R.Sujarani². ¹Asst. Professor, School of Computing, International Conference on Computing Communication and Networking 2014.
- 5- **Lightweight Symmetric Encryption Algorithm for Secure Database.** Author 1: Hanan A. Al-Souly. Author 2: Abeer S. Al-Sheddi. Author 3: Heba A. Kurdi. *Science and Information Conference 2013.*
- 6- **Wireless underground sensor networks: research challenges,** Akyildiz, E.P. Stuntebeck, Ad-Hoc Networks 4 (2006) 669–686.
- 7- **System-Architectures for Sensor Networks Issues, Alternatives, and Directions"**J. Feng, F. Koushanfar, M. Potkonjak, IEEE International Conf on Computer Design (ICCD), Germany, 2002. pp. 226- 231.
- 8- **Recommendation for Cryptographic Key Generation,** NIST SP 800-133...http://csrc.nist.gov/publications/nistpublications/800-57/sp800-57_part1_rev3_general, 2012.
- 9- **Key Generation Using Genetic Algorithm** for Image Encryption. Aarti Soni¹, Suyash Agrawal²RESEARCH ARTICLE. © 2013, IJCSMC All Rights Reserved. 376.
- 10- **Secure Database Encryption in Web Applications,** Amandeep kaur¹ , Mrs. Shailja Kumari² Oct 13, 2016.

Evanescent field Mach-Zehnder interferometer sensor for concentration measurement

Ruaa Khalil Musa¹, Salah Al deen Adnan², Ali Mahdi Hammadi³

Engineer¹, Assistant Professor^{2,3}

^{1,2} Laser and Optoelectronics Engineering Department, University of Technology/Baghdad,

³ College of Electrical and Electronic Techniques, Middle Technical University.

ruaa.alsafi92@gmail.com¹, dr.salahadnan@gmail.com², draliopic@gmail.com³

Abstract:

Optical fibers have been widely used in the field of sensing. In this paper, Mach-Zehnder interferometer is designed and constructed for detecting the concentration of solutions based on the excitation of the evanescent wave at the cladding/core interface. Laser diode (LD) with wavelength of 810 nm has been used. 3 cm of cladding has been removed in the middle of 1 m (SMF-28) for the two arms by using hydrofluoric acid (HF). One arm is isolated from the external perturbation, and the other arm is immersed in different concentrations of sucrose solutions range from 10% to 50% and sodium chloride (NaCl) solutions range from 5% to 25%. As the concentration of solution increases the output power decreases and the wavelength shifts toward the red region. The sensitivities of this sensor for different concentration of sucrose solutions and NaCl solutions are 0.017 nm/(% w/v) and 0.0474 nm/(% w/v), respectively.

Key words: Mach-Zehnder interferometer (MZI), evanescent field, concentration, wavelength shift, sensitivity.

متحسس المجال الزائل ماخ زندر لقياس التركيز

رؤى خليل موسى¹, صلاح الدين عدنان طه², علي مهدي حمادي³

مهندسة¹, استاذ مساعد^{2,3}

قسم هندسه الليزر والالكترونيات البصريه / الجامعه التكنولوجيه^{1,2}, كليه التقنيات الهندسيه الكهربائيه والالكترونيه /
الجامعة التقنية الوسطى³

الخلاصه:

قد استخدمت الالياف الضوئية على نطاق واسع في مجال التحسس. في هذه الورقة تم تصميم وبناء "ماخ زندر التداخل" للكشف عن تركيز المحاليل على اساس تحفيز الموجه الزائله على السطح الفاصل للقلب/القشره. قد استخدم ليزر الصمام الثنائي (LD) مع طول موجي 810 نانومتر. تم ازالة 3 cm من القشره في منتصف 1 m (SMF-28) للذراعين باستخدام حامض الهيدروفلوريك (HF). يتم عزل ذراع واحد من الاضطراب الخارجي, وغمر الذراع الاخر في تراكيز مختلفة من محاليل السكروز تتراوح من 10% الى 50% وتتراوح محاليل كلوريد الصوديوم من 5% الى 25%. كما يزيد تركيز المحلول تقل الطاقة الخارجه ويتحرك الطول الموجي نحو المنطقه الحمراء. الحساسيه لهذا المتحسس لتراكيز مختلفه من محاليل السكروز ومحاليل كلوريد الصوديوم هي 0.017 nm/(% w/v) و 0.0474 nm/(% w/v), على التوالي.

الكلمات المفتاحيه: ماخ زندر التداخل, المجال الزائل, التركيز, تحرك الطول الموجي, الحساسيه.

Introduction:

Optical fiber sensors have been used in several applications such as chemical, biological, and environmental industries, for the measurements of temperature, liquid level, strain, and Refractive index [1].

Optical fiber sensor offers several advantages compared to electronic sensor due to their features like light weight, robust to environment, non-electrical devices, immune to electromagnetic interference (EMI) and radio frequency interference (RFI), high resolution, dynamic range, high sensitivity, allow remote sensing, allow to access into inaccessible areas, small size[2-4].

The refractive index (RI) is the very essential parameter in these applications particularly in bio-sensing for biochemical reactions or controlling molecular bindings and in food industries or chemical in order to control the quality [5].

In the past various refractive index sensors such as Abbe and Rayleigh refractometers were demonstrated to measure the RI but they have the disadvantages of weight and big size [6]. Nowadays fiber optic refractive index sensors are widely used for these applications [7].

Recently, Fiber optic Mach-Zehnder interferometer (MZI) sensors are widely used in various chemical and physical sensing applications. In this paper, MZI is used because of several advantages such as simple structure, ease of fabrication, ability of responding to various measurands, and low cost [8].

Mach-Zehnder Interferometer Sensor:

Mach-Zehnder Interferometer sensor is one of the most sensitive configurations of fiber optic sensors [9], which can be used as an evanescent field sensor. The emitted light from the source is divided by the first 3dB coupler into two equal parts, transmitting in different paths, and then they are combined by the second 3 dB coupler. The reference arm isn't exposed to the measurand, and the sensing arm is exposed to the measurand which is introduced as cladding, this induces a phase difference between the signals resulted in an interference, the output signal shows a sinusoidal variation is directly proportional to the refractive index change of the measurand [10-12]. The schematic diagram of Mach-Zehnder interferometer is shown in Figure (1) [13].

The advantages of MZI sensors are reduced noise due to intensity fluctuations, reduce undesired feedback effect, and any small change in the optical path length of the sensing arm will produce a large change in the output. The optical path length of the sensing arm is changed by changing the physical length of it (under the effect of temperature or pressure) or by changing the effective refractive index of it (by changing the refractive index of the cladding or the refractive index of the guiding layer) [11]. The input signal E_{in} splits into two identical parts, the signals in the two arms of the interferometer are described by [11]:

$$E_r = \frac{E_{in}}{\sqrt{2}} \quad (1)$$

$$E_s = \frac{E_{in}}{\sqrt{2}} \quad (2)$$

Where E_r and E_s are the signals in the reference and sensing arm respectively. The two signals transmit with different paths, until they reach the second coupler. $\Delta\phi$ is the additional optical phase, which is introduced in the sensing arm. Before the second coupler, the two signals are given by [11]:

$$E_r = \frac{E_{in}}{\sqrt{2}} e^{j\omega t} \quad (3)$$

$$\frac{E_{in}}{\sqrt{2}} e^{j(\omega t + \Delta\phi)} \quad (4)$$

Where ω is the angular frequency. At output, the two signals are recombined, E_{out} is given by [11]:

$$\begin{aligned} E_{out} &= E_r + E_s \\ &= \frac{E_{in}}{\sqrt{2}} (e^{j\omega t} + e^{j(\omega t + \Delta\phi)}) \end{aligned} \quad (5)$$

The interference of two beams is given by [14]:

$$I = I_r + I_s + 2\sqrt{I_r I_s} \cos(\Delta\phi) \quad (6)$$

Where I_r and I_s are the intensities of reference and sensing arm.

Output power of Mach-Zehnder Interferometer is described by [15]:

$$p_{out} = p_{in} \cos^2(0.5 \Delta\phi) \quad (7)$$

The phase difference between the sensing arm and reference arm is described by [16]:

$$\Delta\phi = \frac{2\pi}{\lambda} L \Delta n_{eff} \quad (8)$$

Where L is the interaction length (the sensing area length), λ is the wavelength in the vacuum, and Δn_{eff} is the change in the effective refractive index of the mode.

Each solution is referred to as the mode of structure. Each mode is described by its effective index, the effective index it's a parameter that governs the electromagnetic wave as it transmits along the fiber [11].

Experimental Method:

Sodium chloride (NaCl) and sucrose have been used as guiding liquids with various concentrations. The concentrations of NaCl solutions range from 5% to 25% and for sucrose solutions range from 10% to 50%. The refractive index for NaCl and Sucrose solutions at each concentration is measured by using Abbe refractometer.

For the sensing and reference arms, 3 cm of outer plastic jacket in the middle of 1 m of SMF-28 has been removed by immersing the fiber in acetone; the buffer is also removed by acetone. The cladding is partially etched by using hydrofluoric acid (HF) with 40% concentration for 35 minutes to obtain high sensitive region to the surrounding concentrations. The schematic diagram of a Mach-Zehnder interferometer concentration sensor is shown in Figure (2).

The system consists of laser diode (LD) with wavelength of 810 nm, the first (3dB) optical coupler (splitting ratio 50:50) is used to split the light into two identical beams, the coupler is connected with two identical SMF-28 (equal etching length) using (FC to ST) adapter, to combine the light beams the two ends of the fibers are connected to the second (3dB) coupler also with (splitting ratio 50:50) using (FC to ST) adapter. The output of the coupler is connected to a power meter (Fiber Optic Communications Training System EF-970/R promax) and/or Optical Spectrum Analyzer model (HR 2000). The experimental setup of the (MZI) concentration sensor is shown in Figure (3).

When the emitted light entered the first optical coupler, the light beam is divided into two equal beams, the first beam entered in the reference arm, which is isolated from perturbation and the second beam entered on the sensing arm which is immersed in distilled water and different concentrations of Sucrose and NaCl solutions. The beam, then suffer a phase shift due to the external concentrations where the output interference pattern between the two beams is taken by an Optical Spectrum Analyzer, and the output power is taken by the power meter. All measurements are carried out at room temperature.

Results and Discussion:

Figures (4) and (5) show the relationship between refractive index and concentration of NaCl and Sucrose solutions, respectively.

From the Figures the refractive index is directly proportional to the concentration, as concentration of guiding liquid increases refractive index increases.

The reference arm is isolated from any external perturbation, the variation which is induced in the sensing arm is due to the change in the concentration of NaCl solutions range from 5% to 25%, and Sucrose solutions range from 10% to 50%. Figures (6) and (7) show the interference pattern for different concentration of Sucrose and NaCl solutions, respectively.

According to Equation (8) as the concentration of solution increases (the refractive index of the guiding layer increases) the effective refractive index of propagation mode in the sensing arm increases, this will lead to increase the shift towards long wavelength (red region), also the curves show that as the concentration of NaCl and Sucrose solutions increase the intensity decreases. The sensitivity of this sensor ($s = \frac{\Delta\lambda}{\Delta C}$) for sucrose and NaCl solutions is 0.017 nm/ (% w/v) and 0.0474 nm/ (% w/v), respectively, as shown in Figures (8) and (9).

According to Equation (7) as the concentration of solution increases (the refractive index of the guiding layer increases), the phase shift increases this lead to decrease in the output power. The relationship between concentration of Sucrose and NaCl solutions and output power are shown in Figures (10) and (11), respectively.

Conclusion:

A Mach-Zehnder Interferometer sensor based on the excitation of evanescent field has been demonstrated where the variation

of the surrounding concentration is detected by measuring a shift in the wavelength. A red shift in the output spectrum is observed with increasing of concentration. The sensitivity of this sensor for sucrose solutions in the range of 10% to 50% is 0.017 nm/(% w/v) and for

NaCl solutions in the range of 5% to 25% is 0.0474 nm/(% w/v). This sensor can be used for measuring concentration in various applications such as medical, food industry, pharmaceutical, environmental controlling systems, and monitoring the quality of drinking water.

References:

- [1] L. Li, L. Xia, Z. Xie, and D. Liu, "all-fiber Mach-Zehnder interferometers for sensing applications", *Optics Express*, Vol.20, No.10, pp. 11109-11120, 7 May 2012.
- [2] R. B. Malla , A. Sen and N.W. Garrick , "A special fiber optic sensor for measuring wheel loads of vehicles on Highway", *Sensors*, Vol.8, No.4, pp. 2551-2568 ,2008.
- [3] B.P. Pal, "Fundamentals of fibre optics in telecommunication and sensor systems", Bohem press, New Delhi, 1992.
- [4] K.A. Fidanboyly , and H. S. Efendioglu , "FIBER OPTIC SENSORS AND THEIR APPLICATIONS ", *International Advanced Technologies Symposium (IATS'09)*, Vol. 6 , pp.1-6 ,May 2009.
- [5] P. Lu, L. Men, K. Sooley, and Q. Chen, " Tapered fiber Mach–Zehnder interferometer for simultaneous measurement of refractive index and temperature", *Applied Physics Letters*, Vol.94, No.13, pp. 131110, 30 Mar 2009.
- [6] J. Zhou, Y. Wang, C. Liao, B.Sun, J.He, G.Yin, S. Liu, Z.Li, G. Wang, X. Zhong, and J.ZhaoK, " Intensity modulated refractive index sensor based on optical fiber Michelson interferometer", *Sensors and Actuators B: Chemical* ,Vol.208, pp. 315-319, 11 November 2014.
- [7] V. Rastogi, K. Kamakshi, R. K. Patra, A. Kumar and J. Rai, " DESIGN AND FABRICATION OF SINGLE MODE FIBRE OPTIC REFRACTIVE INDEX SENSOR ", *International conference on optics and photonics, CSIO, India*, pp. 1-4 , Nov 2009.
- [8] R. Mehra, H. Shahani, and A. Khan, " Mach zehnder Interferometer and it's Applications", *International Journal of Computer Applications*, Vol.1, No.9, pp.110-118, Feb 2010.
- [9] A. Ghatak and K. Thyagarajan, "An introduction to fiber optics", Cambridge university press, 1998.
- [10] Miao Yu, " Fiber Optic Sensor Technology", https://sem.org/wpcontent/uploads/2016/03/-fiber_optic_sensor_technology.pdf , Feb 6, 2008.
- [11] K. YADAV, N.G. Tarr, and P.D. Waldron , " Perforated Mach-Zehnder Interferometer Evanescent Field Sensor in Silicon-on-Insulator", *International Society for Optics and Photonics* , Vol. 6796 ,pp. 1-6, September 2006.

[12] Z. TIAN, and S.S.H. Yam , " IN-LINE OPTICAL FIBER INTERFEROMETRIC REFRACTIVE INDEX SENSORS", Journal of Lightwave Technology , Vol. 27, No. 13, pp. 2296-2306 ,August 2008.

[13] Z. Q. Tou , "FIBER OPTICS CHEMICAL SENSORS BASED ON RESPONSIVE POLYMERS", Ph.D thesis, Chemical and Biomedical Engineering, Nanyang Technological University, 2015.

[14] K .Qin , " Slow Light Mach-Zehnder Interferometer for Optical Label-free Biosensing", M.Sc thesis, Electrical Engineering, Vanderbilt University ,May 2014.

[15] C.Yi. Tai , C. Grivas, and J.S. Wilkinson," UV photosensitivity in a Ta/sub 2/O/sub 5/ rib waveguide Mach-Zehnder interferometer", IEEE Photonics Technology Letters ,Vol.16, No. 6, pp. 1522 – 1524, 24 May 2004.

[16] F.T. Dullo, V. Sokolov,C. Chauvet , S. Lindecrantz, S.A. Solbø, and O.G. Hellesø , " temperature sensitivity of waveguide Mach-Zehnder interferometer", SPIE OPTO. International Society for Optics and Photonics, Vol. 8988, pp. 89881T-89881T, May 2013.

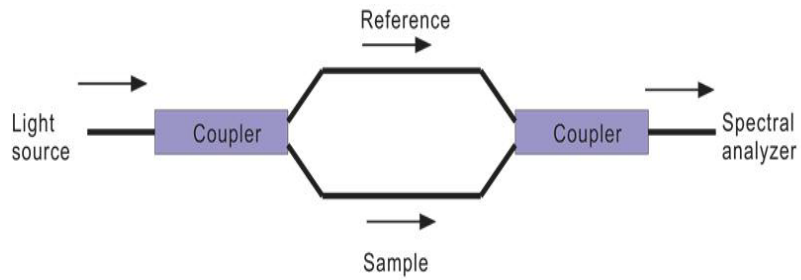


Figure (1): The schematic diagram of Mach-Zehnder Interferometer [13].

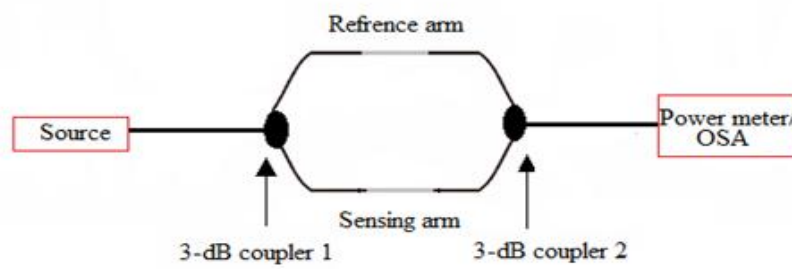


Figure (2): The schematic diagram of a MZI concentration sensor.

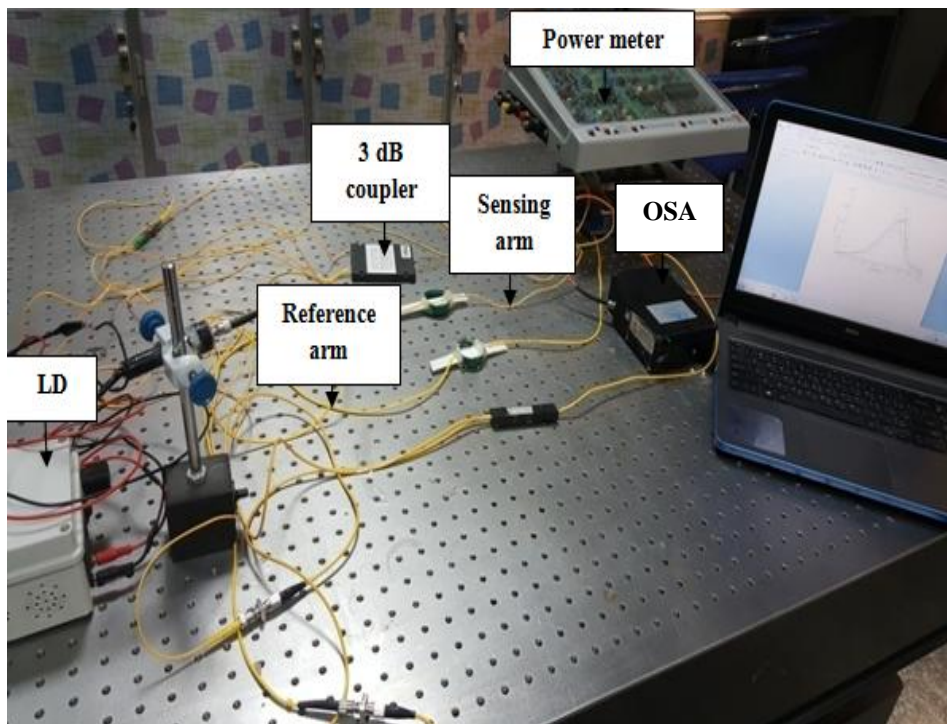


Figure (3): The experimental setup of the MZI concentration sensor.

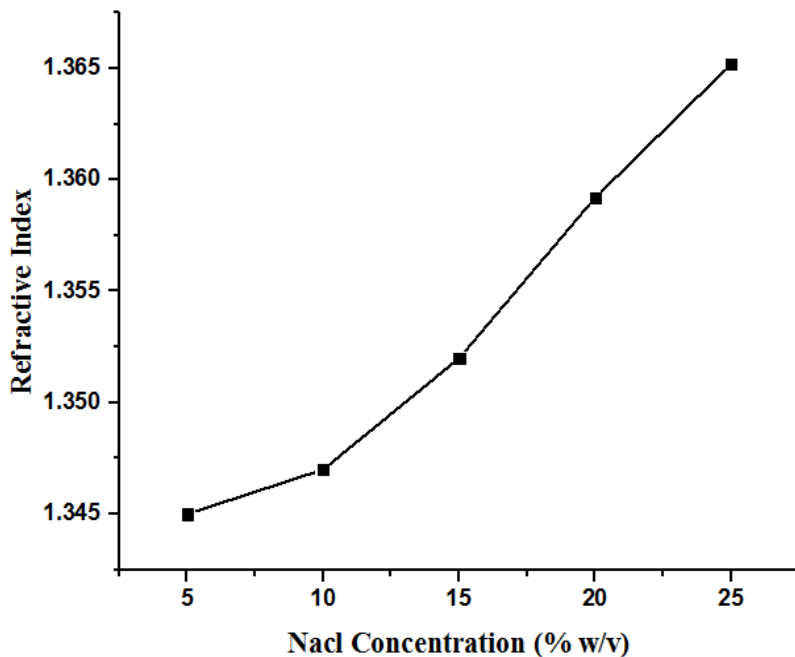


Figure (4): The relationship between concentration and refractive index of NaCl solutions.

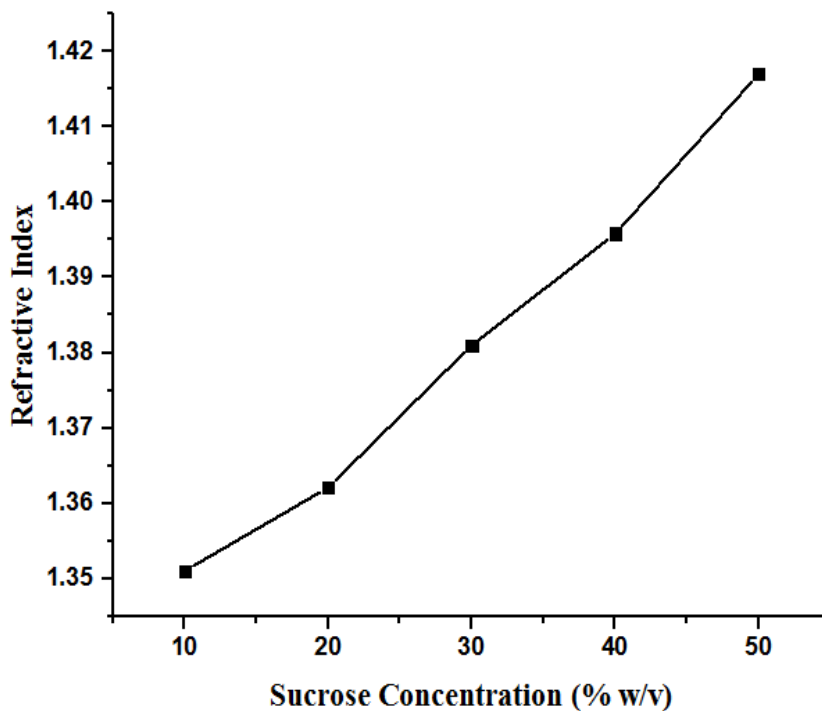


Figure (5): The relationship between concentration and refractive index of sucrose solutions.

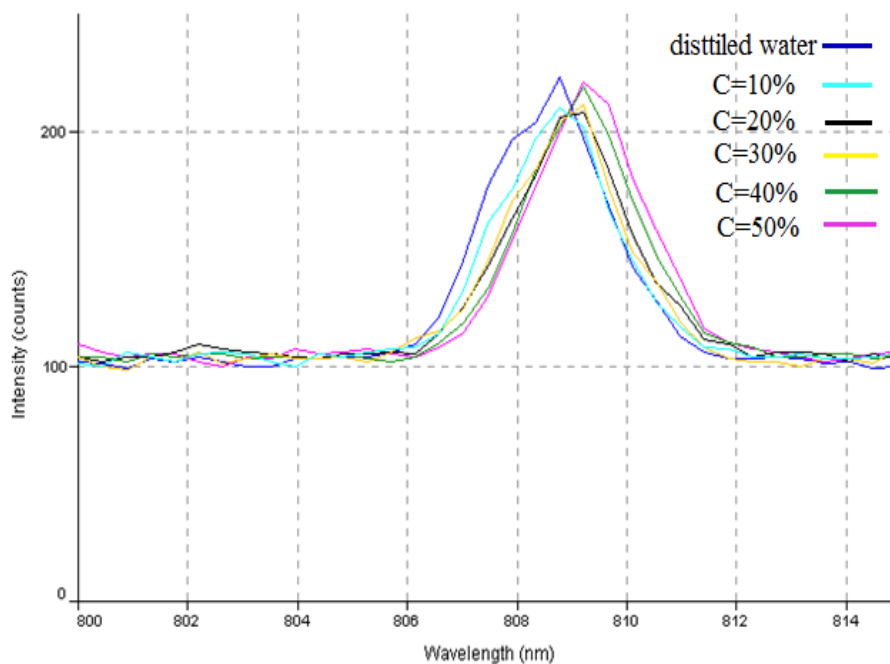


Figure (6): Interference spectra of MZI sensor for different concentrations of Sucrose solutions.

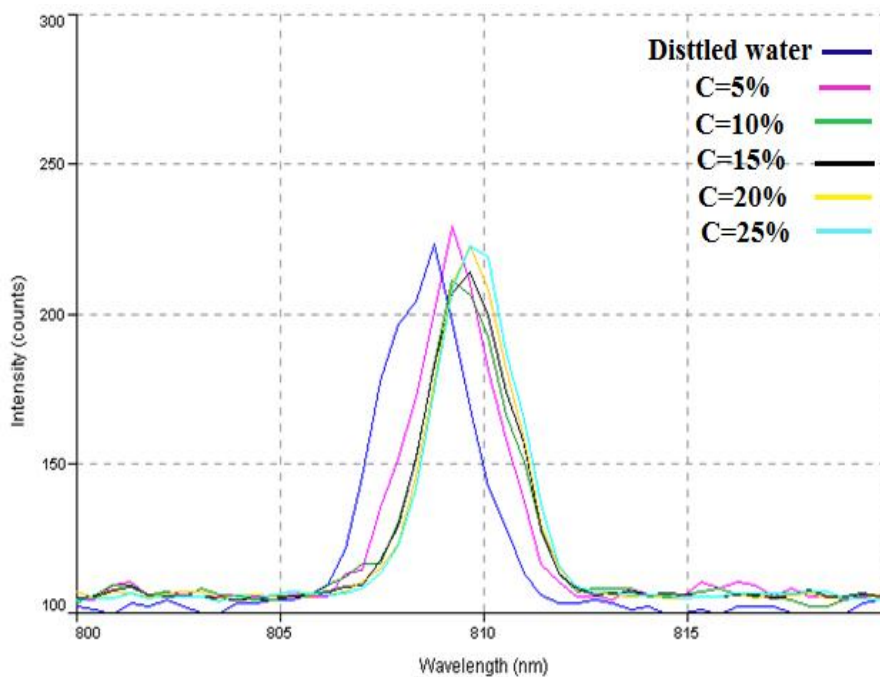


Figure (7): Interference spectra of MZI sensor for different concentrations of NaCl solutions.

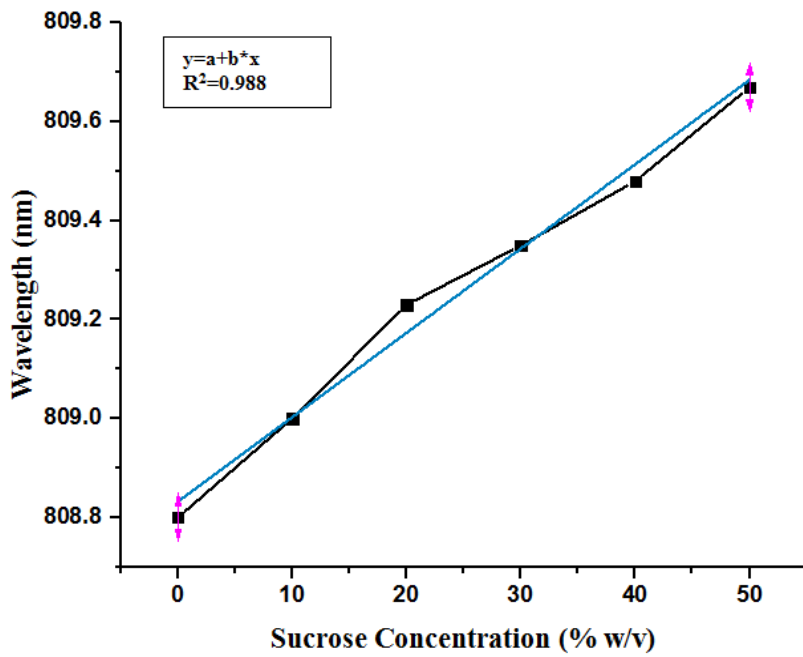


Figure (8): The relationship between wavelength and different concentrations of Sucrose solutions.

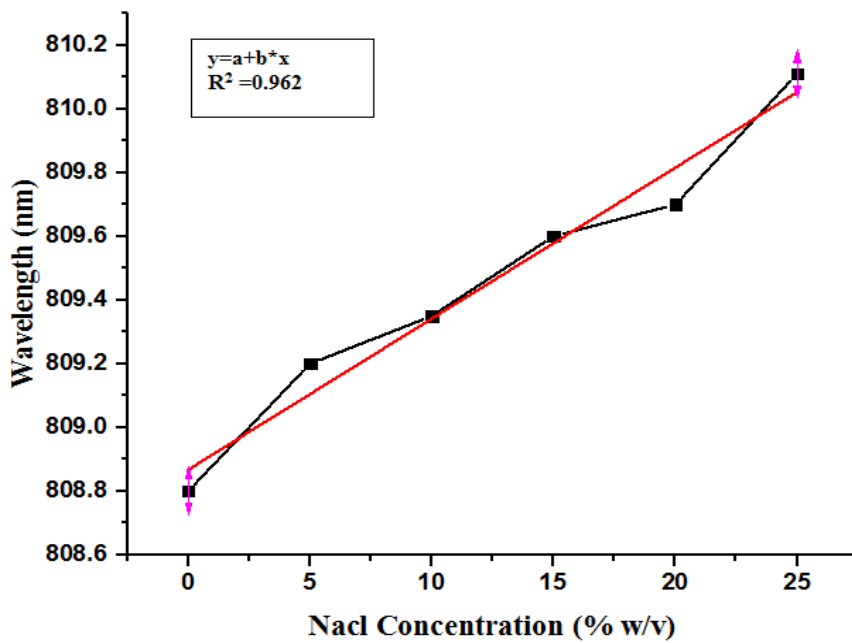


Figure (9): The relationship between wavelength and different concentrations of NaCl solutions.

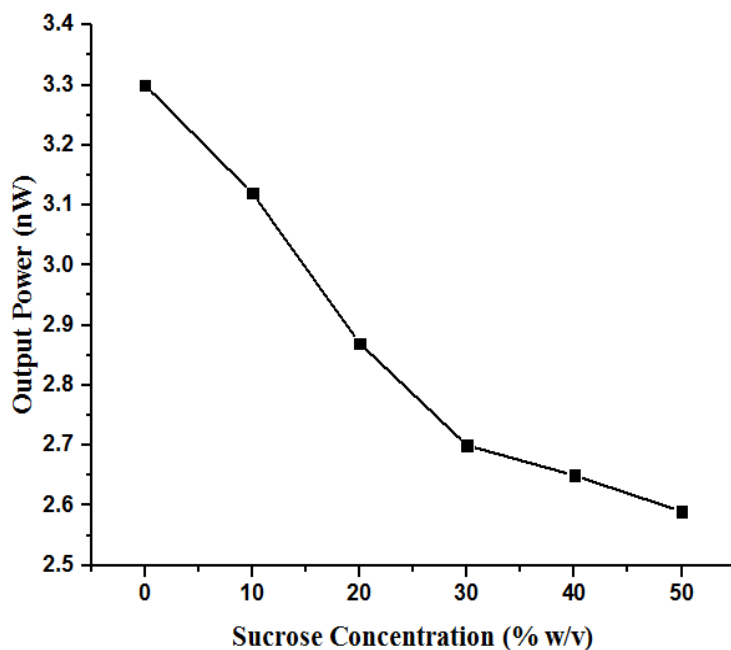


Figure (10): The relationship between output power and different concentrations of sucrose solutions.

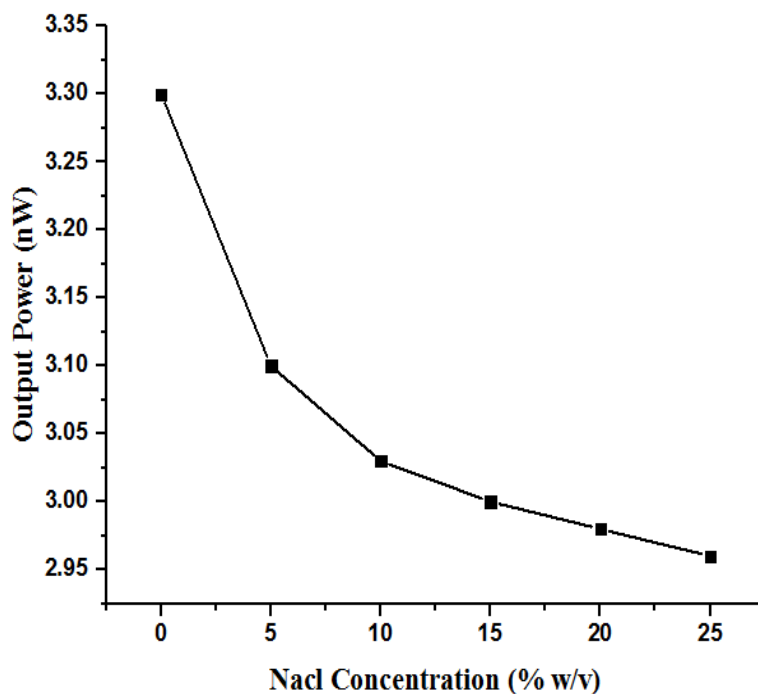


Figure (11): The relationship between output power and different concentrations of NaCl solutions.

Single phase Cascaded H-Bridge Multilevel Inverter study and comparison of different levels

Asst.prof. Jameel Kadhum Abed
 Technical College
 Middle Technical University
drjameel55@yahoo.com

Muhannad Jabbar Munati Electrical Engineering
 Institute of Technology Baghdad
 Middle Technical University
m.j.mnati@gmail.com

Bassam Mohammed Yaseen
 Master student in Electrical Engineering Technical College
 Middle Technical University
bsam88king@yahoo.com

Abstract:

Multi-level inverter used in applications that require high power and medium voltage. It can be used in: homes, factories, as well as in the military and medical aspects. This paper deals with study of Cascaded H-bridge and comparison between different levels for this type (three level, five level and seven level are presenting in this study). The comparison based on the design, the cost and the total harmonic distortion. The design tends to be more complicated when increasing the number of levels because of using more sources, more H-bridges and more connection wires. The control becomes more complexity as well as the inverter will be expensive and heavy as compared to low levels. Considering to the results of Matlab\ Simulink which illustrate the total harmonic distortion is being low when increasing the level and this will be an important matter in the output voltage. The level number of multi-level inverter is choosing according to the type of load.

Key words: Cascaded H-Bridge multilevel inverter, Sinusoidal pulse width modulation techniques

عاكس متعدد المستويات قنطرة H تتالي احادي الطور دراسة ومقارنة المستويات المختلفة

الخلاصة:

العاكس متعدد المستويات (Multilevel Inverter) يستخدم في التطبيقات التي تتطلب قدرة عالية وفولتية متوسطة. يمكن استخدامه في المنازل, المصانع, كذلك في الجوانب الطبية والعسكرية. هذا البحث يختص بدراسة العاكس متعدد المستويات نوع Cascaded H-Bridge ومقارنة بين مستويات مختلفة لهذا النوع (ثلاث, خمس وسبعة مستويات). المقارنة اعتمدت على التصميم, الكلفة والتشوه التوافقي الكلي (Total Harmonic Distortion). التصميم يكون اكثر تعقيداً عند زيادة عدد المستويات بسبب استخدام مصادر, خلية H-bridge وتوصيلات اكثر. التحكم بالمفاتيح اكثر صعوبة عند زيادة عدد المستويات كذلك العاكس يصبح مكلف واثقل بالمقارنة مع المستوي الاقل. بالنظر الى نتائج Matlab التي توضح التشوه التوافقي الكلي (Total Harmonic Distortion) يكون اقل عند زيادة المستوى وهذا امر مهم في موجة الفولتية الخارجة. مستوى العاكس متعدد المستويات (Multilevel Inverter) يختار حسب نوع الحمل.

الكلمات المفتاحية: العاكس متعدد المستويات نوع Cascaded H-Bridge, مستوى العاكس متعدد

المستويات

I. Introduction:

Development of the industries has led to increased need for using high power equipment in megawatts level. For purpose of providing energy to this equipment the multilevel inverter appeared. Multilevel inverter is a device which converts Direct Voltage Source (DCV) to Alternating Voltage Source (ACV). It consists of a group of semiconductor and generates stepped voltage with staircase waveform. Increasing the number of steps lead to smooth signal with reduces distortion and the shape of the wave approaching to sine wave. There are many power applications need multilevel inverter such as variable speed drive, flexible AC transmission systems (FACTS) and renewable energy such as wind, full cells and photovoltaic [1,2]. There are different topologies of multilevel inverter: Neutral point clamped multilevel inverter or Diode clamped multilevel inverter [3,4], Fly capacitance

multilevel inverter and Cascaded H-bridge multilevel inverter [5,6]. Neutral point clamped multilevel inverter and Fly capacitance multilevel inverter are single DC source but Cascaded H-bridge multilevel inverter uses multi DC source. Cascaded H-bridge multilevel inverter preferably employ instead of the other two types because it's required less number of components but also need separate DC source in each level [7]. The multilevel inverter obtains an alternating current output voltage with a staircase waveform [8].

The main features of multi-level inverter are:[9]

1. Less distortion and lower dv/dt of output voltage.
2. Minimum distortion of input current.
3. They generate smaller common-mode (CM) voltage, thus reducing the stress in the motor bearings. In addition, using sophisticated modulation methods, CM voltages can be eliminated.
4. Operate with low switching frequency, which reduce switching loss.

Multilevel inverter circuits have been appearing for more than 30 years. First appeared in 1975.[10]

II. Cascaded H Bridge Multilevel Inverter (CHBMLI)

The set of H-Bridge (Full Bridge) inverter with separate DC Sources are connected in cascade to configure the cascaded H-Bridge multilevel inverter [11]. Figure (1) shows the circuit diagram of an n level inverter. The output voltage generates by each single H-bridge of an inverter have three different value of voltage: $+V_{DC}$, 0 and $-V_{DC}$. The output voltage generated by cascade H-Bridge inverter is the total voltage generated by each H-bridge cell [12]. The required number of semiconductor switches are $2(n-1)$ where n is the number of level. The number of DC sources is equal to the number of H-Bridge cells. The cost and the weight of this inverter is less than Diode clamped multilevel inverter and Flying Capacitor multilevel inverter but the losses of it are more as compared with the other two types [13]. The voltage unbalance of H-bridge multilevel inverter is very low. It can be used in many applications such as motor drive system, photovoltaic cell, solar and fuel cell.

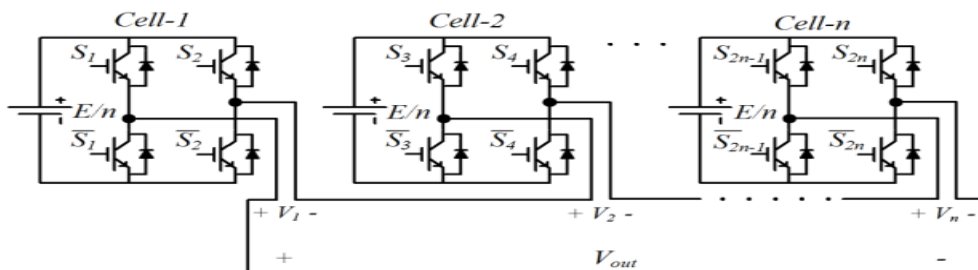


Figure (1). Circuit diagram of an n level inverter [12]

i. Single phase three level CHBMLI

Figure (2) shows the circuit of single phase three level CHBMLI. The circuit consisting of single DC source and four switches (single H-bridge cell).

of output voltage of this level is shown in figure (3). The three levels are $+V_{DC}$, 0 and $-V_{DC}$. Different operation cases of three level CHB inverter are explained below in table1.

Table1. Switches status of three level CHBMLI [14]

Case	Output voltage	S ₁	S ₂	S ₃	S ₄
1	0	1	0	1	0
2	+V _{DC}	1	0	0	1
3	0	0	1	0	1
4	-V _{DC}	0	1	1	0

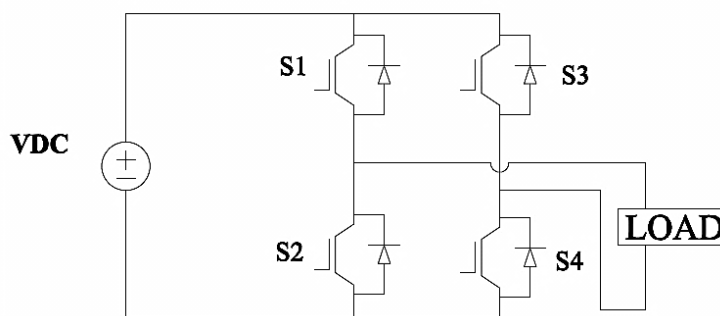


Figure (2). Circuit of single phase three level CHBMLI [14]

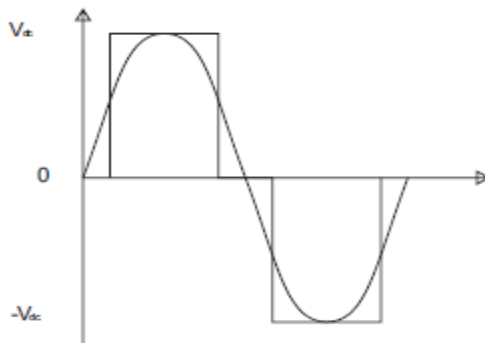


Figure (3). Output voltage waveform of three level CHBMLI [14]

ii. Single phase five level CHBMLI

Figure (4) shows the circuit of single phase five level CHBMLI. The circuit consisting of dual DC sources and eight switches (two H-Bridge cells). The output voltage of five level inverter is generated by two H-bridge cell. The voltage of the first H-Bridge

cell is V_1 and the second H-Bridge cell is V_2 . The total voltage of five level inverter is the sum of V_1 and V_2 . Figure (5) shows the waveform of output voltage of this level. The five levels are $0, +V_{DC}, +2V_{DC}, -V_{DC}$ and $-2V_{DC}$. Different operation cases of five level CHB inverter are explained below in table2.

Table2. Switches status of five level CHBMLI [14]

Case	Output Voltage	S ₁	S ₂	S ₃	S ₄	S ₅	S ₆	S ₇	S ₈
1	0	1	0	1	0	1	0	1	0
2	+V _{DC}	1	0	0	1	1	0	1	0
3	+2V _{DC}	1	0	0	1	1	0	0	1
4	+V _{DC}	1	0	1	0	1	0	0	1
5	0	0	1	0	1	1	0	1	0
6	-V _{DC}	0	1	0	1	0	1	1	0
7	-2V _{DC}	0	1	1	0	0	1	1	0
8	-V _{DC}	0	1	1	0	0	1	0	1

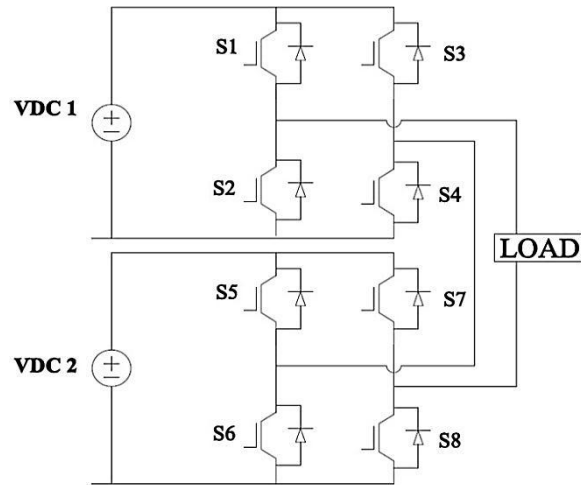


Figure (4). Circuit of single phase five level CHBMLI [14]

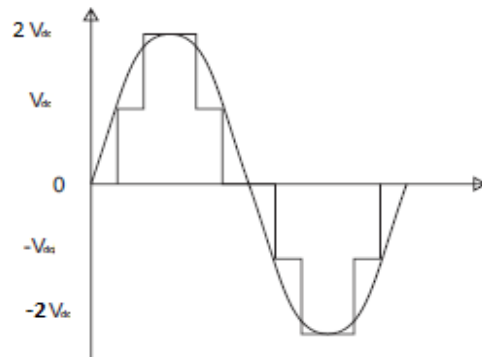


Figure (5). Output voltage waveform of five level CHBMLI [14]

iii. Single phase seven level CHBMLI

Figure (6) shows the circuit of single phase seven level CHBMLI. The circuit consisting of twelve switches (three H-Bridge cells) and three DC sources. The waveform of output voltage of seven level multilevel inverter

is shown in figure (7). The seven levels are $0, +V_{DC}, +2V_{DC}, +3V_{DC}, -V_{DC}, -2V_{DC}$ and $-3V_{DC}$. Different operation cases of seven level CHB inverter are explained in table3.

Table 3. Switches status of seven level CHBMLI [14]

Case	Output Voltage	S ₁	S ₂	S ₃	S ₄	S ₅	S ₆	S ₇	S ₈	S ₉	S ₁₀	S ₁₁	S ₁₂
1	0	1	0	1	0	1	0	1	0	1	0	1	0
2	+V _{DC}	1	0	0	1	1	0	1	0	1	0	1	0
3	+2V _{DC}	1	0	0	1	1	0	0	1	1	0	1	0
4	+3V _{DC}	1	0	0	1	1	0	0	1	1	0	0	1
5	+2V _{DC}	0	1	0	1	1	0	0	1	1	0	0	1
6	+V _{DC}	0	1	0	1	0	1	0	1	1	0	0	1
7	0	0	1	0	1	0	1	0	1	0	1	0	1
8	-V _{DC}	0	1	1	0	0	1	0	1	0	1	0	1
9	-2V _{DC}	0	1	1	0	0	1	1	0	0	1	0	1
10	-3V _{DC}	0	1	1	0	0	1	1	0	0	1	1	0
11	-2V _{DC}	0	1	0	1	0	1	1	0	0	1	1	0
12	-V _{DC}	0	1	0	1	0	1	0	1	0	1	1	0

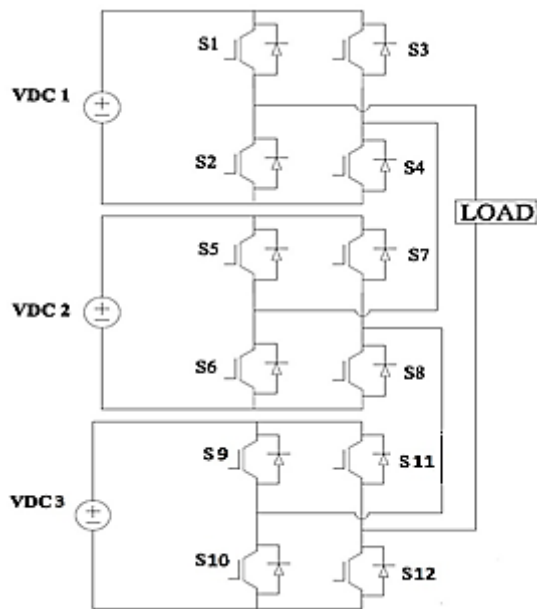


Figure (6). Circuit of seven level CHBMLI [14]

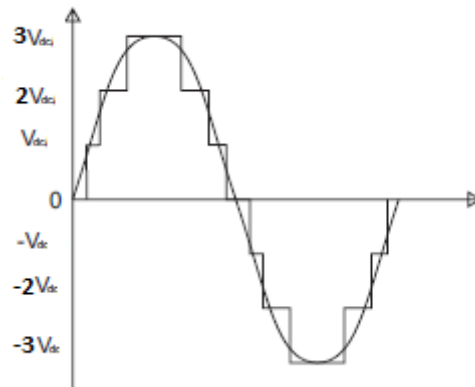


Figure (7). Output voltage waveform of seven level CHBMLI [14]

Table 4. Comparison between three level, five level and seven level of CHBMLI / phase

Parameters	Three level	Five level	Seven level
Number of cells	1	2	3
Number of switches	4	8	12
THD	52.23%	26.63%	18.01%
Cost	Less	Medium	More
Weight	Less	Medium	More

III. Sinusoidal PWM techniques (SPWM)

Different multicarrier techniques are used to decrease the distortion of multilevel inverter [15]. SPWM is one of these techniques, the sinusoidal wave is a modulating signal and the triangular waves are carrier signals. An n level inverter need (n-1) carrier signal [16]. The pulses of gates are generated as a result of comparing a sinusoidal modulating signal with a

triangular carrier signals. Figures (8, 9 and 10) Shows carrier signals with a reference modulating signal of three, five and seven level CHB inverter respectively. The carrier signals are in the same phase and amplitude but different from each other in the dc level [17]. The main advantage of this technique is decreasing the size of the filter to minimum and therefore reduces the cost, size and weight of an inverter.

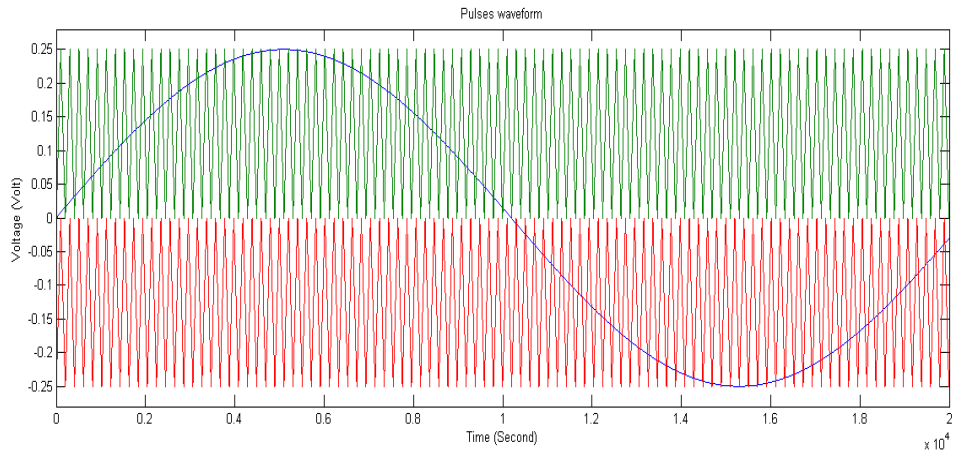


Figure (8). Carrier and Reference signals of three level CHBMLI

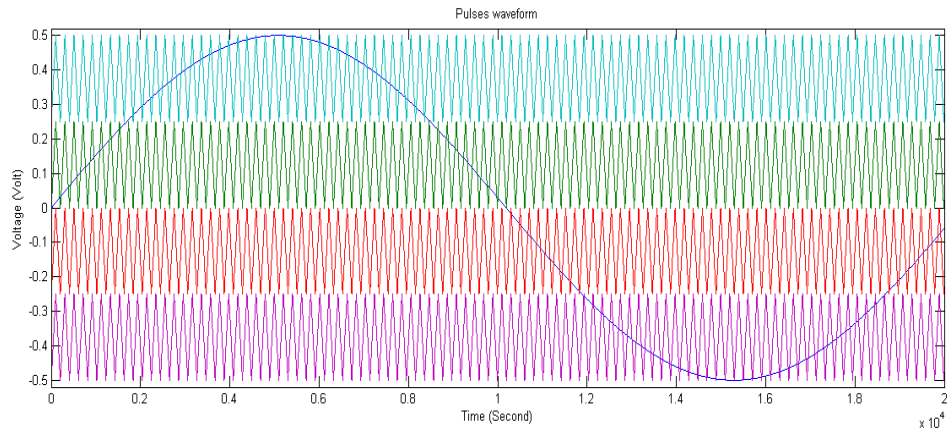


Figure (9). Carrier and Reference signals of five level CHBMLI

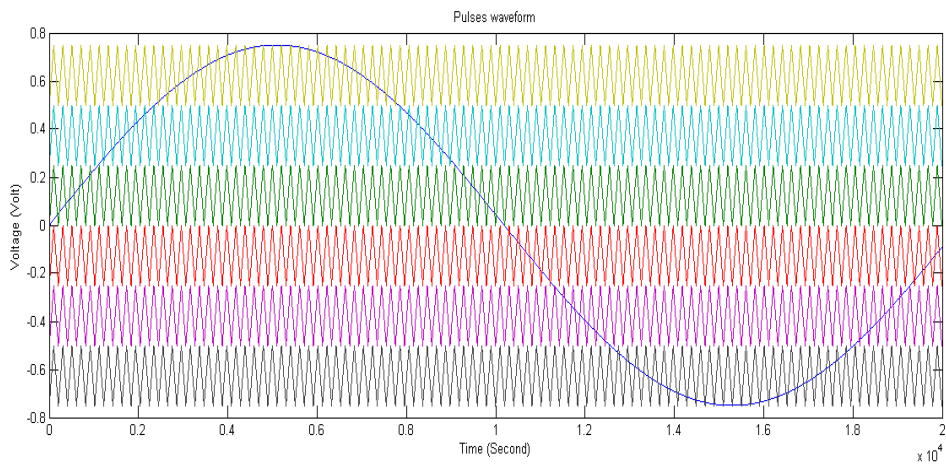


Figure (10). Carrier and Reference signals of seven level CHBMLI

V. Results:

Design of CHBMLI and the results of output voltage waveforms, output current waveforms and values of THD are obtained by

Matlab\ Simulink 2010 version 7.11.0. The figures below show the results of three, five and seven level respectively with resistive and inductive load ($R=100\Omega$ and $L=0.5H$).

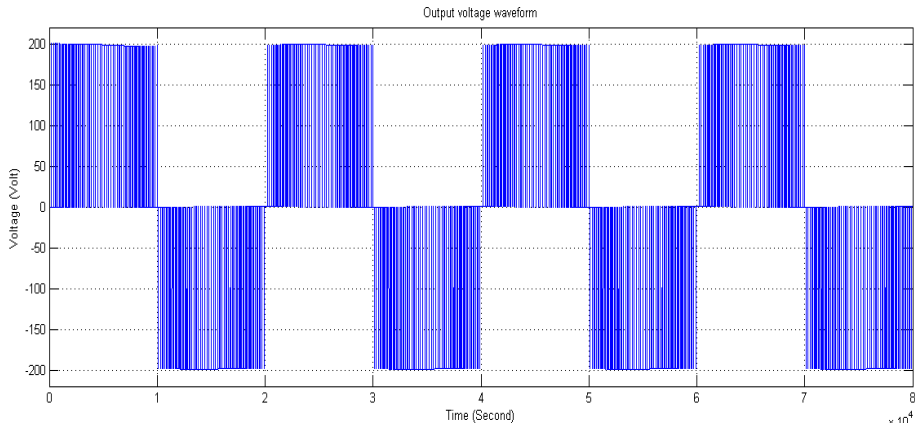


Figure (11). Output voltage waveform of three level

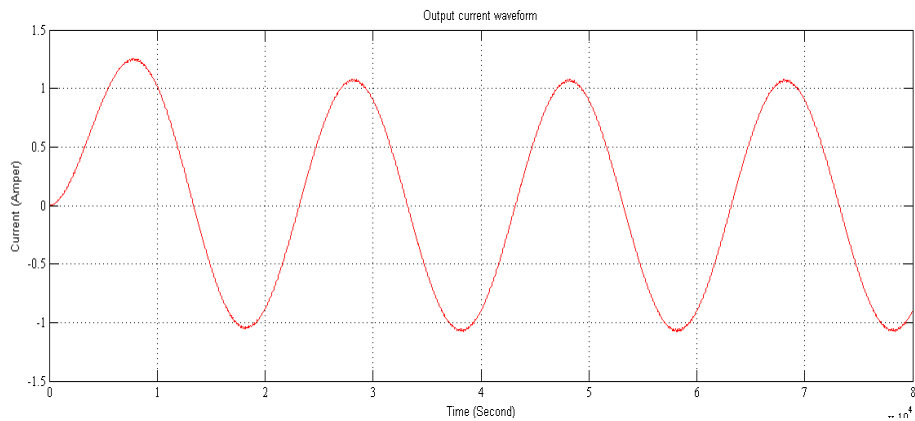


Figure (12). Output current waveform of three level

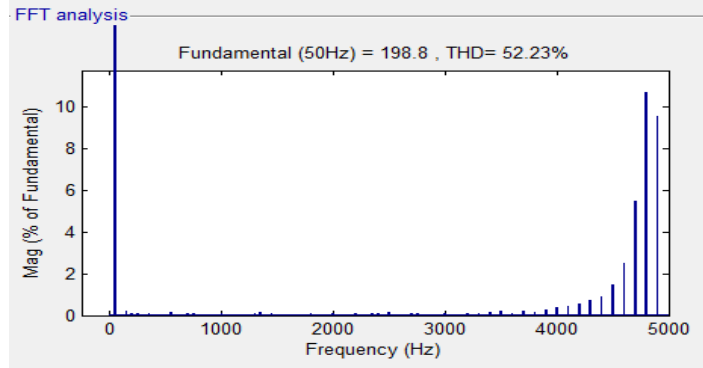


Figure (13). THD of three level

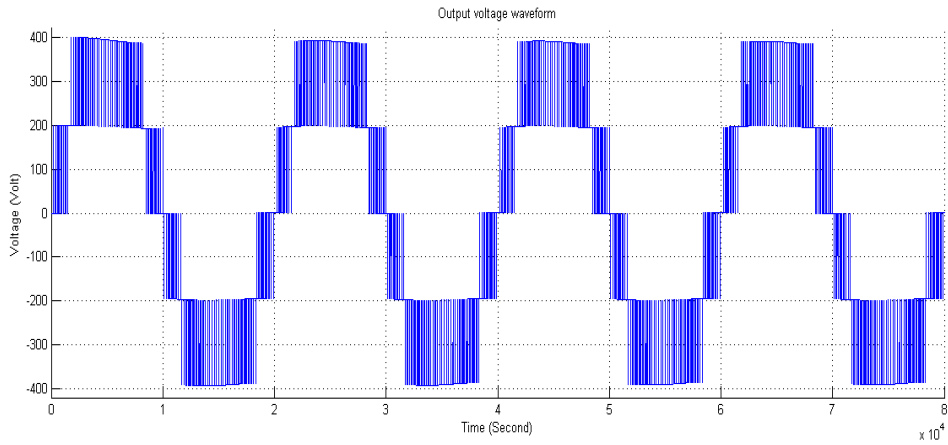


Figure (14). Output voltage waveform of five level

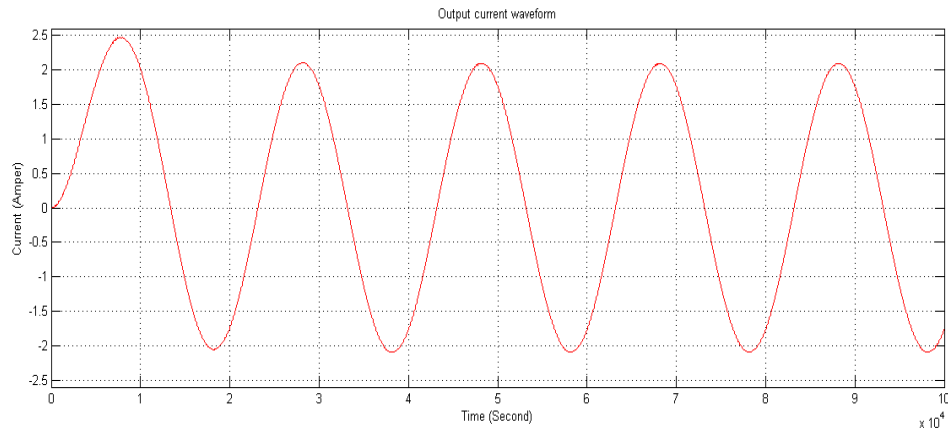


Figure (15). Output current waveform of five level

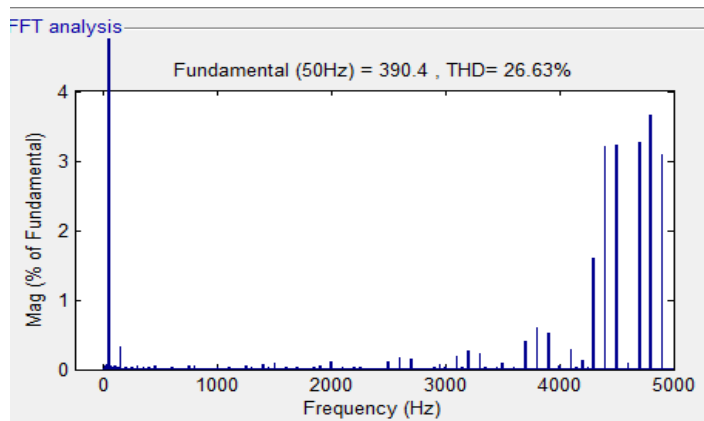


Figure (16). THD of five level

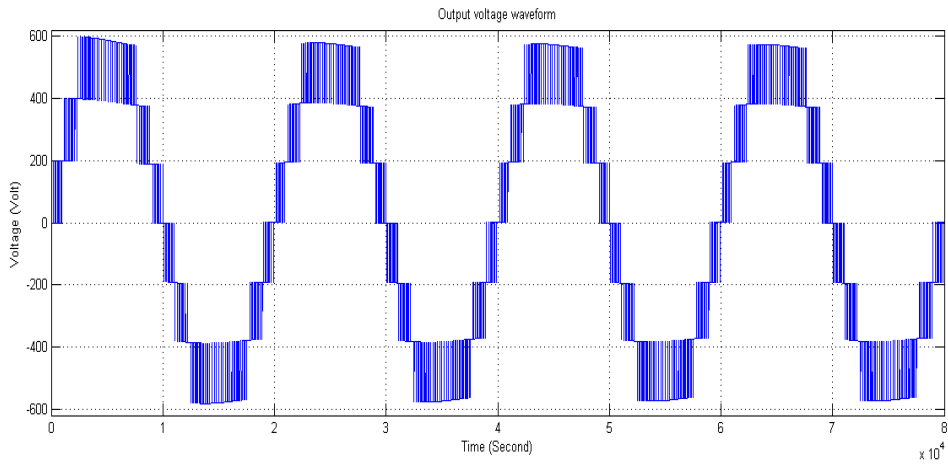


Figure (17). Output voltage waveform of seven level

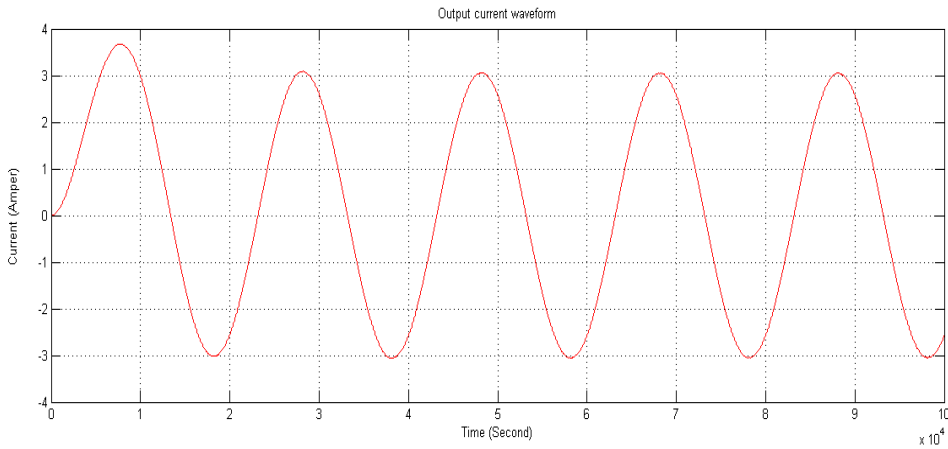


Figure (18). Output current waveform of seven level

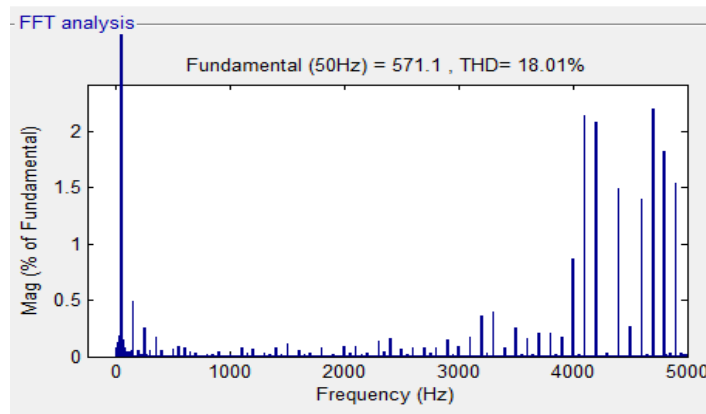


Figure (19). THD of seven level

V. Conclusion:

This paper deals with the study and comparison of cascaded H-Bridge topology with different levels. The comparison has three different level three, five and seven level and the method of control which use is SPWM. The result of MATLAB\Simulink appears less distortion at high level i.e. total harmonic distortion (THD) decreases with the increase in the number of level. The output voltage waveform of high level is improving and approaching more to the sinusoidal waveform. The output current of seven level is more than output currents of five level and three level. These are the advantages of increasing the number of level. But the cost, size and weight are increasing as well as the design is more complicated in high level of Multilevel Inverter.

References:

- [1]. F. Z. Peng, "A generalized multilevel inverter topology with self voltage balancing," IEEE Transactions on Industry Applications, vol. 37, pp. 611-618, 2000.
- [2] A. Shojaei, S. H. Fathi and N. Farokhnia, "Power Sharing Improvement in Cascaded Multilevel Inverters," 14th International Power Electronics and Motion Control Conference, EPE-PEMC 2010 , PP. T3-88 - T3-92,2010J.
- Clerk Maxwell, A Treatise on Electricity and Magnetism, 3rd ed., vol. 2. Oxford: Clarendon, pp.68–73, 1992.
- [3] Pradyumn Chaturvedi, Shailendra Jain, and Pramod Agarwal, "Carrier-Based Neutral Point Potential Regulator With Reduced Switching Losses for Three Level Diode Clamped Inverter," IEEE transactions on industrial electronics, vol. 61, no. 2, pp.387-389, February 2014.

- [4] A. Nabae, I. Takahashi, H. Agaki, "A New Neutral-Point-Clamped PWM Inverter," *IEEE Transactions on Industry Applications*, Vol. IA-17, No. 5, pp. 518-523, Sep./Oct., 1981.
- [5] R. F. Z. Peng, J-S Lai, "Multilevel Converters – A New Breed of Power Converters" *IEEE Transactions on Industry Applications*, Vol. 32, No. 3, PP. 509-517, May/June 1996.
- [6] Azli N.A., and Choong Y. C. "Analysis on the Performance of a Three-phase Cascaded H-Bridge Multilevel Inverter," *IEEE International on Power and Energy Conference*, vol., no., pp. 405-410, November 2006.
- [7] Booma N, and Sridhar N. "Nine level cascaded H-bridge multilevel DC-link inverter," *International Conference on Emerging Trends in Electrical and Computer Technology*, pp. 315-320, March 2011
- [8] R. H. Baker, "Switching circuit," U.S. Patent 4 210 826, July 1980.
- [9] E. Cengelci, S. U. Sulistijo, B. O. Woom, P. Enjeti, R. Teodorescu, and F. Blaabjerge, "A new medium voltage PWM inverter topology for adjustable speed drives," in *Conf. Rec. IEEE-IAS Annu. Meeting*, St. Louis, MO pp. 1416–1423, Oct. 1998.
- [10] R. H. Baker and L. H. Bannister, "Electric power converter," U.S. Patent 3 867 643, Feb. 1975.
- [11] Mariusz Malinowski, Senior Member, IEEE, K. Gopakumar, Senior Member, IEEE, Jose Rodriguez, Senior Member, IEEE, and Marcelo A. Perez, Member IEEE "A Survey on Cascaded Multilevel Inverters". Vol. 57, No. 7, pp 2197-2206, July 2010.
- [12] Prasad K.N.V., Kumar G.R., Kiran T.V. and Narayana G.S. "Comparison of different topologies of cascaded H-Bridge multilevel inverter," *International Conference on Computer Communication and Informatics*, pp. 1-6, Jan. 2013.

- [13] Ch.Krishna kantha, P.Deepthi Sree ,
 “Analysis, Simulation & Comparison of
 Various Multilevel Inverters Using
 Different PWM Strategies “,IOSR
 Journal of Electrical and Electronics
 Engineering (IOSR-JEEE) e-ISSN: 2278-
 1676,p-ISSN: 2320-3331, Volume 9,
 Issue 2 Ver. VII, PP 54-65, Mar – Apr.
 2014.
- [14] B. Harish, U.Raja Kiran, B. Madan
 and Soubhagya Kumar Dash, “Power
 Quality Improvement of DC-AC
 Converter by Using Cascaded H-Bridge
 Multilevel Inverter”, International
 Journal of Advanced Research in
 Electrical, Electronics and
 Instrumentation Engineering, Vol. 3,
 Issue 2, PP 7171-7178, February 2014
- [15] José Rodríguez, Jih-Sheng Lai and
 Fang Zheng Peng, “Multi-level Inverters:
 A Survey of Topologies, Controls, and
 Applications “,IEEE TRANSACTIONS
 ON INDUSTRIAL ELECTRONICS,
 VOL. 49, NO. 4, pp 724-737. August
 2002
- [16] B.Subhanandhini and V.Jegethesan
 “Application of hysteresis pulse width
 modulation for multilevel
 inverters,” IEEE international conference
 on advances in engineering science and
 management, pp.387-389, march 2012
- [17] S. Y. Mosazaden, S. H. Fathi and
 H. Radmanesh, “New High Frequency
 Switching Method of Cascaded
 Multilevel Inverters in PV Application
 “,IEEE Conference on Power
 Engineering and Renewable Energy.
 DOI:
 10.1109/ICPERE.2012.6287235, July
 2012

Design of Maximum power Tracking System by Automatic Control of Solar Cell Panel to the Sun Direction

Kader H.A. Al-Shara

Al-Farabi University College, Department of Computer Engineering

Kaderalshara@yahoo.com

Abstract:

Renewable energy is an area of significant investment and importance for future generations. The basis of this project is to design a new automatic control system for solar panel that tracking maximum power tracking according to the direction of sun ray. This project is an analysis of maximum power that can generate from the solar panel. This project needed to investigate the system parameter that affected the input sun ray to the solar panel. The system parameter that needs to investigate is weather, cell type, number of cells, temperature and the intensity of the sun. The system parameter is important to create the maximum power that can be generated by the design solar panel. In this paper, the main purpose is to design a system which controls the direction of the solar panel base on the sun direction and the main system parameter is the intensity of sun in daily mode. The system uses the motor type for controlling the angle of the solar panel base on the maximum intensity of sun ray. The validity of this proposed system achieved the maximum power of 101 Watt compared with the conventional types.

Keywords: Solar cell, Renewable Energy, Polycrystalline, maximum power.

تصميم منظومه سيطره اوتوتيكي لخلايا الطاقة الشمسية باتجاه اشعة الشمس للحصول على اكبر مقدار من الطاقة.

الطاقة المتجدده تعتبر من الفروع الحديثه والاستثمارية المهمه لمستقبل الطاقة. البحث المقدم يقترح تصميم منظومة سيطرة جديدة للخلايا الشمسية التي باستطاعتها مواكبة حركة الشمس تزامنيا. و تم التطرق للعناصر المهمه التي تتحكم في دوران خلايا الشمس باتجاه اشعة الشمس الساقطة. علاوة الى ذلك تم اضافته عناصر ثانويه لمحاكاة عمل النظام الحقيقي كحالة الطقس , عدد الخلايا , نوع الخلية الشمسية , درجة الحرارة , وكمية اشعة الشمس الساقطة. العناصر التي تم تضمينها تعتبر مهمه للحصول على اكبر مقدار من الطاقة الكهربائيه المتولده من خلال هذا التصميم. في هذا البحث تم التطرق ايضا على نظام السيطره لمواكبة حركة الخلايا الشمسية تزامنيا مع حركة واتجاه الشمس باستخدام ماطور احادي الطور للسيطره على زوايه انحراف الخلايا الشمسية تزامنيا مع حركة اكبر كمية لاشعة الشمس الساقطة. ان موثوقية المنظومة المقترحه حققت مقدار طاقه قدره 101 واط مقارنه بالنماذج الاخرى.

الكلمات المفتاحية: خلايا شمسية, اكبر من الطاقة, الطاقة المتجدده,

1. Introduction

Nowadays, the electrical system is widely used in the world. Consuming of electrical energy is increasing from day to day with the growing demand for electrical users that follows the massive jump of new technology in electrical component. The electrical consumption in South Asia increases 20% from 1980 to 2012 because the demand of the electrical user rapidly increases. [1-3].

For Example, in Malaysia, the greatest power plant generation of electricity currently use is a thermal power plant and hydroelectric power plant supported by TNB Company. Thermal power plants can cause much affection for our environment. The burning of coal for thermal power plant that release carbon dioxide and methane gases that can affect the greenhouse effect for the environment. The hydroelectric is a one of green energy, but it can't accommodate the demand of users today. The hydroelectric limited the production of electricity that can't increase easily. The service and maintenance of turbine fan of hydroelectric also need high cost to make sure the turbine is working every time. Based on the above listed challenges, the proposed based on a solar panel system can help to solve this problem. The solar energy is reliable resources that can be a cost-effective contingency [4]. Solar panel system also can provide virtually power system without affecting the

environment problem because it is secure and save green energy [5]. The maintenance cost of solar panel is less than the hydroelectric that need more workers to maintain the process is running smoothly [6]. But, the installation of solar panel needs high cost to get the higher wattage compare to another power plant like hydroelectric and combustion of coal. The designing of the maximum power, solar panel can solve a little bit installation cost. By designing the system, it can save the space and cost forget the high output electrical wattage of solar panel. The remainder of this manuscript is organized as follows: Section two presents the Solar Panel Model. Section Three focuses on the scheme of the proposed system, and Section Four concludes the paper.

2. Solar Panel Model

A solar cell is modeled as a current source with a diode and represented as an equivalent circuit as shown in Figure 1.

The parameter's value of solar cell like diode, resistor and current will change the output power of I-V curve.

The model of solar panel is obtained by connecting of solar cells in series and parallel. The interconnection of solar panel is shown in Figure 2, which shows how the output power is produce depends on the designing of connection of solar cell. The output power that will produce for each type of connection in solar panel will differ. The selection of connection

optimization is necessary to obtain the maximum power that can be generated by solar panel

2.1 System Design

The derived equations represented a mathematical analysis for calculating the maximum output power (P_{max}) from the solar panel model. The basic equation is mainly based on previously published articles [7-8].

$$I = I_{pv} - I_0(e^{bV} - 1) \quad (1)$$

$$I_{pv} = 2.54 \sin\left[\frac{\pi}{12}(t - 6)\right] \quad (2)$$

$$P = IV \quad (3)$$

$$P = (I_{pv} - I_0(e^{bV} - 1))(V) \quad (4)$$

$$\frac{dP}{dV} = (I_{pv} - I_0(e^{bV} - 1)) - (I_0 b e^{bV} - 1)(V) = I_{pv} + I_0 - I_0 e^{bV}(1 + bV) \quad (5)$$

$$I_{pv} + I_0 - I_0 e^{bV}(1 + bV) = 0 \quad (6)$$

Let,

$$b = \frac{1}{2}, \quad I_0 = 4.1 \times 10^{-5}$$

Then,

$$\frac{2.54}{4.1 \times 10^{-5}} \sin\left[\frac{\pi}{12}(t-6)\right] = e^{\frac{V}{2}} \left(1 + \frac{V}{2}\right) - 1 \quad (7)$$

Final equation is,

$$P_{max} = \left(\left[2.54 \sin\left[\frac{\pi}{12}(t_{max} - 6)\right] - I_0 \left(e^{\frac{V_{max}}{2}} - 1 \right) \right] V_{max} \right) \quad (8)$$

Where, I, V, t and b represent the voltage, current, time and solar sale absorption constant, respectively.

Figure 3-4 shows the detailed of the project schematic diagram for the system. A couple of solar panels are installed in the single control motor. The motor is controlled from the main control station in order to move a solar panel as a function of sun direction. The motor is automatically operated in daytime only.

3.1 System Performance

3.2 Ideal Photovoltaic Cell Array

The Figure 5 shows the simulation of ideal photovoltaic cell in a standard condition. The input signal of the simulation is constant that are 25 °C of temperature and 1k W/m² of Irradiation. The signal is in optimum condition to get the maximum power from the photovoltaic cell.

The parameter that need to change in solar cell are short circuit current (I_{scn}), Open circuit voltage (V_{ocn}), Maximum Current (I_{mp}), and the Maximum Voltage (V_{mp}) to get the maximum power that can be generated by solar cell.

Figure 6-7 show the result for I-V and P-V graph of ideal solar cell. The curve explains the value of the maximum power of the solar panel. The graph shows that the maximum power that generated is 1000 W during maximum voltage at 90 V. The result is for ideal solar cell value that can be controlled by changing the parameter of the solar cell. The changing of the parameter may affect the value of output power of solar panel.

3.3 Simulation Model

For the designed simulation, the 100 of cell is combining to be a solar panel. The simple circuit of the simulation is shown in Figure 8 below. The simulation of the system is comparing the output power of solar panel from different input concentration of sun that called irradiation. The input irradiation is entering to the system from 0 to 1000 W/m². Then, it will connect to the Simulink-PS Converter to convert the unit less Simulink input Irradiation to a physical signal. The physical signals directly connect to the input Ir for solar panel. The output from the 100 panel block diagram is connected to the current sensor and voltage sensor. The function of the current sensor is directly converted the output signal from the current measured to the physical signal proportional to the current. Then, the voltage signal is quite similar to the current sensor but its change the voltage measured signal. From these two sensors, the output power can calculate by product of the signal from current and voltage sensor. The value of current (I), voltage (V), and power (P) is export to the MATLAB by using a workspace block diagram.

After running the simulation in Simulink MATLAB, the output data will export to the MATLAB to plotting the graphs. The graph is to analyze the relationship between current, voltage, and power to the change of input irradiation.

The simulation results obtained Fig.9

presents the increasing of output power under the changing of irradiance. From the graph above, the maximum power can be defined during the input irradiance is at the optimum value. The maximum power that can be generated from the simulation is 160.9 W.

4. System Performance with difference type of Solar cell

The first step for the mathematical analysis of solar panel is defining the parameter that need to calculate in the formula. The value of each parameter depends on the data sheet of Monocrystalline type solar module SPM-100M and Polycrystalline type solar module SPM-20M. Table 1 and Table 2 shows the list of parameter from the datasheets given. Moreover, other solar cell system parameters are based on the previously published articles in [9-11].

Based on the various system parameters listed in Table 1 and Table 2, the parameter value is set as a constant value for the mathematical analysis. This result of mathematical analysis is evaluated by comparing the difference in temperature value. Table 3 shows the value of difference of for evaluating the output power of solar panel. Two types of solar panel are comparing the result by changing the temperature.

4.1 Performance of Monocrystalline solar panel type.

The Figure 10 shows the results of Current and voltage for monocrystalline solar panel type. The graph represents the value of voltage is

decreasing under high temperature. To archive the maximum voltage that can generate is maintain the solar panel under lower temperature. The value of current for the monocrystalline solar panel is around 5.6A to 6A under the difference of temperature. The current a little bit increasing when the temperature is increased.

The Figure 11 shows the relationship between power and voltage from the monocrystalline solar panel type. The graph above proves that the maximum power can be achieved by decreasing the value of temperature. The maximum power that can generate is 101 W at 10 °C, 95 W at 25 °C, 87 W at 45 °C and 74 W at 75°C.

4.2 Performance of Polycrystalline solar panel.

Figure 12 represents the I-V curve for polycrystalline type solar panel. The output voltage of this solar panel is similar to the monocrystalline solar panel. But, from the graph below the output current of this solar panel type is smaller compared to the monocrystalline solar panel. The result shows the output current only 1 A to 1.5 A.

Finally, Figure 13 depicts the graph of P-V curve of polycrystalline type solar panel is plotted. The graph shows that the power is decreasing under the high temperature. The graph shows the Maximum power from this solar panel type is lower than monocrystalline type. The maximum power from this solar panel is shown in Figure 4.15 below. The maximum power is 19.2 W

at 10 °C, 19.0 W at 25 °C, 18.4 W at 45 °C and 17 W at 75 °C. The ratio of the output power and temperature is lower compared to the monocrystalline solar panel type.

5. Conclusion

In this paper, a new model of dual solar cell is designed to compare the output power result with different parameters. The result shows the relationship between maximum output power with the difference irradiance or concentration of sun. The simulation represents the design of maximum power, solar panel system according to the sun direction to achieve the first step towards real time environment. The solar panel must be in optimum irradiation to achieve maximum power from solar panel. The solar panel must be controlled perpendicularly directly according sun direction to get the optimum of irradiation. Otherwise, the shadowing effect will occur if the solar panel system at fixed condition. The cloudy and rainy weather also gives the negative impact to the generation of maximum power. The mathematical analysis of the maximum power solar panel is implemented in MATLAB programming by comparing the two different types of solar panel datasheet. From the result, the effect of temperature for the monocrytalline type and the polycrystalline type of solar panel can be analyzed. The result shows the polycrystalline solar panel more efficient compare with the monocrystalline solar panel.

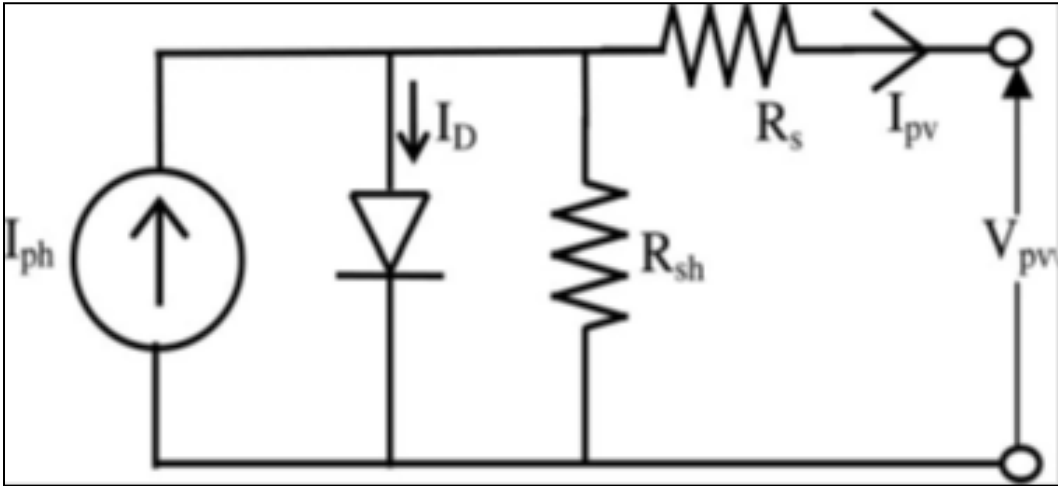


Figure 1: Equivalent Circuit of Solar Cell [3].

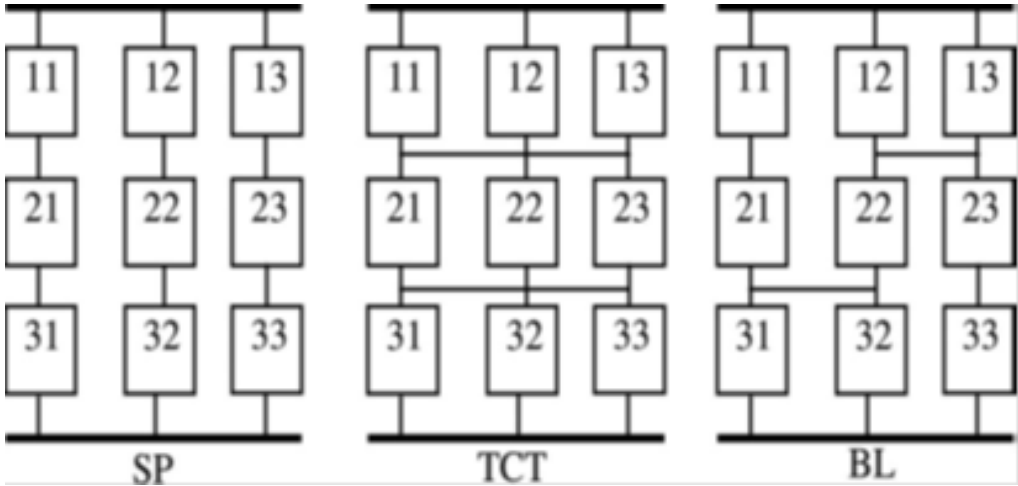


Figure 2: Series and Parallel connection of Solar Cell in a Solar Panel. [3]

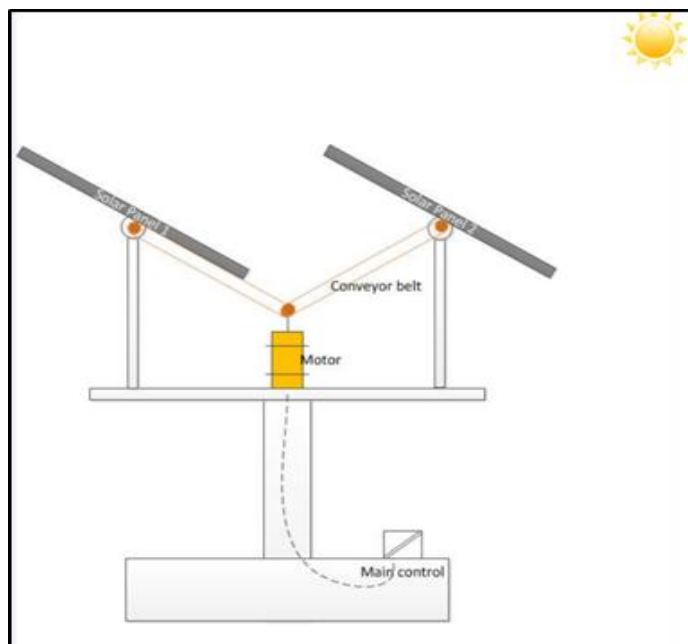


Figure 3: Proposed Design of Dual Solar Panel.

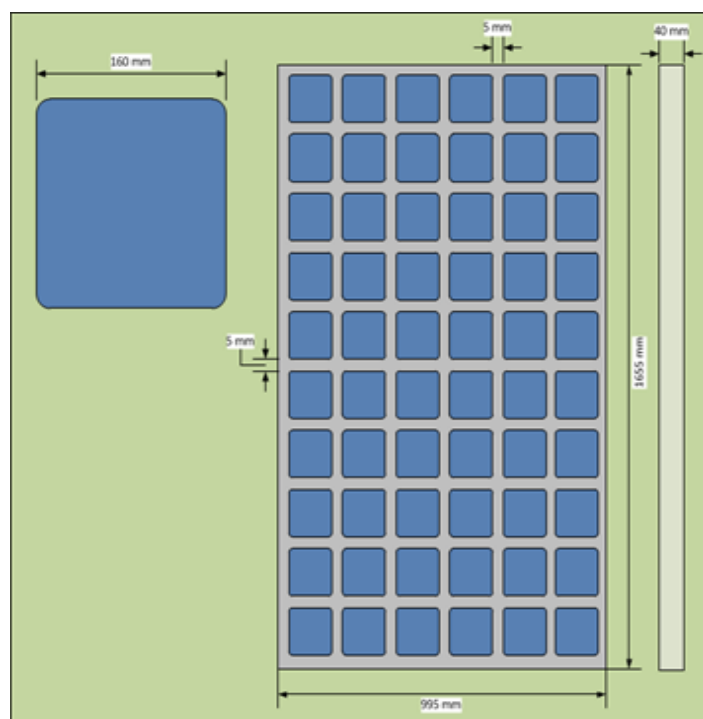


Figure 4: Dimension of Solar Panel Design

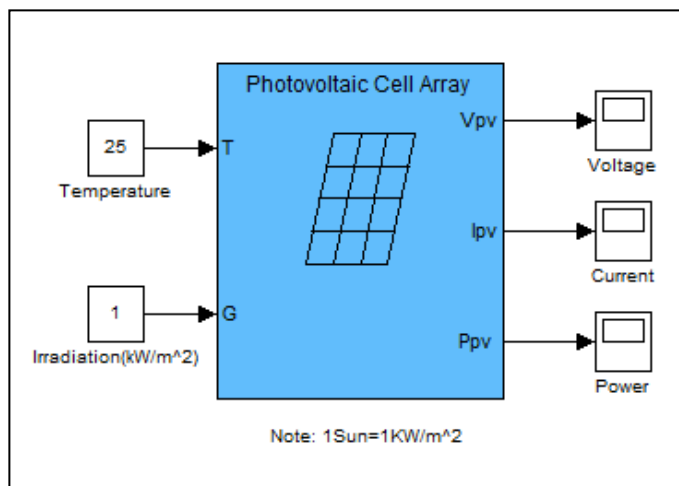


Figure 5: Simulation of Ideal Photovoltaic cell Array.

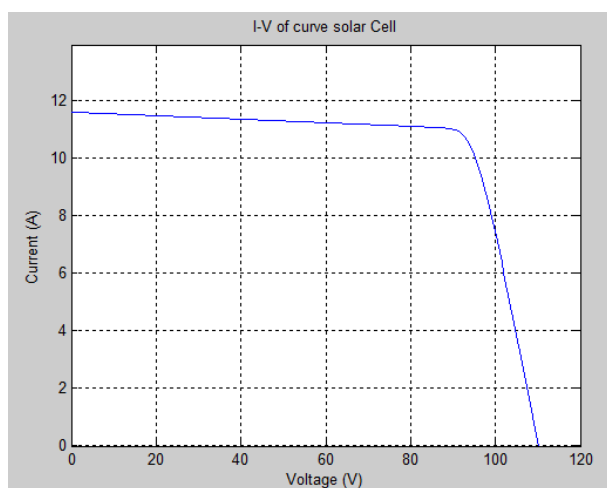


Figure 6: Ideal Solar cell I-V Graph.

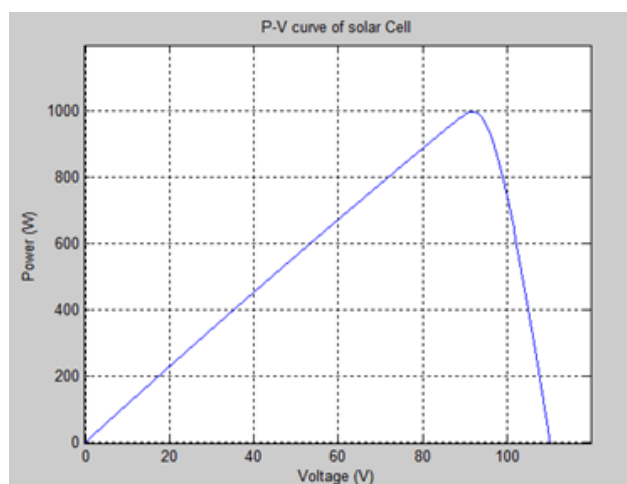


Figure 7: Ideal Solar cell P-V graph

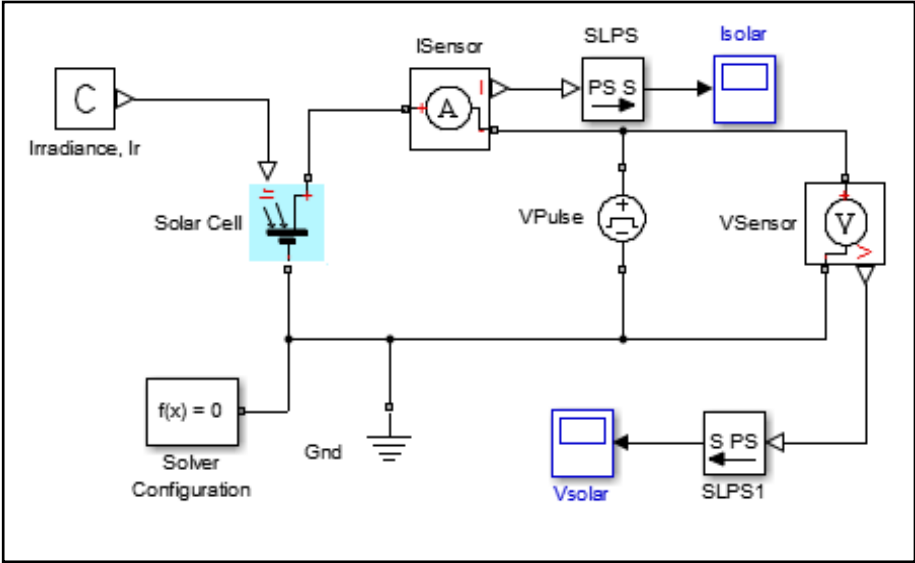


Figure 8: Simulation of Solar Panel System.

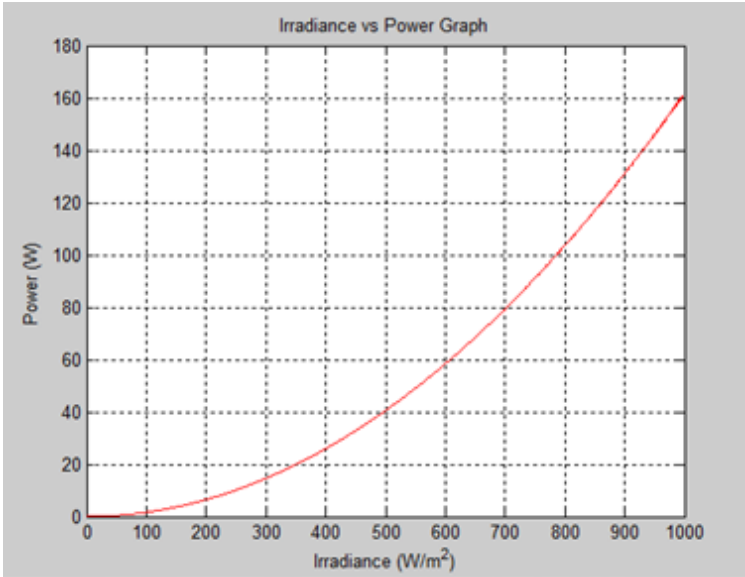


Figure 9: The simulation output Power over Irradiance Graph

Table1: Parameters of SPM100-M Monocrystalline type solar panel.

Parameters	Values
Maximum Power, P_{max}	20 W
Maximum Power Voltage, V_{mp}	18.32 V
Maximum Power Current, I_{mp}	1.09 A
Open-circuit Voltage, V_{oc}	22.06 V
Short-circuit Current, I_{sc}	1.17 A
Series Fuse Rating	10 A
NOTC	47 °C

Table 2: Parameters of SPM020-P polycrystalline type solar panel

Parameters	Values
Maximum Power, P_{max}	20 W
Maximum Power Voltage, V_{mp}	18.32 V
Maximum Power Current, I_{mp}	1.09 A
Open-circuit Voltage, V_{oc}	22.06 V
Short-circuit Current, I_{sc}	1.17 A
Series Fuse Rating	10 A
NOTC	47 °C

Table 3: Table of Changing Temperature with Maximum Irradiation of Sun.

Irradiation of Sun (W/m^2)	Temperature (°C)
1000	10
1000	25
1000	45
1000	75

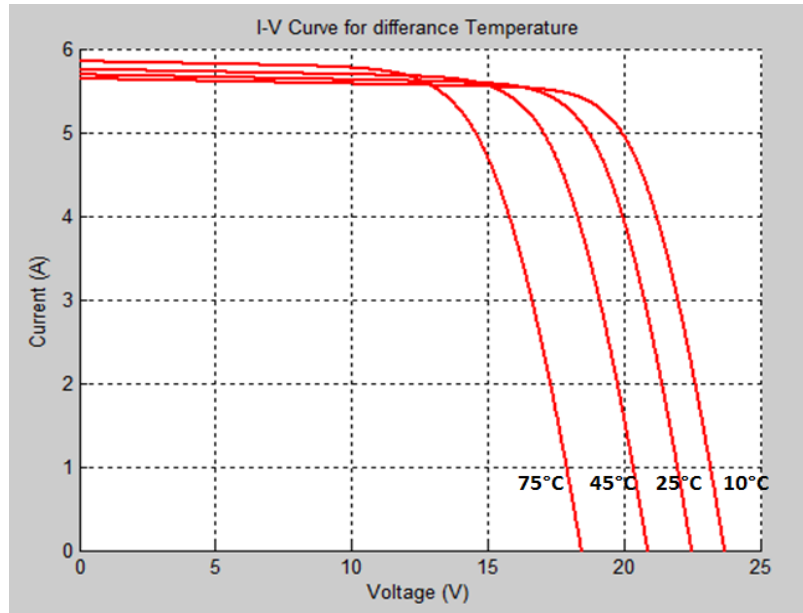


Figure 10: I-V Curve of Monocrystalline SPM100-M Model

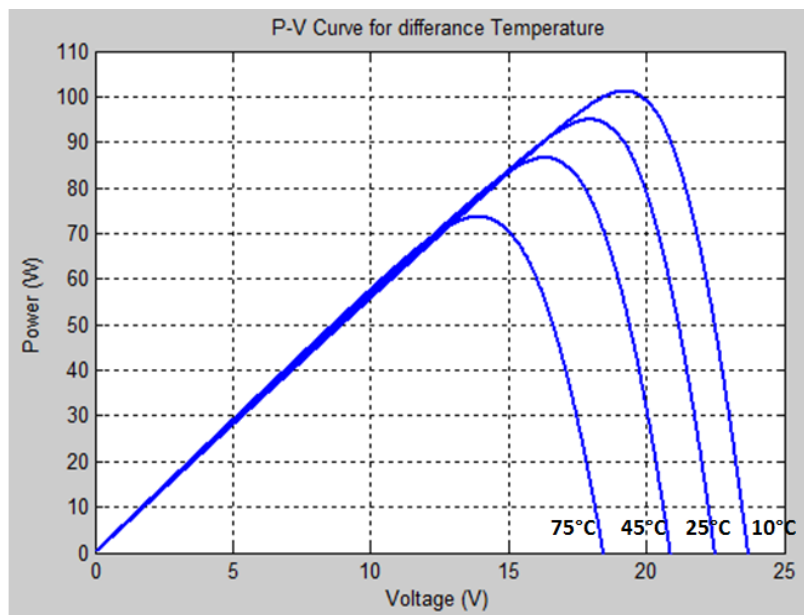


Figure 11: P-V Curve of Monocrystalline SPM100-M Model.

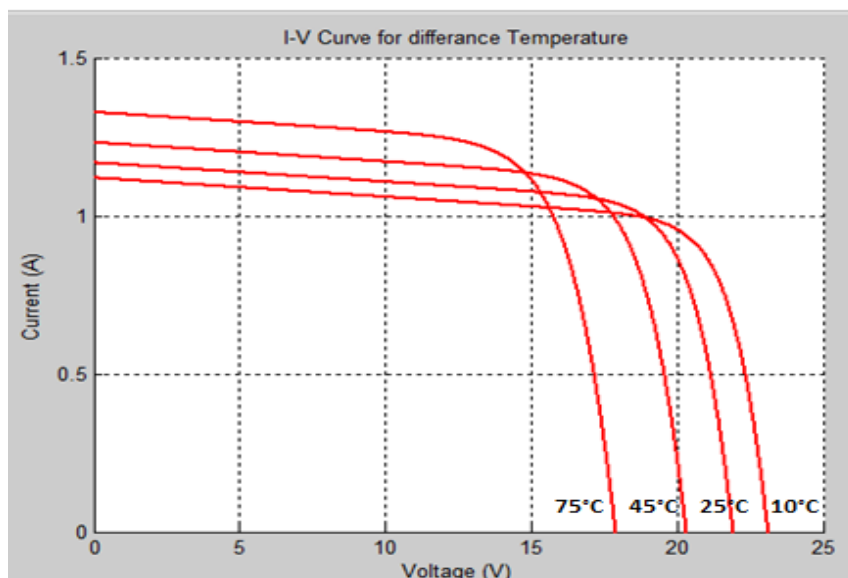


Figure 12: I-V Curve of Polycrystalline SPM020-P Model.

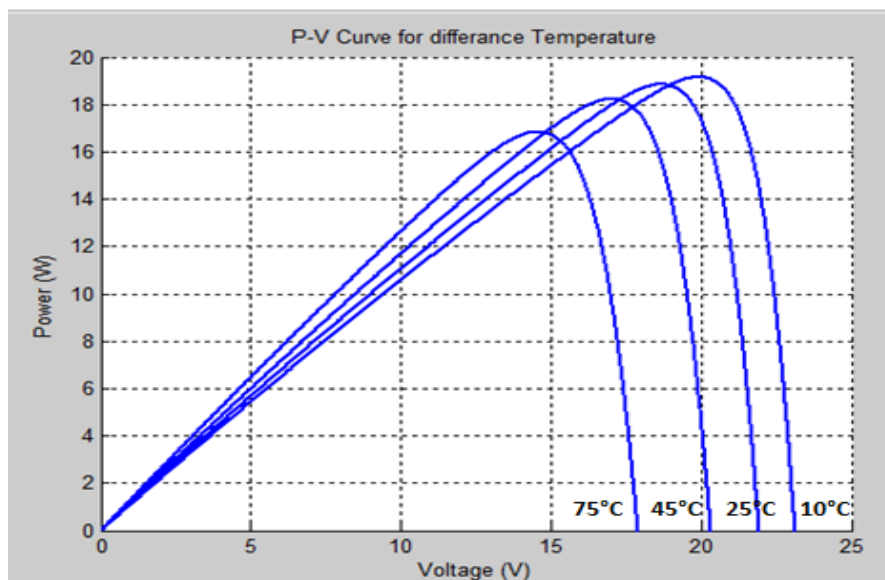


Figure 13: P-V Curve of Polycrystalline SPM020-P Model

References

- 1- Malaysia Energy Information Hub, MEIH, [Online]. Available: <http://www.st.gov.my/>
- 2- Sera,S.;Rodriguez,P.: PV panel mode based on datasheet values, IEEE International Symposium on Industrial Electronics, ISIE 2007, 4-7 June 2007, pp.2392 – 2396.
- 3-P.Srinivasa Rao, C.N. Saravana“Maximum Power from PV Arrays Using a Fixed Configuration under Different Shading Conditions,” IEEE Journals of Photovoltaic: Vol. 4., pp.12, 2014.
- 4-Miller, Michael “Maximum Power from a Solar Panel,” Undergraduate Journal of Mathematical Modeling: One + Two: Vol. 3: Iss.1, pp: 12-22, 2010.
- 5-Liu, S.; Dougal, R.A.: Dynamic Multiphysics Model for Solar Array, IEEE Trans. On Energy Conversation, Vol. 17, No.2, June 2002, pp. 285-294.
- 6-Pure Energies, [Online]. Available: <http://pureenergies.com/us/blog/top-10-countries-using-solar-power>.
- 7-H. M. Moniruzzaman, M. Patwary, R. Mosaddequr “Solar Panel System with an Automated Solar Tracker,” IEEE Journals of Photovoltaic, vol.6, pp.65, 2011.
- 8-Sheila Glasbey, Solar Electricity Handbook, “A Simple Practical Guide to Solar Energy”, Greenstream Publishing,U.K, 2012.
- 9- Miller, Michael “Maximum Power from a Solar Panel,” Undergraduate Journal of Mathematical Modeling: One + Two: Vol. 3: Iss.1, pp: 12-22, 2010.
- 10- V. P. Sethi, K. Sumathy, S. Yuvarajan, D. S. Pal (2012) “Mathematical Model for Computing Maximum Power Output of a PV Solar Module and Experimental Validation,” Journal of Fundamentals of Renewable Energy and Applications: Vol. 2, pp.20-33, 2012.
- 11-Kashif Ishaque, Zainal Salam, Syafaruddin “A comprehensive MATLAB Simulink PV system simulator with partial shading capability based on two-diode model,” Solar Energy 85 (2011), pp. 2217-2227.

Creating continuous model review for material cement in Kirkuk plant when fuzzy and randomly demand with acceleration (speed up) waiting period by application.

Dr. Abdul muneem k. Hamadi Alshokri

Counting department – Madent Alelem College.

أنشاء أنموذج مراجعة مستمرة لمخزون مادة السمنت في معمل كركوك عند
ضبابية وعشوائية الطلب لتعجيل فترة الأنتظار مع تطبيق عملي .

أ.م.د.عبدالمنعم كاظم حمادي الشكري

قسم المحاسبة – كلية مدينة العلم الجامعة

munaam53@yahoo.com

Abstract:

Many production companies suffering lot of problems concerning the management of inventory, especially in identify the amounts inventory should storage .In the actual market is very difficult to determine the precise value of the request for it to be random in most cases and that the adoption of these companies on the personal experiences and some of simple mathematical techniques leads to uncertainty determinant amounts of stock.

Where in this research create a model continuous for inventory due to demand is random fuzzy which has a fuzzy numbers for a following the trigonometric function for cement product which belong to cement plant Kirkuk at year 2015 and on a seasonal basis has been create a mathematical model after data distribution test which obtained upon request during the waiting period after removal of fuzzy where the test was using statistical program (spss) finding that distributed normally (normal distribution).

the research target to accelerate waiting period and identify the period which achieved highest economic typical quantitative by the lower expected cost with reduce the deficit and determine the best point to restore demand after conducting the required mathematical and statistical analyzes of the data by writing algorithm of proposed and It was using special mathematical criteria of quantitative methods in addition to the application importance and inventory effectiveness of the potential model in determining the economic quantities of production when the demand is random and fuzzy and reduced investment in inventories which leading to lower total costs of inventory to a minimum and so as to give solutions for research problem.

Key words: Continuous review of inventory, Fuzzy random demand Waiting time, Fuzzy trigonometric numbers.

المستخلص :

أن معظم الشركات الصناعية وشركات الإنتاج تتعرض للكثير من المشاكل المتعلقة بإنتاج وخزن وتسويق المنتج وخاصة فيما يتعلق بتحديد كميات المخزون الواجب الاحتفاظ بها , لذلك من الصعب عمليا تحديد قيمة دقيقة للطلب لذلك يكون الطلب عشوائي في معظم الأحيان ومن ذلك فان اعتماد الشركات على الخبرات الشخصية وبعض الأساليب الرياضية التقليدية البسيطة ينتج عنه تحديد غير دقيق لكميات الخزين .

في هذا البحث تم إنشاء أنموذج مراجعة مستمرة للمخزون لكون الطلب عشوائي ضبابي ذو أرقام ضبابية تتبع الدالة المثلثية لمنتج السمنت لمعمل سمنت كركوك لسنة (2015)م وعلى أساس فصلي , وتم إنشاء الأنموذج بعد اختبار توزيع البيانات المستحصل عليها للطلب خلال فترة الانتظار بعد إزالة الضبابية حيث تم الاختبار باستخدام البرنامج الاحصائي (spss) وتبين أنها تتوزع توزيع طبيعيا (Normal distribution).

ويهدف البحث الى تعجيل فترة الانتظار وتحديد الفترة التي تحقق اعلى كمية اقتصادية مثلى للإنتاج باقل كلف كلية متوقعة وتقليل العجز المتوقع وكذلك تحديد افضل نقطة لاعادة الطلب وباجراء التحليلات الرياضية والاحصائية المطلوبة للبيانات لصياغة خوارزمية للأنموذج المقترح واستعمالا لمعايير حسابية خاصة بالاساليب الكمية ولذلك اتضحت اهمية تطبيق هذا الانموذج وكفائتها في الحد من الاثار الناجمة عن التقلبات البيئية التي تواجهها الشركة من خلال السيطرة على مستوى الطلب وكلف الاحتفاظ بالخزين فضلا عن اهمية تطبيق انموذج الخزين وبيان فعاليته في تحديد الكميات الاقتصادية المثلى للإنتاج عندما تكون كميات الطلب الضبابية عشوائية وبذلك سيتم تقليل الاحتفاظ في الخزين مما يؤدي انخفاض الكلف الاجمالية للخزين الى ادنى حد ممكن وبذلك ستوجد حولا مقترحة لمشكلة البحث

الكلمات المفتاحية : المراجعة المستمرة للمخزون, الطلب الضبابي العشوائي, وقت الانتظار, الأعداد الضبابية المثلثية.

1 -Introduction:

Are important tasks management of store things that cannot be dispensed with in all companies and factories, the fact that the stock represents a portion of the capital of the company or factory value ranges between 15-25% of the invested capital. So that the storage is to keep a certain determinant quantities according to a scientific study of a commodity or raw material for a period of time to wait for the sale or used with storage costs. In practice, demand for goods is variable depending on consumer demand for the types of goods, as well as the waiting time. It is also variable depending on the circumstances that may be encountered by the external supplier. This leads to delaying the arrival of applications in a timely manner in some cases. The need for the consumer and the costs of storage because the increase in inventory generates a problem because it leads to idle capital and exploitation of storage space without interest and the lack of inventory generates another problem

leading to loss which generated by the company because of the inability to meet the actual demand of the consumer so The company's management is facing the problem of determining the optimal value of inventory and timely supply for the issuance of an order to suppliers and optimal quantity for each supply order.

In this research, an optimal model will be constructed to control the storage of cement for the Kirkuk plant for the year 2015 by studying the continuous review system of the reservoirs under the alternative of the random demand with a deficit due to the instability of the demand quantities and the uncertainties that prevail. Fuzzy logic for handling data uncertainties this logic will provide an easy and simple way to obtain specific conclusions from inaccurate and ambiguous data, and then the waiting time will be increased production and reduce the expected deficit as well as to determine the optimal waiting period that achieves the highest optimal economic quantity. Production at the

lowest total cost unexpected with lost fuzzy environment.

$E[\tilde{x}_L]$:The expected demand rate during the waiting period is fuzzy.

h: The cost of storage per ton during the season.

L: Wait time (variable decision), consisting of several components (i th) of the components of the minimum time () and the normal time of (b_r) with the cost of pressure per unit of time under the following assumption ($C1 \leq C2 \leq C3$) The rang wait time is ().

Lr: Length of waiting time with its components (r 1,2

2 - The methodology:

1 -2 Model Assumptions:

We will use the following assumptions to development of a model for fuzzy probability storage with compression of waiting time components: (5)

A: The cost of preparing the order for each order.

\hat{D} :The rate of demand during seasonal is random and fuzzy in nature.

The waiting period is compressed for the minimum duration as follows:

$$L_n = \sum_{j=1}^n a_j$$

$$Lr = L_n + \sum_{K=r+1}^n (b_k - a_k)$$

For $r = 0,1, \dots, n$

$$b_r > a_r, L_{r-1} > L_r$$

Q: The economic size of the production quantity.

Q_r :The economic size of the production quantity at the time of waiting (r).

C_L : The cost of compressing the waiting time for each cycle.

B_r : The amount of disability in each cycle.

B: The percentage of applications that are not executed due to depletion of deposits, which can be accepted by the plant management, and between $(0 \leq B \leq 1)$

π :Cost of disability per ton.

π_0 :Profit per ton.

$\bar{\pi}$:Total loss resulting from unsatisfied demand

$$\bar{\pi} = \pi + (1 - B)\pi_0$$

2 – 2 Mathematical formula:

From the assumptions above and given that a small portion of (B) during the period of entry into stock can be deferred requests so the total cost will be extracted through the following formula:

$C(Q,R,L)$ = setup cost + holding cost + stock-out cost +lead-time crashing cost

$$= A \frac{D}{Q} + h \left[\frac{Q}{2} + R - E[x_L] + (1 - B)E[B_r] \right] + \frac{D}{Q} [\bar{\pi}E[B_r]] + \frac{D}{Q} \dots \dots (1)$$

$$= \frac{D}{Q} [A + \bar{\pi}E[B_r]] + h \left[\frac{Q}{2} + R - E[x_L] + (1 - B)E[B_r] \right] \dots \dots (2)$$

Here the demand is considered as a random variable so the demand can be expressed vaguely and the total costs will be treated as a random variable so the cost function will be written as follows:

$$C(Q, R, L) = \frac{\hat{D}}{Q} [A + \bar{\pi}E[(\tilde{x}_L - R)^+]] + h \left[\frac{Q}{2} + R - E[\tilde{x}_L] + (1 - B)E[(\tilde{x}_L - R)^+] \right] \dots \dots (3)$$

$$E[B_r] = E[(\tilde{x}_L - R)^+]$$

The demand during the waiting period is different depending on the length of the waiting period in the uncertain environment, so the estimation of the demand during the waiting period is based on the

inaccurate perception, so the demand during the waiting period is fuzzy.

Whereas:

X: Demand weekly.

$$x_L = x_2 L$$

$$0 \leq x_1 \leq x_2 \leq x_3$$

Therefore, the expected value during the waiting period for the demand is fuzzy blurred and is extracted from the following equation:

$$E[\tilde{x}_L] = E[\tilde{x}] * L$$

$$E[\tilde{x}_L] = \frac{x_1 + 2 * x_2 + x_3}{4} \dots \dots (4)$$

The model of continuous review of reservoirs under the fuzzy random cloud environment is as follows:

$$\tilde{C}(Q, R, L) = \frac{\tilde{b}}{Q} [A + \pi E[(\tilde{x}_L - R)^+] + C(L)] + h \left[\frac{Q}{2} + R - E[\tilde{x}_L] + (1 - B)E[(xL - R)^+] \right] \dots \dots (5)$$

There are two cases to calculate the expected deficit when the re-demand point is within range:

$$R \text{ in } (x_1 L, x_3 L)$$

Provided that the re-order point is greater or equal to the expected demand during the waiting period

$$R \geq E[\tilde{x}_L]$$

Cas1: $R \in [x_1 L, x_2 L]$

Re - order demand point as following figure:

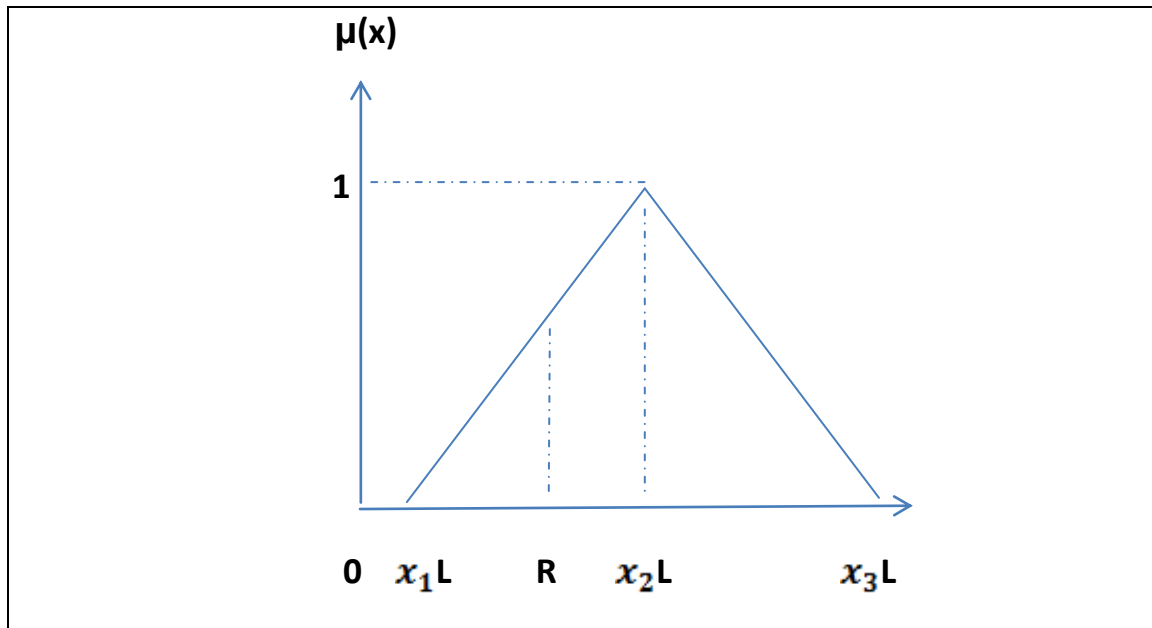


Figure (1) when $R \in (x_1L, x_2L)$

The expected disability in this case can be derived from the following:

$$E[(\tilde{x}_L - R)^+] = \int_R^{x_3L} (t - R) d\Phi(t) = \int_R^{x_2L} (t - R) d\Phi(t) + \int_{x_2L}^{x_3L} (t - R) d\Phi(t) \dots (6)$$

$$= \frac{2x_2L^2 - x_2L((x_1 - x_3)L + 4R) + 2Rx_1L + R^2 - x_1x_3L^2}{4(x_3 - x_1)L} \dots \dots \dots (7)$$

Whereas:

$$\phi(t) = \begin{cases} 0 & \text{for } t \leq x_1L \\ \left(\frac{t - x_1L}{2(x_2 - x_1)L}\right) & \text{for } x_1L \leq t \leq x_2L \\ \left(\frac{t + x_3L - 2x_2L}{2(x_3 - x_2)L}\right) & \text{for } x_2L \leq t \leq x_3L \\ 1 & \text{Otherwise} \end{cases}$$

Assuming:

$$E[\tilde{x}_L] = t$$

Hanes the expected total cost for storage when $R \in$ (Calculate by following formula When the total cost equation is derived for (Q):

$$E[\tilde{C}(Q, R, L)] = \frac{E[\tilde{d}]}{Q} \left[A + \bar{\pi} \left(\frac{2x_2L^2 - x_2L((x_1 - x_3)L + 4R) + 2Rx_1L + R^2 - x_1x_3L^2}{4(x_3 - x_1)L} \right) + C(L) \right]$$

$$h \left[\frac{Q}{2} + R - E[\tilde{x}_L] + (1 - B) \left(\frac{2x_2L^2 - x_2L((x_1 - x_3)L + 4R) + 2Rx_1L + R^2 - x_1x_3L^2}{4(x_3 - x_1)L} \right) \right] \dots (8)$$

$$\frac{\partial}{\partial Q} E[\tilde{C}(Q, R, L)] = 0$$

We get the formula by calculate the optimal economic size.

$$\begin{aligned} & Q^2 \\ &= \frac{2E[\tilde{d}]}{h} \left[\left[A + \bar{\pi} \left(\frac{2x_2L^2 - x_2L((x_1 - x_3)L + 4R) + 2Rx_1L + R^2 - x_1x_3L^2}{4(X_3 - X_1)L} \right) \right] \right. \\ & \left. + C(L) \right] \dots \dots \dots (9) \end{aligned}$$

$$Q. = \sqrt{\frac{2E[\tilde{d}]}{h} \left[\left[A + \bar{\pi} \left(\frac{2x_2L^2 - x_2L((x_1 - x_3)L + 4R) + 2Rx_1L + R^2 - x_1x_3L^2}{2(x_3 - x_1)L} \right) \right] + C(L) \right]} \dots \dots (10)$$

Case 2: Let $R \in (x_2L, x_3L)$

Therefore, the total expected cost of storage when $R(\epsilon)$ calculated from the following formula as shown figure :

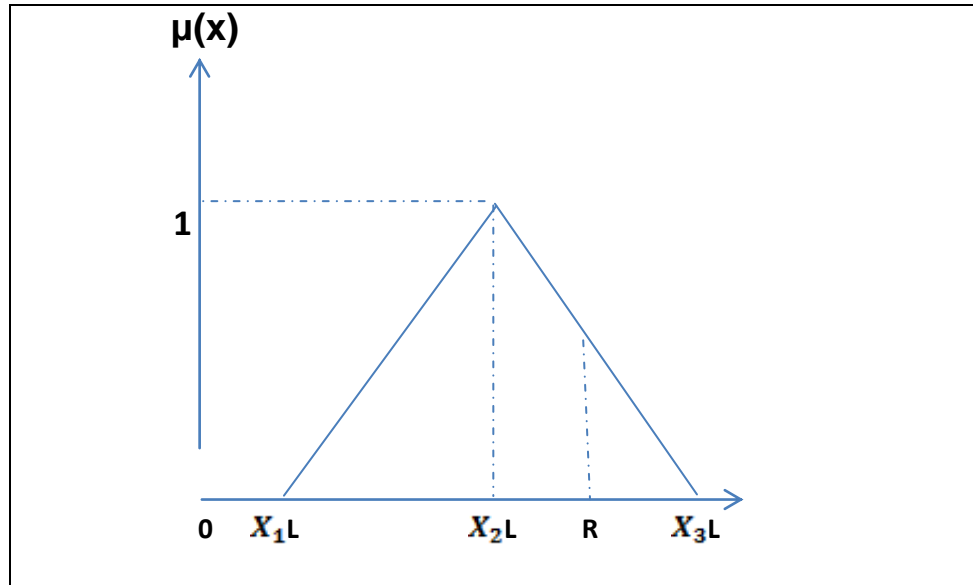


Figure 2 when $R \in [X_2L, X_3L]$

The expected disability in this case can be derived from the following formula:

$$E[(\tilde{x}_L - R)^+] = \int_R^{x_3L} (t - R) d\Phi(t) \quad \dots \dots \dots (11)$$

$$= \frac{(x_3L - R)^2}{4(x_3 - x_2)L} \quad \dots \dots (12)$$

The expected total cost of storage when $R(\epsilon)$ is calculated from the following formula:

$$E[\tilde{C}(Q, R)] = \frac{E[\tilde{d}]}{Q} \left[A + \bar{\pi} \left(\frac{(x_3L - R)^2}{4(x_3 - x_2)L} \right) + C(L) \right] + h \left[\frac{Q}{2} + R - E[\tilde{x}_L] + (1 - B) \left[\frac{(x_3L - R)^2}{4(x_3 - x_2)L} \right] \right] \dots (13)$$

When we derivative the total cost equation for(Q) we get:

$$\frac{\partial}{\partial Q} E[\tilde{C}(Q, R, L)] = 0$$

From this we get the formula by calculated the optimal economic size.

$$Q^2 = \frac{2E[\tilde{d}]}{h} \left[\left[A + \bar{\pi} \left(\frac{(x_3L - R)^2}{4(x_3 - x_2)L} \right) \right] + C(L) \right] \dots (14)$$

$$Q = \sqrt{\frac{2E[\tilde{d}]}{h} \left[\left[A + \bar{\pi} \left(\frac{(x_3L - R)^2}{4(x_3 - x_2)L} \right) \right] + C(L) \right]} \dots \dots \dots (15)$$

3 -Practical view:

1-3 Introduction:

percent in the ton industry One of the cement and al trabalhudid, hageralgebs, white oil and will be the process of mixing materials involved measured ratios globally scientifically and practically passing through malty process to produce the cement material.

2- 3 The model data:

The formulation of data demand weekly for the first seasonal (January, February and March) , as indicated in the following table:

For the purpose of applying the model of the problem in question has been relying on seasonal data for the year 2015, as the required data collected for the Cement Plant of Kirkuk - General Company for Iraqi Cement, for a period of one year and on a seasonal basis, which was obtained fuzzy quantity demand for the cement material where the first, third season data adoption for year (2015), as well as obtained the special costs of such material has been the cement industry relies on hageralklis, a raw material essential in the cement industry where interference by (75-80%)

Table (1) shows the weekly demand during the first seasonal

Months	X_1	X_2	X_3	E[x]
January				
First week	5209	5567	6144	5621.75
Second week	5114	5494	6038	5535
Third week	4928	5472	6006	5469.5
Fourth week	4833	5399	5904	5383.75
February				
First week	4495	4769	5521	4888.5
Second week	4333	4536	5045	4612.5
Third week	4353	4719	5087	4719.5
Fourth week	4515	4952	5563	4995.5
Marche				
First week	5764	6532	7035	6465.75
Second week	6168	6608	7003	6596.75
Third week	5657	6495	7145	6448
Fourth week	6275	6645	7177	6685.5

Source : Preparing the researcher based on the company records:

3-3 Distribution of the application during the waiting period:

When reviewing the statistical analysis of the demand during the waiting period for each chapter after removing the fuzzy using the following law $E[\tilde{x}]$ = It was found that the normal distribution is distributed where the data were tested by using the statistical program (SPSS).

Table (2) shows the normal distribution of the first chapter

Descriptive Statistics						
	N	Minimum	Maximum	Sum	Mean	Std. Deviation
	Statistic	Statistic	Statistic	Statistic	Statistic	Statistic
The First Season	12	4612.50	6685.50	67422.0	5618.50	758.40276

A Test distribution is Normal

b. Calculated from data

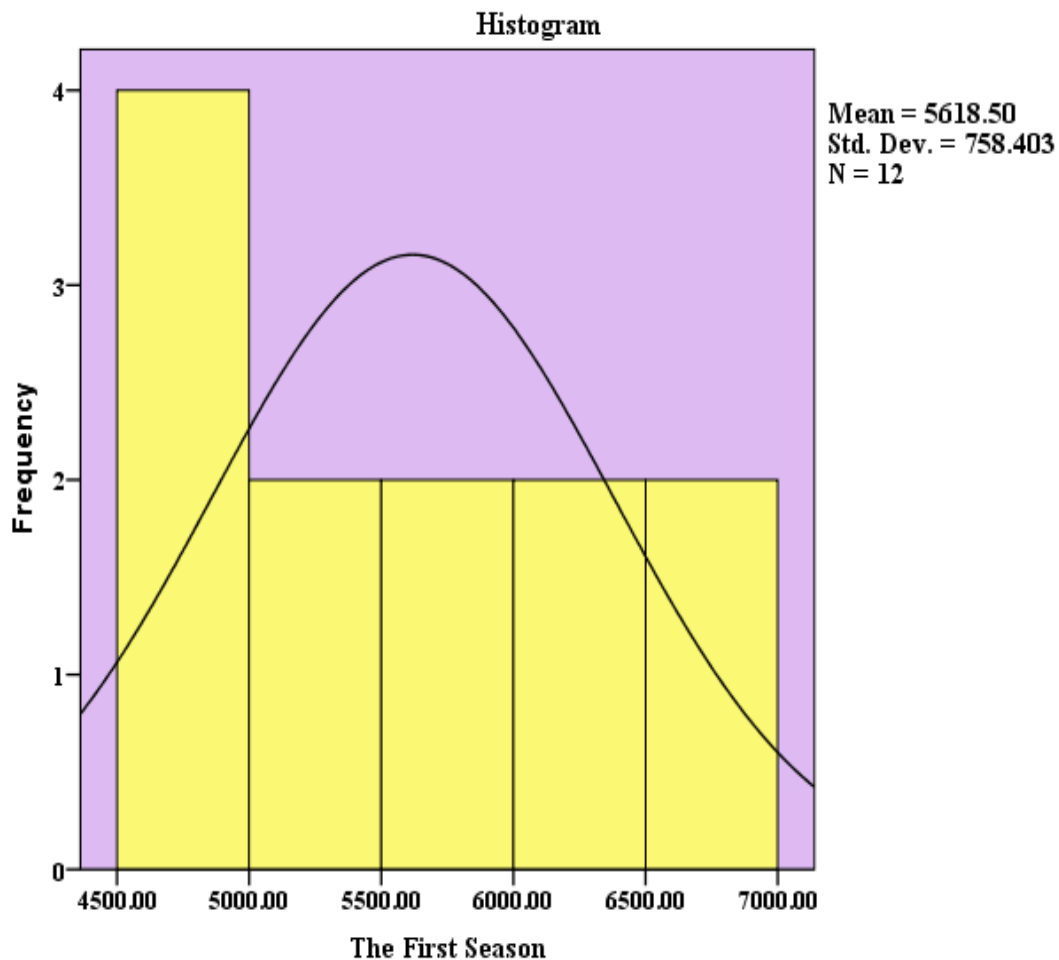


Figure (3) normal distribution of first seasonal

Table (3) shows the weekly demand rate during the first seasonal

X1	X2	X3
5139	5599	6139

Table (4) shows the probability of fuzzy demand during the seasonal.

Probability Demand

Demand	Probability
$d1=(70024,70140,70370)$	0.15
$d2=$	0.18
$d3=(70070,70130,70221)$	0.20
$d4=(70105,70250,70320)$	0.22
$d5=(70150,70330,70400)$	0.25

Table) (5) shows the weekly demand during the second quarter (April, May, June)

Months	X_1	X_2	X_3	$E[X]$
April				
First week	8566	8731	9544	8893
Second week	8433	8724	9540	8855.25
Third week	8280	8635	9216	8692.5
Fourth week	8413	8642	9220	8729.25
May				
First week	8701	9217	9908	9260.75
Second week	8569	9276	10239	9340
Third week	:8357	9045	9423	8967.5
Fourth week	8913	8986	9754	9159.75
Jun				
First week	6413	6743	7620	6879.75
Second week	6457	7003	7832	7073.75
Third week	6348	6796	7638	6943
Fourth week	6522	6950	7814	7059

Source: Preparing the researcher based on the company records

Table (6) shows the normal distribution of second seasonal

Descriptive Statistics						
	N	Minimum	Maximum	Sum	Mean	Std. Deviation
	Statistic	Statistic	Statistic	Statistic	Statistic	Statistic
The Second Season	12	6879.75	9340.00	99853.50	8321.1250	1003.83828

a. Test distribution is Normal.

b. Calculated from data

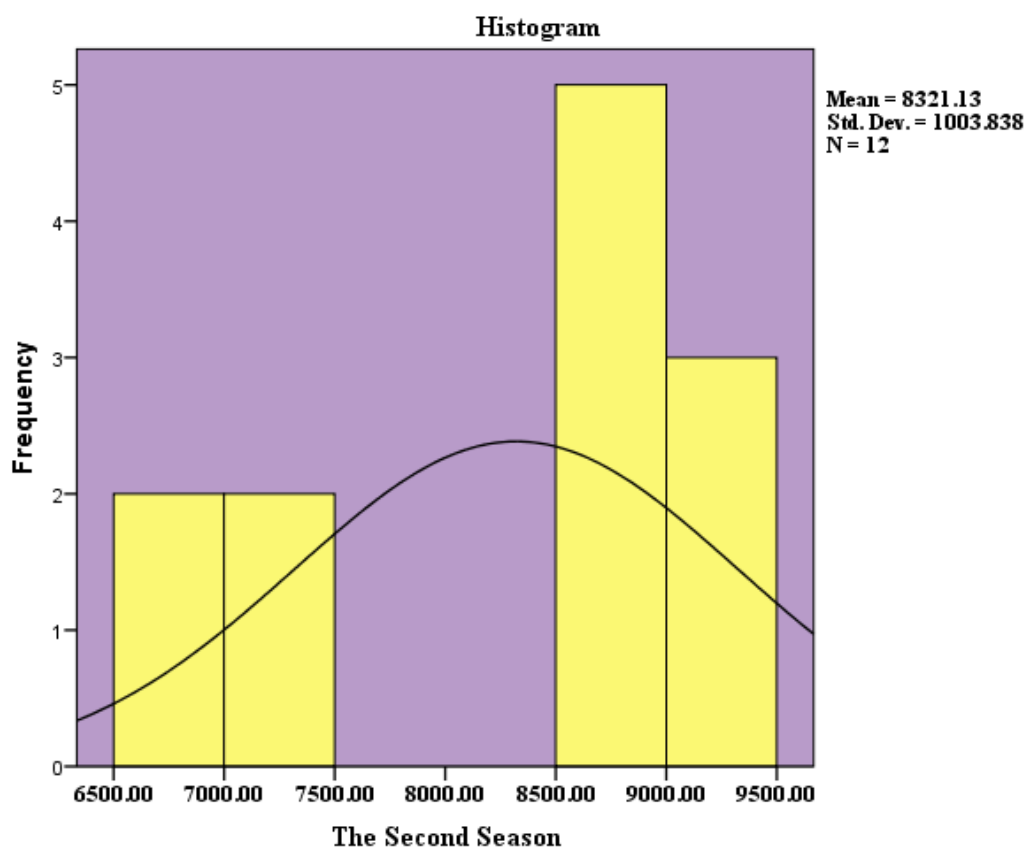


Figure (4) normal distribution of second seasonal

Table (7) shows the average weekly demand during the second seasonal

X1	X2	X3
7831	8229	8979

Table (8) shows the probability fuzzy probability demand average during

Demand	Probability
d1=	0.27
d2=(94010,96994,97530)	0.24
d3=(91989,92250,93122)	0.19
d4=(90928,92835,93202)	0.16
d5=	0.14

Source: Preparing the researcher based on the company records

Table (9) shows the costs used in the model

Season \ cost	α	H	β	$\bar{\pi}$	π_0	π	A
First season	0.35	4500	0.2	20100	20125	4000	16362192
Second season	0.4	4500	0.4	16075	20125	4000	21942309

Table (10) shows the components of the waiting time

Contents waiting time	1	2	3
Normal time	15	10	10
Reduce time	8	3	3
Crash cost	297000	300000	365000

5-Model Algorithm:

First step:

Calculate the length of the waiting period (L_r) with the compression of its components to the maximum of normal time by applying the following formula: (5)

$$L_n = \sum_{j=1}^n a_j$$

$$L_r = L_n + \sum_{k=r+1}^n (b_k - a_k)$$

$$L_0 = 35 \text{ days (5 weeks)}$$

$$L_1 = 35 - 7 = 28 \text{ days (4 weeks)}$$

$$L_2 = 28 - 7 = 21 \text{ days (3 weeks)}$$

$$L_3 = 21 - 7 = 14 \text{ days (2 weeks)}$$

and

$$L_3 = \min_{0 \leq r \leq n} L_r = 2 \text{ weeks}$$

$$L_0 = \max_{0 \leq r \leq n} L_r = 5 \text{ weeks}$$

Table (11) shows reduced waiting periods

R	L_r
0	5
1	4
2	3
3	2

4 - Application the model of fuzzy probability storage:

This paragraph is devoted to the application of a model of fuzzy probability storage in the framework of the algorithm to be clarified based on the seasonal demand data of the product collected so that we can draw conclusions and discuss them.

Second step:

Calculate expected demand during the waiting period through the following formula:

$$E[\tilde{x}_L] = E[\tilde{x}] * L_r$$

$$E[\tilde{x}] = \frac{x_1 + 2 * x_2 + x_3}{4}$$

Third step:

Calculate the standard deviation of the demand during the waiting period by the following formula:

Whereas:

$$\bar{X} = \frac{\sum X_i}{n}$$

Fourth step:

Calculate the Redemption Point (R) through the following formula:

$$R = E[\tilde{x}] * L_r + \sqrt{L_r} * \sigma * K_{ai}$$

Fifth Step:

Calculate the degree of affiliation of the application during the waiting period through the following formula:

$$\mu(x) = \begin{cases} \frac{E(x)L - x_1L}{x_2L - x_1L} & \text{for } x_1L \leq E(x)L \leq x_2L \\ \frac{E(x)L - x_3L}{x_2L - x_3L} & \text{for } x_3L \leq E(x)L \leq x_3L \\ 0 & \text{otherwise} \end{cases}$$

Sixth Step:

Calculate expected **deficit** of demand during the waiting period.

Case (1) if $R \in (x_1L, x_2L)$

The expected deficit is calculated by applying equation (7).

Case (2) if $R \in (x_2L, x_3L)$

The expected deficit is calculated using the equation (12).

Seventh step:

Calculate expected demand during the quarter by the following formula:

$$E[\tilde{d}] = \sum_{i=1}^n E[\tilde{d}_i] * P_i$$

whereas:

$$E[\tilde{d}_i] = \frac{(d_{i1} + (d_{i2} * 2) + d_{i3})}{4}$$

Eighth Step:

Calculate the cost of pressure C (L) through the following law:

$$C(L) = Cr(L_{r-1} - L) + \sum_{K=1}^{r-1} C_K(b_k - c_k)$$

Table (12) shows the calculation of the cost of accelerating (speed up) the waiting time

R	C(L)
0	0 <i>for $35 \geq L$</i>
1	$297000(35 - L) = 10395000 - 297000L$ <i>for $35 \leq L$</i>
2	$300000(28 - L) + 297000 * 7 = 8400000 - 300000L + 2079000$ <i>for $28 \leq L$</i>
3	365000 <i>for $21 \leq L$</i>

Table (13) shows the cost of accelerating the waiting time for each stag

Crash lead –time	Lr	C(L)
0	5	0
1	4	2079000
2	3	4179000
3	2	6734000

Ninth Step:

The economic size of the production quantities is calculated by the following formula:

CAS 1: IF $R \in (X_1, X_2)$ By applying equation (10) .

CAS 2: IF $R \in (X_2L, X_3L)$ By applying equation (15) .

Tenth Step:

Calculate the expected total cost of the storage through the following formula:

CAS 1: IF $R \in$ By applying equation (8):

CAS 2: IF $R \in (x_2L, x_3L)$ By applying equation (13):

Table (14) shows the optimal solution for third seasonal.

Crash lead - time	L	MC	Q	R	SHORTS
0	5	125969228.6	27080.8	28736.91	355
1	4	125934942.5	27205.51	23050.38	262.37
2	3	12461077805	27392.42	17354.66	174.16
3	2	127628443.6	27912.32	11644.56	92.88

Table (15) shows the best solution for fourth seasonal.

Crash lead - time	L	MC	Q	R	SHORTS
0	5	163412924.4	35425.56	42149	502
1	4	1631809618	35515.67	33772.5	382.88
2	3	163221426.9	35651.2	25387.9	266.6
3	2	164597679.6	36103.38	16990.7	155.94

6 - Results:

the table(14) show us that the best waiting period is when (L = 3) a week, (21 days), which is to accelerate the waiting period for two (14) days, meaning that we can only accelerate the components of the first and second waiting period. (27392.42) tons, or about (27392) tons during this period at the lowest total cost expected by (12461077805) dinars and the point of re-demand is when the stock reaches (17354.66) tons, or about (17355) tons with an attempt to reduce the amount The expected deficit to (174.16) tons or about (174) tons during this period of this seasonal (third seasonal) , while for the second seasonal , the economic quantity of the (35651.2) tons (35651) tons when the waiting

period (L = 3) a week is the best waiting period because it achieves the highest quantity at the lowest total cost expected by (163221426.9) dinars and the point of re-demand is when the stock reaches (25387.9)) And that the expected deficit during this period is (266.6) tons during the waiting period for this seasonal (fourth seasonal).

7 – Conclusions:

1-The company does not adopt the scientific methods in determining the actual quantities of demand for the cement product. An annual plan is drawn up based on personal estimates.

2-The use of fuzzy logic in inventory management is more effective and flexible for decision makers in determining the

optimal quantities of traditional methods.

3-Through the study and analysis it became clear that the demand for the cement product is affected by the seasonal factors in its fluctuations due to the adoption of most companies on personal experience and some simple mathematical methods that lead to the identification of inaccurate amounts of storage, because in practice it is difficult to determine the exact value of the request, The demand is often vague.

8 - Recommendations:

1 -Conducting studies in the field of inventory management in the with a random and fuzzy environment and applying it to productive companies in Iraq because they lack inventory systems based on modern methods and methods of inventory management.

2- Adoption of modern scientific methods in determining the optimal economic volume of demand or production to

develop a seasonally plan or annual study.

3 -Using the applications of the theory of aggregates fuzzy in various areas to remove the uncertainty and volatility that prevail in the Iraqi production environment.

4- Develop seasonally and annual plans using modern scientific methods in determining the economic quantities of production.

References:

1-Alshamerti, Hamid Saad Nur Operations Research / Concept and Application, First Edition, Baghdad, Memory Library 2010.

2- Ali, Abdullah Hassan, "Building a model of my obscure inventory control with practical application" Master Thesis, Baghdad University, Faculty of Management and Economics, 2006.

3-Jassem, Abdullah Basim "Best strategy for management of fuzzy inventory applied research in the Baghdad Company for soft drinks," Master Baghdad

University, Faculty of Management and Economics, 2016.

4-Homsi, Daniel, "Models of Probable Inventory Management and Planning Horizon Theory", Master Thesis, Damascus University, Faculty of Management and Economics, 2009.

5-Shah, Nita H. & soni, Hardik N, "Continuous Review Inventory Model with Fuzzy Stochastic Demand and Variable Lead Time", Applied Industrial Engineering an International Journal .NO.1 (2), PP.7- 24, 2012 .

6-Soni, Hardik N. & Manisha Joshi, "A Periodic Review Inventory Model With Controllable Lead Time and Backorder Rate in Fuzzy-Stochastic Environment" Journal of Applied Fuzzy Information and Engineering.NO.1, pp 101-114 , 2015.

7-Taleizadeh,Ata Allah &Niaki, Seyed Taghi Akhavan & Aryanezhad, Mir-Bahador & Shafii, Nima, (2013), "A hybrid method of fuzzy simulation and genetic algorithm to optimize

constrained inventory control systems with stochastic replenishments and fuzzy demand" Information Sciences, No.220; PP.425-441.

8-Tyworth, John E.& Juo, Yuanming & Ganeshan, Ram, (1996), "Inventory control under gamma demand and random lead time" ,Journal of business logistic,No.1,PP.291-304.

9-Yao, Jing shying & change, Jershan, (2003), "Inventor without backorder with fuzzy total cost and fuzzy storing cost defuzzified by centroid and signed distance" , Elsevier : European Journal, No.148, PP.401-409.

10-Zadeh, L.A., (1965), "Fuzzy Sets", Information and control, No.8, PP. 338-353.